HAWASSA UNIVERSITY

INSTITUTE OF TECHNOLOGY

QUANTIFYING SURFACE AND GROUND WATER AVAILABILITY OF THE MEKI RIVER, CENTRAL RIFT VALLEY LAKES BASIN, ETHIOPIA.

MSc THESIS

SALAME ABDI AHMED

December, 2024

HAWASSA, ETHIOPIA

QUANTIFYING SURFACE AND GROUND WATER AVAILABILITY OF THE MEKI RIVER, CENTRAL RIFT VALLEY LAKES BASIN, ETHIOPIA.

BY

SALAME ABDI AHMED

A THESIS SUBMITTED TO THE

FACULTY OF BIOSYSTEMS AND WATER RESOURCES ENGINEERING,

DEPARTMENT OF HYDRAULIC ENGINEERING

HAWASSA UNIVERSITY INSTITUTE OF TECHNOLOGY, SCHOOL OF GRADUATE STUDIES, HAWASSA UNIVERSITY HAWASSA, ETHIOPIA

IN PARTIAL FULFILLMENT OF THE

REQUIREMENTS FOR THE

DEGREE OF

MASTER OF SCIENCE IN HYDRAULIC ENGINEERING

(SPECIALIZATION: HYDRAULIC ENGINEERING)

December, 2024

HAWASSA, ETHIOPIA

DECLARATION

I, **Salame Abdi Ahmed**, hereby declare that this is my original work and I have not and will not submit it to any other university for consideration of a similar degree or other equivalent awards. All sources of information used in the creation of this thesis have been properly acknowledged.

Signature_____

Date_____

ADVISOR'S APPROVAL SHEET

SCHOOL OF GRADUATING STUDIES

HAWASSA UNIVERSITY

This is to certify that the thesis entitled **"Quantifying Surface and Groundwater Availability in the Meki River, Central Rift Valley Lakes Basin, Ethiopia."** submitted in partial fulfillment of the requirements for the degree of Master's with specialization in Hydraulic Engineering, the Graduate Program of the Department of Hydraulic and Water Resources Engineering and has been carried out by **Salame Abdi ID. No.0013/13**, under our supervision.

Therefore, we recommend that the student has fulfilled the requirements and hence hereby can submit the thesis to the department.

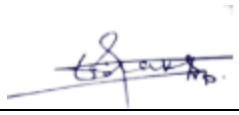

Dr. Sirak Tekleab		6/12/2024
Name Major Advisor	Signature	Date
_____	_____	_____
Name Co-Advisor	Signature	Date

EXAMINER'S APPROVAL SHEET

SCHOOL OF GRADUATE STUDIES

HAWASSA UNIVERSITY

We, the undersigned, members of the Board of Examiners of the final open defense by Salame Abdi have read and evaluated his thesis entitled **Quantifying Surface and Groundwater Availability in the Meki River, Central Rift Valley Lakes Basin, Ethiopia."**, and examined the candidate. This is, therefore, to certify that the thesis has been accepted in partial fulfillment of the requirements for the degree.

Dr. Sirak Tekleab		6/12/2024
Name of Major Advisor	Signature	Date
_____	_____	_____
Name of Internal Examiner-I	Signature	Date
_____	_____	_____
Name of Internal Examiner-II	Signature	Date
Dr. Bahru Mekuria		Nov 29, 2024
Name of External examiner	Signature	Date
_____	_____	_____
SGS Approval	Signature	Date

ACKNOWLEDGMENT

First and foremost, I extend my heartfelt gratitude to the Almighty for granting me this significant moment. I am deeply thankful for the blessings of health, serenity, fortitude, and resilience that have enabled me to achieve my goals.

I am deeply appreciative of my advisor, Sirak Tekleab (Ph.D.), and co-advisor, Petros Yohenes (MSc.), for their unwavering support, professional guidance, invaluable feedback, and timely assistance at every phase of my thesis. Their friendship and constructive criticism have been instrumental in shaping my work.

Lastly, I wish to express my deepest love and respect to my family and friends for their consistent support, concern, encouragement, and the positive social atmosphere they provided during my thesis journey.

LIST OF ABBREVIATIONS

SWAT	Soil and Water Assessment Tool
Arc SWAT	SWAT Integrated with ArcGIS
NMA	National meteorology agency, Ethiopian
DEM	Digital Elevation Model
GW-SW	Groundwater and surface water
OIDA	Ontario Irrigation Development Authority
JICA	Japan International Cooperation Agency
WWAP	United Nations World Water Assessment Programm
OEPO	Oromia Environmental Protection Office
HGS	HydroGeoSphere
GW	Ground water
GSFLOW	Coupled groundwater and surface water Flow, model
MoWIE	Ministry of Water, Irrigation, and Energy, Ethiopian
GUI	Graphical User Interface
MODFLOW	Modular groundwater model
SCS	Soil Conservation System
RMSE	Root Mean Square Error
USACE	United States of Army Corps of Engineering
ME	Mean absolute
MAE	Mean absolute error
ARCGIS	Aeronautical Reconnaissance Coverage Geographic Information System
R^2	Coefficient of Determination
SWAT_CUP	Soil and water assessment tool -Calibration and Uncertainty Procedures
SUFI2	Sequential Uncertainty Fitting
HRU	Hydrological Response Unit

SLR	Solar radiation
NSE	Nash Sutcliff Efficiency
WND	Wind speed
WXGEN	Weather Generator

TABLE CONTENT

LIST OF TABLES

LIST OF FIGURES

ABSTRACTS

Quantifying surface water (SW) and groundwater (GW) availability is crucial for effective water resource management. This study assesses SW and GW in the Meki River sub-basin, central Rift Valley, Ethiopia, by SWAT and MODFLOW models. Integrating SWAT and MODFLOW. This study analyzed hydrological dynamics and groundwater resources for a period 2000 to 2020. SWAT divided the watershed into 18 sub-basins and 86 Hydrological Response Units (HRUs), simulating over 21 years with a three-year warm-up period. The SWAT model, calibrated and validated for 2000–2013, successfully simulated hydrological processes. Model performance was robust, with R^2 values of 0.76 and 0.85 and NSE values of 0.61 and 0.74, following 1000 simulations during calibration and validation. Critical parameters influencing streamflow included CN2, SOL_K, and GWQMN.

Using SWAT-derived GW recharge and evapotranspiration, the MODFLOW-NWT model simulated groundwater flow. Calibration with PEST ensured accuracy, achieving a strong correlation (R^2 = 0.9922) between observed and simulated groundwater levels across 62 piezometers. Error metrics (RMSE = 9.46 m, MAE = 7.22 m) confirmed model accuracy. Spatial analyses showed heterogeneous groundwater flow influenced by local conditions and SW interactions.

River-aquifer interactions revealed significant groundwater discharge to rivers, with daily discharge (91,198.128 m^3/day) exceeding recharge (24,866.406 m^3/day). The steady-state model showed balanced inflows and outflows, with recharge and river discharge being major inputs. This calibrated model offers a solid framework for managing groundwater resources in the Meki River sub-basin, supporting sustainable water management and planning. Groundwater flow primarily moved from the western escarpment towards the Tora-Koshe-Dugda ridge, influenced by varying hydraulic conductivity. The steady-state model balanced inflows and outflows (40.947 Mm^3/year), with recharge (23.5 Mm^3/year) and river contributions (9.1 Mm^3/year) as key inputs. Evapotranspiration, river discharge, and extraction also played significant roles.

Keywords: SWAT, MODFLOW, surface water, groundwater, recharge, river-groundwater interaction

1. INTRODUCTION

1.1 Background

Water scarcity is a critical global concern, especially in arid and semi-arid regions where water availability is a key challenge (Jackson et al., 2001). Surface water and groundwater have long been treated as separate resources. However, there is growing acknowledgment of their ongoing interplay as fundamental components of the hydrological cycle, impacted by a variety of meteorological and physiographic conditions (Winter et al., 1998; Dowlatabadi et al., 2015). Integrating these interrelated resources is increasingly important for ensuring sustainable water resource management (Sophocleous, 2002; Khan & Khan, 2019; Woessner, 2020). In Africa, water resources are critical for sustaining lives and ecosystems, with groundwater frequently serving as the primary water source in rural areas (Hiscock, 2011).

In Africa, water resources are critical for sustaining lives and ecosystems, with groundwater frequently serving as the primary water source in rural areas (Hiscock, 2011). However, issues such as over-pumping and diminishing groundwater levels endanger water security and socioeconomic growth across the continent (Abebe et al., 2014). Understanding watershed hydrology is critical for sustainable water management in places with high groundwater-surface water interaction (Bailey et al., 2016; Dowlatabadi & Zomorodian, 2016; Guevara Ochoa et al., 2020). Effective management of surface and groundwater resources is critical, especially in areas with strong surface-groundwater interactions, such as Ethiopia (Ayenew, 1998; Legesse and Ayenew, 2006; Zeray, 2006).

Ethiopia, endowed with twelve river basins and abundant natural water resources, faces significant challenges in managing surface runoff and groundwater for irrigation and other uses (Awulachew et al., 2007; MoWIE, 2010). Despite the country's rich water potential, unequal utilization of surface water and groundwater resources, combined with significant population growth and environmental degradation, intensifies water scarcity issues (Ako et al., 2010).

The Meki River sub-basin, located in Ethiopia's Central Rift Valley Lakes Basin, stands out as a critical area for water resource management. The region mainly relies on agriculture, particularly the growth of important crops, fruits, and vegetables (Hagos et al., 2020). The Meki

River, a lifeline for local communities, sustains agricultural activities crucial for the area's socioeconomic well-being.

Integrated management strategies are pivotal in addressing water scarcity challenges and ensuring sustainable water resource utilization in the Meki River sub-basin. Effective management of surface and groundwater resources is crucial not only for securing water supplies but also for supporting the region's agricultural productivity and overall development. This study aims to integrate advanced modeling tools like the Soil & Water Assessment Tool (SWAT) and MODFLOW to quantifying surface water and groundwater availability in the Meki River sub-basin. The study aims to provide robust water resource management methods that contribute to the region's sustainable development goals by bridging the gap between understanding of interrelated surface and ground water dynamics.

1.2. Statement of problems

Groundwater and surface water are critical resources in Ethiopia, contributing significantly to poverty reduction and food security. Groundwater, in particular, meets more than 80% of home water requirements and is rapidly being used for agricultural purposes (Pavelic et al., 2012; Ohenhen et al., 2023; Mengistu et al., 2019; Hulluka et al., 2023). However, excessive groundwater extraction has overtaken natural replenishment rates, resulting in a consistent drop in groundwater levels and quality (Rusli et al., 2023). In the Rift Valley Lakes Basin (RVLB), notably in the Meki River sub-basin, complex hydrogeological circumstances, excessive water abstraction, and watershed degradation have resulted in declining water tables and ecological disruptions (Ayenew 2001; Berhanu et al. 2014). Alongside these pressures, human impacts on groundwater dynamics in the region remain understudied, underscoring the urgent need for more comprehensive research.

Surface water in the Meki River sub-basin is crucial for the area. The Meki River plays a key role in supporting agriculture, which is the main source of income and livelihood for the local community. The Meki River supports the cultivation of essential crops and fruits, driving economic growth and enhancing local livelihoods through agriculture (Hagos et al., 2020). However, surface water resources are also under pressure due to erratic rainfall patterns,

growing irrigation demands, and environmental degradation. These factors contribute to fluctuating river flows, intensifying water scarcity issues. Despite the interconnection between surface water and groundwater systems, previous studies have often examined them separately, missing crucial interactions that affect overall water availability.

The Meki River basin, in central Ethiopia, is critical for water resources, sustaining agricultural, domestic water supply, and ecosystem services. Rising water demands, climate unpredictability, and land use changes all pose challenges to the basin's long-term water management. To address these concerns, it is critical to quantify surface and groundwater availability using advanced modeling methods like SWAT and MODFLOW.

1.3. Objective

General objectives

The main objective in this study is to quantify the surface water and ground water availability in Meki River sub basin.

1.3.1. Specific objectives

In order to achieve the general objective of the study, the following specific objectives are set for major milestones of the study: -

- To quantify the spatial and temporal variation of stream flow in the basin.
- To quantify the spatial variations of groundwater in the basin.
- Estimate the spatial variations surface water – groundwater interaction.

1.4. Research questions

Research questions are designed to address specific concerns or issues. Therefore, this study explores and answers the following research questions:

1. What are the spatial and temporal variations of streamflow in the basin?
2. How do the spatial variations of groundwater differ across the basin?
3. What are the spatial variations in surface water–groundwater interaction within the basin?

1.5. Scope of the study

This research emphasis on quantifying surface and groundwater availability in the Meki River sub basin using hydrological and hydrogeological models SWAT and MODFLOW. It investigates hydrological dynamics, emphasizing stream flow, groundwater variations, and

surface water – groundwater interaction within the basin. Objectives include analyzing temporal variations of stream flow, quantifying groundwater levels across different locations, and estimating spatial variations in surface water – groundwater interaction. This study aims to comprehensively understand the hydrological processes in the basin by addressing these key parameters.

1.6. The significance of the study

This study makes major contributions This study provides significant contributions in several areas: firstly, it enhances our understanding of hydrological dynamics in the basin by analyzing temporal and spatial variations in streamflow and groundwater levels, crucial for effective water management. Secondly, it informs targeted strategies for sustainable water use by accurately quantifying spatial variations in groundwater and surface water interactions, aiding in risk mitigation. Lastly, the research advances hydrological parameter quantification, particularly in temporal variations of streamflow and spatial variation of groundwater, thereby improving modeling techniques and methodologies in hydrological science. Overall, this study offers valuable insights into basin hydrology, benefiting both scientific understanding and practical water resource management efforts.

1.7. Organization of the Thesis

This thesis is organized into five chapters. Chapter 1 provides an introduction to the research topic, outlines the research objectives and questions, and highlights the significance of the study. Chapter 2 presents a comprehensive literature review, discussing relevant studies and research related to the quantification of surface water and groundwater availability using the integrated SWAT and MODFLOW model based on recharge linking. Chapter 3 describes the methodology, including data collection, model setup, and calibration/validation procedures. Chapter 4 presents the results of the modeling analysis and discusses the findings in relation to the research objectives. Finally, Chapter 5 presents the conclusions, summarizes the key findings, and provides recommendations for future research and water resource management in the Meki River basin.

2. LITERATURE REVIEW

2.1. Overview of groundwater and surface water availability

The dynamic interplay of groundwater (GW) and surface water (SW) is critical for understanding the flow and availability of water in the hydrological cycle (Sophocleous, 2002). These interactions occur when groundwater discharges into surface water bodies or when surface flows recharge groundwater during peak flow periods (Wake, 2008). Such exchanges are especially important in Ethiopia's Rift Valley, where surface water bodies can recharge groundwater, altering both quality and quantity over time (Fleckenstein et al., 2010). This interwoven relationship is crucial for sustainable water resource management, particularly in areas where water supports agriculture and urban water delivery systems (Hatch et al., 2006; Sophocleous, 2002).

In the Nile River Basin, variations in groundwater flow caused by changes in surface water demand or recharge patterns have a considerable impact on water availability and local ecosystems (Scibek et al., 2007). Seasonal fluctuation in Ethiopia's Central Rift Valley's Meki River Sub-basin has an impact on both groundwater and surface water supplies, making sustainable water usage difficult (Yohannes et al., 2019). A study of the Lake Tana Basin underlined the importance of understanding the spatiotemporal interactions between GW and SW, which can provide useful insights into flow dynamics and resource management (Tigabu et al., 2020). Broader studies across the Nile River Basin highlight the importance of hydrological linkages in water resource planning, especially in light of climatic variability and land use changes (Abate et al., 2015, Gebrehiwot et al., 2019).

In Ethiopia's Central Rift Valley, integrated water availability modeling has proven to be an effective tool for assessing sustainable agricultural intensification options. Such simulation emphasizes the importance of balancing water resource distribution to improve agricultural resilience and sustainability in semi-arid environments (Taye et al., 2022; Legesse et al., 2017). By combining findings from the Meki catchment with broader regional studies, it is clear that effective water resource management necessitates a thorough understanding of groundwater-surface water dynamics in order to address the challenges posed by seasonal variability and competing demands on water resources.

2.2. Overview of Groundwater and surface water interactions

Groundwater (GW) and surface water (SW) are inextricably intertwined in the hydrologic cycle (Sophocleous, 2002). He also says that technologies for measuring groundwater recharge across several spatial and temporal dimensions exist. In recent years, research on the interplay of groundwater and surface water has gained prominence as a critical method to attaining sustainable management of these interrelated water resources (Fleckenstein et al., 2010). According to (Wake, 2008), surface water bodies can either acquire water and solutes from groundwater systems or serve as a source of groundwater recharge, altering groundwater quality in the process.

According to numerous studies, the interaction between groundwater and surface water involves discharge and recharge processes that occur across the soil-water interface (Hatch et al., 2006; Sophocleous, 2002; Scibek et al., 2007). Effective water resource management requires a detailed grasp of the hydrological cycle's components and their interactions. According to (Guzmán et al., 2016), watershed morphology has a substantial impact on groundwater and surface water interactions, which are determined by the hydraulic link.

2.3. Method of quantifying GW& SW availability

Many experts believe that numerous methodologies have been employed to quantify groundwater and surface water interaction across the world, but owing to heterogeneities and the difficulty of combining observations at multiple scales, measuring their interaction remains a challenge (Sophocleous, 2002). The fact that surface water models have daily time steps whereas groundwater models have monthly time steps is a major challenge in combining groundwater and surface water processes (Lamontagne et al., 2014). As a result of this difficulty, a variety of novel modeling tools and methodologies have been created to address it (JOLL & RASSAM, 2009; Lamontagne et al., 2014).

The number of models that consider both GW and SW is continuously increasing. As a result, considerations must be made throughout the selection process to ensure that the model meets the study's objectives, such as data availability, ease of use, simulation accuracy, and budget. Many published basin-scale investigations, including those accessible, have used coupled GW-SW methodologies. Currently, many published basin-scale investigations use four coupled

groundwater and surface water models. Hydro Geosphere (Sudicky et al., 2008), MIKE SHE (Abbott et al., 1986), GSFLOW (Markstorm et al., 2008), and SWAT MODFLOW (Markstorm et al., 2008) are among them are SWAT MODFLOW (Markstorm et al., 2008) and Kim et al. (2008; 2015; Soiphocleous et al., 1999; Bailey et al., 2016). The first two models are appropriate for more advanced simulations. They are totally distributed and grid-based, but they require high-resolution data and a high-capacity computer. The remaining two are semi-distributed and include the most critical physical processes for accurately simulating large-scale basins over extended time periods (Chunn et al., 2019).

2.4. Selection of appropriate model

One of the most important aspects in the modeling process is selecting the appropriate conceptual model for the problem. The most essential data needed in the conceptualization phase include the hydro-stratigraphic unit, surface water bodies, physical and hydraulic constraints, and recharge and discharge zone (Anderson and Woesser, 1992).

The most well-known SW-GW technology is HydroGeoSphere (HGS), which is a three-dimensional finite-element numerical model with an unstructured grid developed by Aquanty (Sudicky et al., 2008). HGS began by modeling variably saturated GW flow with the FRAC3DVS algorithm created by (Therrien, 1992) with other modules such as surface water flow added on over time. HGS has an advantage over most other integrated products on the market today in that it considers both GW and SW flow from the start of each project. This eliminates the need to pair two independent codes in the past, which improves the overall representation of a user's conceptual model. It includes natural physical processes like snowfall and evapotranspiration, as well as the capacity to mimic geologic media with cracks and macro-pores, similar to other integrated models.

HGS is the most powerful fully integrated SW-GW tool accessible among the modules now available, and it can be used to a broad range of scales, from site-specific projects to river basin-wide studies (Aquanty, 2018).

This power, however, comes at a cost, both literally and in terms of computing load. HGS can significantly delay single-core machines, necessitating the use of a powerful system to complete model runs (Brunner and Simmons, 2012.). Furthermore, the incredible level of detail that HGS

is capable of necessitates a large amount of data in order for the model to retain its dominance over alternative options. Simulations can take a long time, which prevents calibration and parameter estimates to the same extent as in other models.

MIKE SHE is used for fully coupled and integrated surface water and groundwater modeling, as well as analysis, planning, and management of a wide range of water resources and environmental problems related to surface water and groundwater, such as surface-water impact from groundwater withdrawal and conjunctive groundwater and surface water use (Abbott et al., 1986).

GSFLOW is an integrated SW-GW model that simulates connected hydrological flow, akin to SWAT-MODFLOW. For GW flow, MODFLOW is used, and for SW flow, the USGS's PRMS (Precipitation-Runoff Modeling System) (Leavesley et al., 1983). MODFLOW, as opposed to SWAT-MODFLOW, is the component model that is primarily responsible for simulating water systems like rivers and lakes. PRMS, like SWAT, works with SW flow and climate data and performs numerical computations using the Hydrological Response Unit (HRU) technique.

As a result, multiple HRUs are defined for a single watershed in order to accurately describe the area's hydrology (Markstrom et al., 2008). Unlike SWAT-MODFLOW, however, GSFLOW's coding allows simulations to be conducted in three different ways: coupled PRMS-only, MODFLOW-only, or MODFLOW only, allowing for greater model calibration flexibility. In the same way that SWAT's PRMS component is discretized by HRU, GSFLOW's PRMS component has similar constraints (Markstrom et al., 2008). As dominant properties for soil, land use, and other factors are scaled up to represent a larger area (Bailey et al., 2016), this results in a more homogeneous representation of the real world than is normally desirable, potentially limiting its use for detailed analysis of local processes in smaller-scale study areas. However, because MODFLOW is the major manager of flow in aquatic bodies, several extra problems may develop.

In recent decades, various conjunctive simulations of surface and groundwater have been performed using SWAT and MODFLOW (Putthividya et al., 2017; Kim et al., 2008; Guzman et al., 2015; Dowlatabadi et al., 2015). There were numerous strategies used in those experiments to integrate SWAT and MODFLOW, but the most viable method was to use recharge rates

between HRUs in SWAT and cells in MODFLOW. These studies were successful in evaluating water availability in many parts of the world, and they provided essential data to assist water management policies.

In this study, SWAT and MODFLOW were configured to run independently and then integrated via recharge rates. These recharge rates were first estimated using the SWAT model and then reported as groundwater recharge values at the HRU level. In the integration phase, the HRU's recharge rate should be exchanged with cells and used as MODFLOW input data. SWAT's semi-distributed properties make it impossible to pinpoint the spatial location of each HRU in subbasins. To reflect HRU locations, one HRU is developed for each sub-basin based on dominant land use, soil, and slope options (Dowlatabadi et al., 2015; Molla et al., 2023).

2.4.1. Hydrological modeling for water resources assessment

Hydrological modeling is essential for assessing water resources because it simulates the movement and availability of water in river basins. Several modeling techniques have been developed to estimate streamflow, water balance components, and groundwater dynamics. Among these approaches, the Soil and Water Assessment Tool (SWAT) has gained prominence due to its ability to mimic hydrological processes in complicated watersheds (Arnold et al., 1998).

SWAT is a semi-distributed, continuous-time, physical-based model that operates on a daily time scale (Arnold et al., 1998, 2012). Within basins, the model is primarily used to evaluate the impact of land management strategies on water resources and non-point-source pollution. The model's core simulation items include water, sediments, nutrients, and pesticides (Menking et al., 2004; Narula and Gosain, 2013). Climate, hydrology, soil temperature and properties, plant development, nutrients, pesticides, land management, water routing, bacteria, and diseases are all critical model components (Kim et al., 2008).

In the SWAT model framework, a watershed is usually divided into multiple sub-basins, each of which is further divided into Hydrologic Response Units (HRUs) (Chung et al., 2010; Aliyari et al., 2019). SWAT's simulation unit is the HRU, which is defined by similar soil types, land use, and slope characteristics (Arnold et al., 1998, 2012; Guzman et al., 2015).

Despite having its own GW module, SWAT is a lumped model (Arnold et al., 1998, 2012; Kim et al., 2008) that does not detail the spatial distribution of aquifer characteristics (e.g., hydraulic conductivity, porosity, specific yield, and specific storage) (Kim et al., 2008; Wei et al., 2019).

Furthermore, SWAT cannot model SW-GW interactions (such as runoff recharge and GW discharge) or the GW level. According to Liu et al. (2020c), two techniques for improving SWAT's performance in modeling GW are to modify the GW module code and connect SWAT to a GW model. Changing SWAT module codes in various studies had a good result in recreating GW flow (Pfannerstill et al., 2013; Nguyan and Dietrich, 2018). However, the new GW code improves only a subset of aquifer system modeling (Pfannerstill et al., 2013; Nguyan and Dietrich, 2018), and the professional skills required to implement the change limit the adoption of this technique.

As a result, the latter coupling technique is usually used, and MODFLOW has advanced faster and is more widely used than the other GW models (Chung et al., 2015; Gao et al., 2019; Izady et al., 2015; Kim et al., 2017). SWAT uses meteorological, topography, land use, and soil data to simulate water balance and flow in river basins. It has been widely used to measure surface water availability, evaluate the effects of land use changes on water resources, and support decision-making processes in a variety of places around the world.

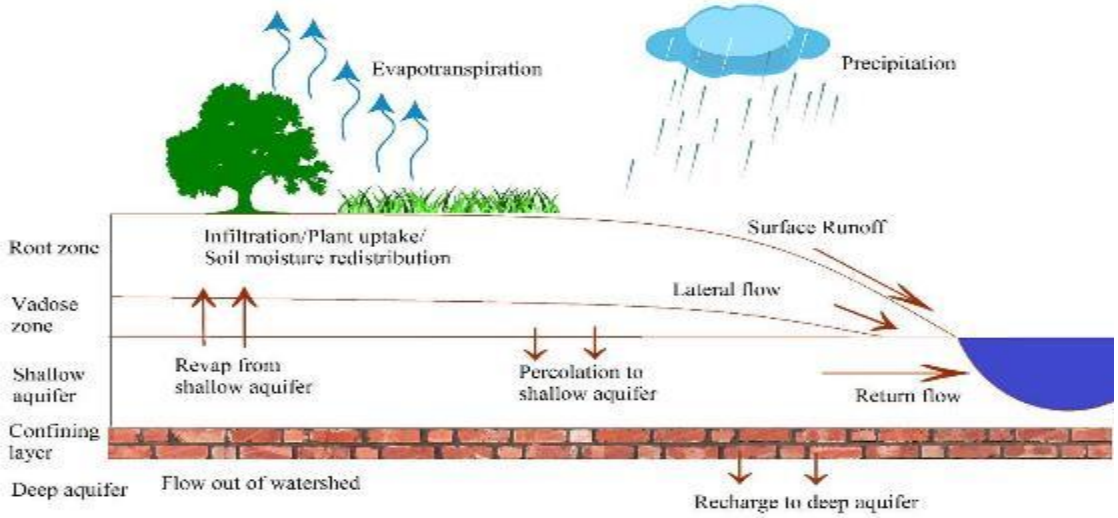

Figure 2.1. Overview of the SWAT model (edited from Neitsch et al,.2012)

2.4.2. Groundwater modeling and assessment

In addition to surface water, groundwater resources play a vital role in sustaining water supplies and meeting various water demands. Groundwater modeling is essential for understanding the dynamics and availability of groundwater systems. One commonly used groundwater modeling tool is the MODFLOW model, which simulates groundwater flow and solute transport in three-dimensional aquifer systems (McDonald and Harbaugh, 1988). The US Geological Survey proposed MODFLOW (McDonald and Harbaugh, 1988), a modular three-dimensional finite difference GW flow model.

The model employs the finite difference approach to solve the GW flow differential equations (Guzman et al., 2015). MODFLOW is a physically based model of subsurface flow that incorporates Darcy's law and mass balance (Kim et al., 2008). The model is designed to replicate a variety of natural or intentionally induced hydrologic processes for different types of aquifers in both steady and transient states (McDonald and Harbaugh, 1988; Kasahara and Wondzell, 2003; Ke, 2014). The model employs the finite difference approach to solve the GW flow differential equations (Guzman et al., 2015). MODFLOW is a physically based model of subsurface flow that incorporates Darcy's law and mass balance (Kim et al., 2008). The model is designed to replicate a variety of natural or intentionally induced hydrologic processes for different types of aquifers in both steady and transient states (McDonald and Harbaugh, 1988; Kasahara and Wondzell, 2003; Ke, 2014).

Generally, MODFLOW has been effectively used in a variety of studies to analyze groundwater recharge, simulate aquifer responses to pumping, and assess the effects of land use changes on groundwater resources. By combining SWAT and MODFLOW models, it is feasible to capture the interactions and feedbacks between surface and groundwater systems, resulting in a comprehensive understanding of a river basin's water resources.

2.5. Application of SWAT and MODFLOW model

The combination of SWAT and MODFLOW models provides a useful tool for estimating both surface and groundwater resources in river basins. This linked modeling approach allows for the assessment of water balance components, streamflow dynamics, irrigation water demand, and

groundwater storage fluctuations. Several studies have used the SWAT and MODFLOW models to estimate water resources in different regions, indicating their usefulness in capturing the intricacies of hydrological processes and connections between surface and groundwater systems (Dowlatabadi et al., 2015; Molla et al., 2023).

2.6. Previous Research on Study area

Numerous studies have been conducted in Ethiopia's Rift Valley Lakes Basin to assess and manage water resources. These research investigated the region's hydrological characteristics, identified water availability and demand patterns, and evaluated the effects of climate change and human activities on water resources (Moges et al., 2015; Bewket and Conway, 2007). Abate H. (2007) conducted modeling studies in the Meki River catchment to investigate the impact of land use change and climate variability on watershed runoff. (Gashew, 1998) examined the hydrogeology and hydrology of Lake Ziway and its surroundings.

The water resources of the Ziway-Langano-Abijata-Shalla Basin were analyzed by Consultant (1970). The primary purpose of the research was to redirect the Meki River into the Awash River in order to extend irrigation in the Amibara area. In their project study of Meki irrigation and rural development, (JICA and OIDA, 2001) placed a heavy emphasis on assessing the basin's water resource potential. As a result, hydrological analysis and lake water balance were incorporated in the research, and Temesgen A. (2008) created a physically based distributed hydrological model to estimate major components of the Meki river basin's hydrologic cycle. In 1975, the Ministry of Overseas Development's Land Resources Division undertook a thorough assessment of the Ziway basin, focusing particularly on Lake Ziway and the Meki River, and offered alternative

Dagnachew Legesse's Ph.D. thesis from 2002 examined the Ziway-Shalla basin's hydrological response to climate and human activity changes. In 1972, Di Pola released a geological map and synopsis of the geology, stratigraphy, structural patterns, and geological map of the main Ethiopian rift from 7000 to 80 40N latitudes, at a scale of 1:60,000. In 1982, Tesfaye Chernet published a regional geology and hydrogeological map of the Ziway-Shalla basin, which included a regional permeability group classification.

In his article "rift valley lakes integrated natural resource development master plan," Halcrow (1989) investigated the area's groundwater and surface water possibilities. Ayenew investigated the overall hydrology and hydrogeology of the Ziway-Shalla basin in his Ph.D. thesis in 1998. The study examined the interaction of groundwater and surface water, as well as water balance and sub-catchment recharge calculations. (Ayenew, 2001) performed numerical groundwater flow modeling of the central main Ethiopian rift lake basin in 2001, evapotranspiration estimation using thematic mapper spectral satellite data in the Ethiopian rift and adjacent highlands in 2003, and Alemu Dribssa's MSc thesis in 2006 examined groundwater-surface water interaction and recent changes in the hydrologic environment of the Lake Ziway catchment.

(Birhanu, 2011) also investigated numerical groundwater flow and used MODFLOW to measure recharge (within the catchment borders) and groundwater flow. The Meki River Basin hydrological system was analyzed and ground water recharge was estimated using a semi-distributed model, and river discharge was estimated using a two-dimensional aerial view using MODFLOW (Ayenew, 2008). (Ayenew T. , 2001a).

However, few studies have used the SWAT-MODFLOW model to fully estimate surface and groundwater availability in the basin. Therefore, this research aims to fill this gap in the literature by applying the SWAT-MODFLOW model to the Meki River basin, which is a sub-basin within the Rift Valley Lakes Basin. (Yifru et al., 2021) study about Assessing the Effect of LULC and Climate Change on Water Yield and Groundwater Recharge and used SWAT-MODFLOW model.

All previous research examined the basin's hydrology, hydrogeology, climate, land use, and numerical groundwater flow modeling, but surface water and groundwater were regarded as separate entities. Groundwater and surface water, on the other hand, are not distinct components of the hydrological cycle, as stated by Winter (1999), and interact in a number of ways across the terrain. Groundwater-surface water interactions are complex processes that occur at multiple geographical and temporal scales. As a result, our work bridged the gap by simulating the

measurement of surface water and groundwater availability with the SWAT and MODFLOW models, which had never been done before.

2.7. Summary and Research Gap

In summary, the literature review highlights the significance of quantifying surface water and groundwater availability in river basins for effective water resources management. The integration of SWAT and MODFLOW models offers a comprehensive approach to assess water balance components, streamflow variations, irrigation water demand, and groundwater dynamics. While previous studies have applied these models individually, there is a research gap in utilizing the SWAT-MODFLOW model for water resources assessment in the Meki River basin within the Central Rift Valley Lakes Basin in Ethiopia. This research aims to address this gap by quantifying the surface water and groundwater availability in the Meki River basin using the SWAT and MODFLOW model, thereby contributing to the knowledge base and supporting sustainable water management practices in the region.

2.8. Model performance and uncertainty evaluation

From the available data, one or two years were utilized for warm-up, 2/3 for calibration, and 1/3 for validation. The SWAT Model was calibrated using SWAT-CUP's Sequential Uncertainty Fitting _version 2 (SUFI-2) interface. SWAT-CUP is a distinct calibration and uncertainty program created by Abbaspour et al. (2004). SUFI-2 is a widely used approach for calibration and uncertainty analysis. (Setegn et al., 2008) and (Yang et al., 2008) analyzed several processes and discovered that SUFI-2 is superior since it produces good results even with the fewest number of runs.

Model performance was evaluated using both graphical and statistical techniques. Moriasi et al. (2007) proposed one dimensionless metric and two error indices among numerous statistical model evaluation methods. In this work, dimensionless Nash-Sutcliffe efficiency (NS) (Nash & Sutcliffe, 1970) and coefficient of determination (R^2) were utilized. The Nash-Sutcliffe efficiency (NS) is a measure of the normalized magnitude of residual variance in comparison to observed flow variation. The NS value runs from $-\infty$ to 1, with 1 representing a perfect match to the 1:1 line, and NS values less than zero reflecting poor model performance. Table 1 shows the

mathematical representations of various strategies, as well as the SWAT model's recommended performance ranges.

Table 2. 1: Model performance rating for stream flow at the daily time scale.

	Equations	
Performance rate	$\text{NSE}=1-\frac{\sum_{i=1}^{N}\left(Q_{si}-Q_{oi}\right)^2}{\Sigma\left(Q_o-\overline{Q_o}\right)^2}$	$R^2 = \frac{\sum_{i=1}^{n}(Q_{si}-\overline{Q_s})(Q_{oi}-\overline{Q_o})^2}{\sum_{i=1}^{n}(Q_{si}-Q_s)^2\sum_{i=1}^{n}(Q_{oi}-\overline{Q_o})^2}$
V. good	$0.75 < \text{NSE} \leq 1.00$	$0.75 < R^2 \leq 1.00$
Good	$0.65 < \text{NSE} \leq 0.75$	$0.65 < R^2 \leq 0.75$
Satisfactory	$0.50 < \text{NSE} \leq 0.65$	$0.50 < R^2 \leq 0.65$
Unsatisfactory	$\text{NSE} \leq 0.50$	$R^2 \leq 0.50$

Source: Moriasi et al. (2007) NS represents Nash-Sutcliffe efficiency. Qobs and Qsim represent measured and simulated flows, respectively, while R2 is the coefficient of determination. The coefficient of determination (R2) was used to assess the strength of correlation among model variables, as well as the mean differences between water balance components at different station densities. The coefficient of determination is the square of the correlation between observed and simulated values, which indicates how much of the measured value variance is explained by the simulation (Krause et al., 2005). It ranges from 0 to 1. The number 1 shows that the simulation's variance is equal to that of the observed time.

3. MATERIALS AND METHODS

3.1. Description of study area

3.1.1. Location of study area

The Meki River sub-basin is part of central Ethiopia's Rift Valley Lakes Basin (RVLB). It has an approximate area of 2,242.042 km². Geographically, the Meki River Subbasin is limited by 38.1667°E to 38.8333°E and 7.8333°N to 8.3333°N. It stretches from the western escarpments of the Ethiopian Rift Valley to the center rift valley level. The river travels eastward and empties into Lake Ziway, a vital freshwater source for the region. The Meki River flows from the Gurage and Woliso highlands and is an important hydrological unit that supports the local ecosystem and human populations (Awulachew et al., 2007).

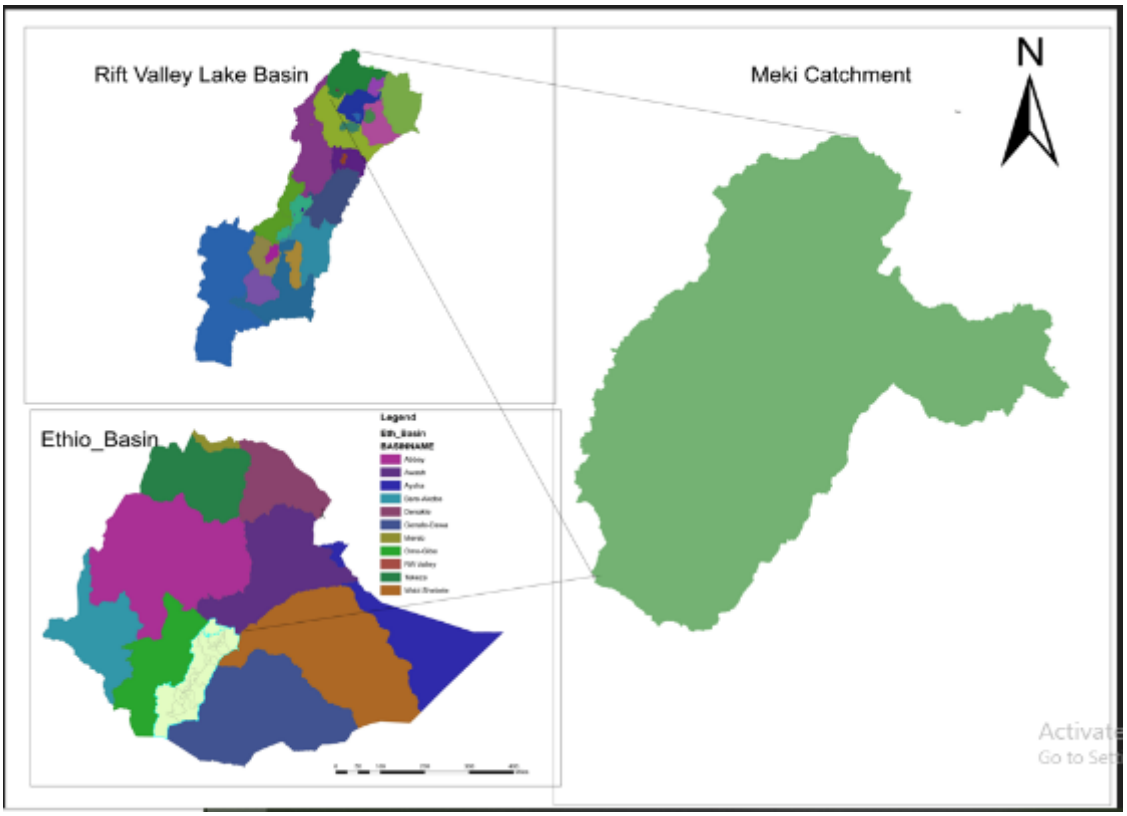

Figure 3.1 Map of study area

3.1.2. Topography of study area

The Meki River sub-basin's terrain features tremendous elevation fluctuations, which have a substantial impact on hydrological processes such as runoff and groundwater recharge. The area can be divided into three physiographic areas: the high plateau on the western summit of the area with elevation range of (2295 – 3611m), the transitional escarpment (1856 – 2294m) and the rift floor (1636 – 1855m) (Abate, 2007). The region's topography transitions from steep slopes in the highlands to flat plains as it moves toward the central basin. This gradient shapes the hydrology of the area, including infiltration rates and overland flow patterns.

The landscape in the Meki River Subbasin ranges from the severely fragmented plains at the foot of the rift to the western Gurage Highlands, which are 1642 to 3611 meters above sea level (Figure 3.2). The upper basin is rocky and steep, as opposed to the lower basin's flat topography and large valley. The Meki River flows from the western highlands and escarpments, including a large marshy part, for approximately 100 kilometers before draining into Lake Ziway. In contrast to escarpments and flat rift floor zones, highland lands have increased drainage density.

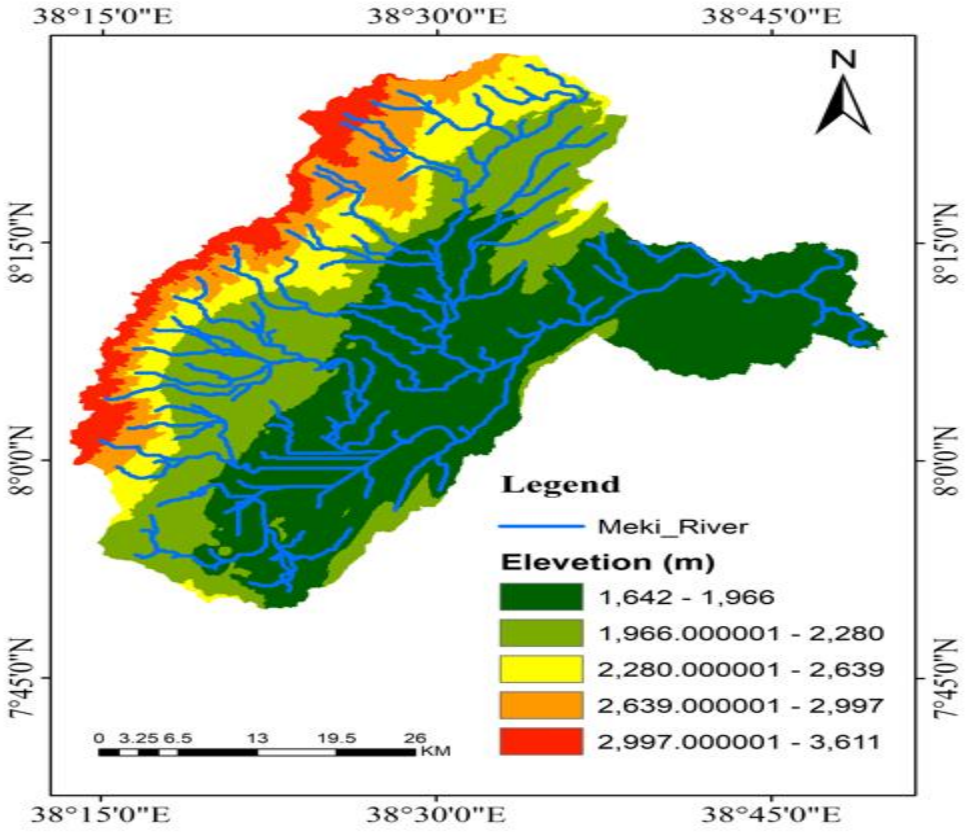

Figure 3.2. Elevation of the study area

3.1.3. Climate of study area

The Meki River sub-basin has a semi-arid to sub-humid climate, influenced by altitudinal variance and seasonal rainfall patterns. The climatic conditions of the area are described here. The average values of the climatic parameters are described in the table below, whereas Figure 3.3 depicts the mean monthly variation of the climatic parameters.

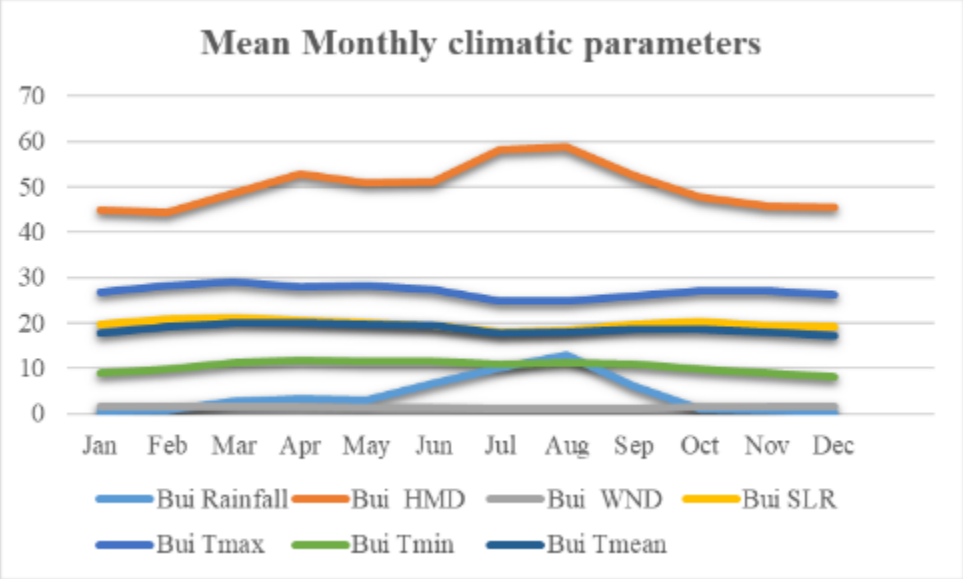

Figure 3.3 Mean monthly climate of the study area (2000_2020)

3.1.3.1. Rainfall

The subbasin's principal water source is rainfall. Precipitation data is included in the 21-year global weather dataset from 2000 to 2020. The findings show that the mean annual precipitation has a bimodal distribution, with the majority of rainfall occurring during the south-east monsoon season from March to May and a few rainfalls recorded from mid-September to November, despite the fact that the overall amount of monsoon is quite small. The SWAT study found that the average annual precipitation is 1252.724 mm.

Table 3.1 Mean annual rainfall

Station	UTM-E(m)	UTM-N (m)	Mean Annual Rainfall(mm)
Bui	450940	920899.9	1457.45
Buta Jira	431236.7	897893.4	1697.93
Ejersa	448360.3	885524.9	1278.78
Koshe	465614.5	911918.6	1134.3
Meki	479841	900995.8	1037.52
Sutan	457836	928981.7	814.66
Tora	436459.8	868772.3	1348.43

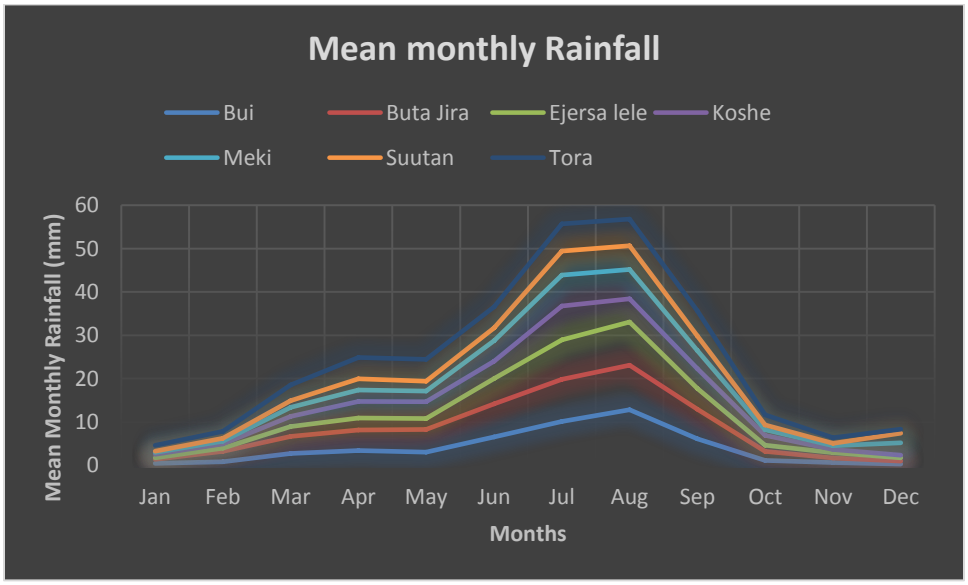

Figure 3. 4 Mean monthly rainfall

3.1.3.2. Temperature

The temperature of both the air and the surface plays an important influence in the process. As the temperature rises, the air can hold more moisture, but there is a limit to how much moisture it can keep at any given temperature. The research area's average yearly temperature ranges from 10.4 to 26.9 degrees Celsius.

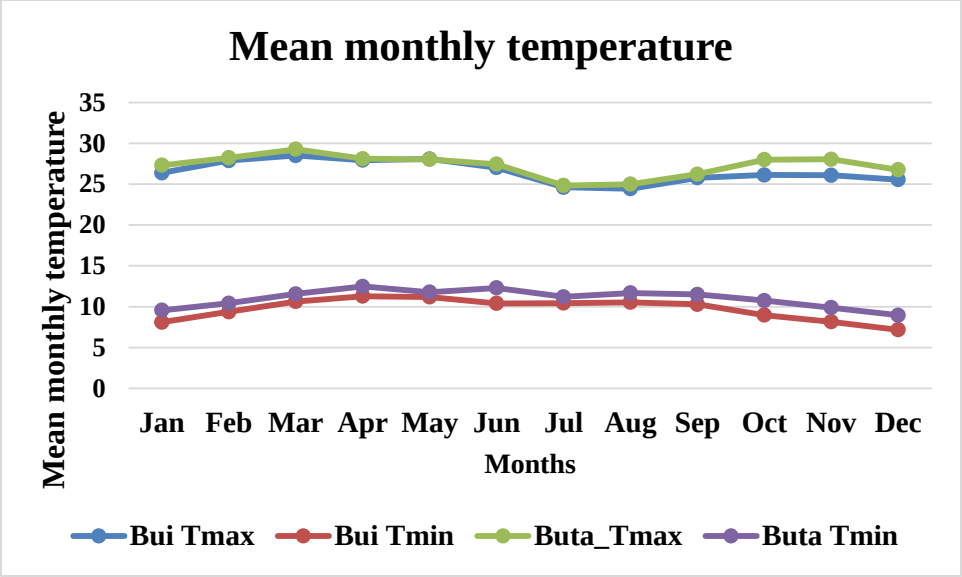

Figure 3.5 Mean monthly temperature

3.1.3.3. Relative Humidity

Relative humidity is the difference between the amount of moisture in the air and the amount required to saturate it at the same temperature. Higher relative humidity figures indicate that the air is approaching saturation, whilst lower values indicate that there is less water vapor in the atmosphere. It indirectly affects evaporation rate. When the relative humidity reaches 100%, evaporation ends.

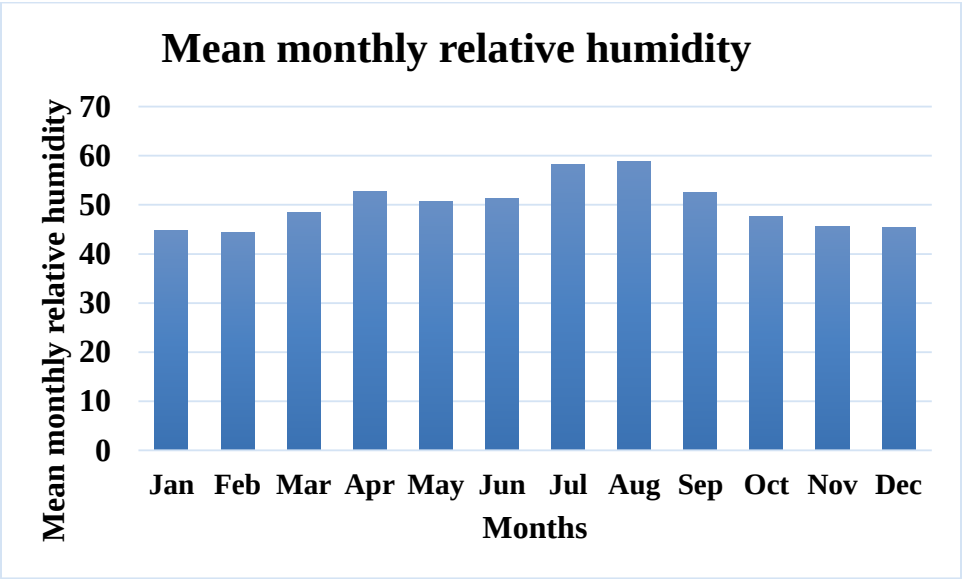

Figure 3.6 Mean monthly relative humidity

3.1.3.4. Sunshine Hours

Evaporation happens practically constantly during the day and night, while it is almost always active when exposed to direct sunlight.

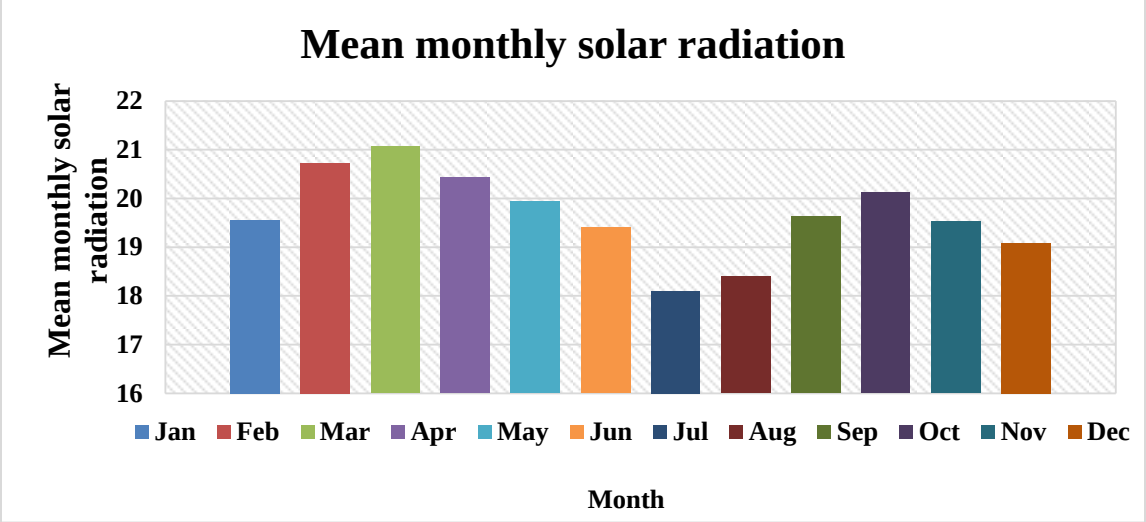

Figure 3.7 Mean monthly solar radiation

3.1.3.5. Wind speed

Wind speed, another important weather component for the SWAT model's input, was collected from meteorological stations in the same way that other variables were. The air above the evaporating surface becomes increasingly saturated as evaporation continues, and when it can no longer absorb any more, evaporation ceases. Evaporation would continue if dry air replaced wet air quickly. As a result, there is a linear relationship between air and moisture distribution, wind speed, and turbulence. Wind speed has a substantial influence on the rate of evaporation, which is collected and formatted in text format for the SWAT input data.

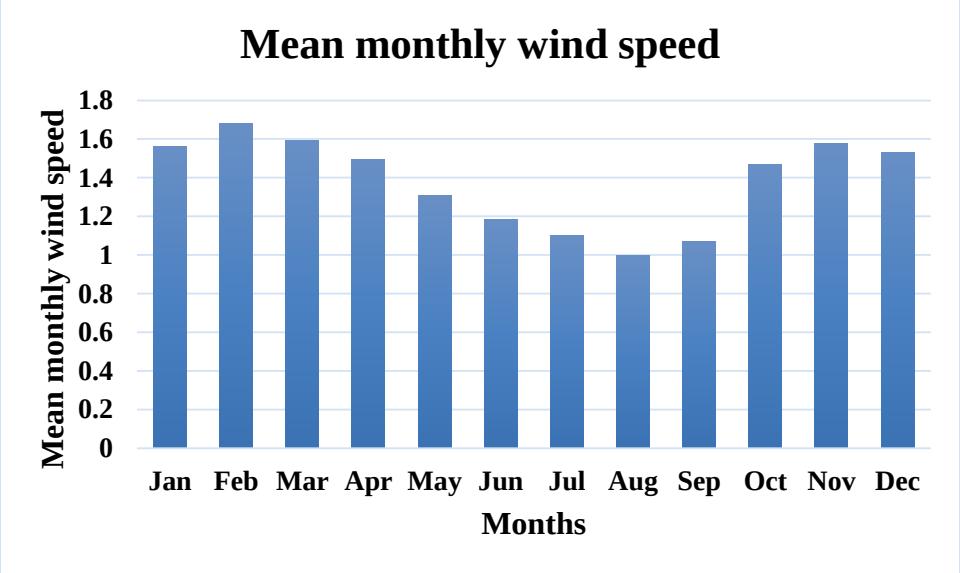

Figure 3.8 Mean monthly wind speed

3.1.4. Land use/ Land cover

Land use is an important factor in hydrological and groundwater research since it influences recharge rates significantly. The primary land uses and covers in Meki include forest, grassland, cropland, marshes, moderately cultivated, shrubland, and water bodies. Topography, climate, and biology all have an impact on the catchment's land cover. The land cover of the rift valley basin has altered considerably in recent years as the population has grown.

3.1.5. Soil Map Data

The SWAT model specifies soil texture, accessible water content, hydraulic conductivity, bulk density, and organic carbon content for each soil type. Soil in the studied area is strongly correlated with parent material and degree of weathering (Makin et al, 1976). The primary parent materials include basalt, ignimbrite, acidic lava, volcanic ash and pumice, and riverine and lacustrine alluvium (Paola 1972). In general, the research area's dominant soil types include Chromic Cambisol, Eutric Cambisol, Eutric Vertisol, Haplic Luvisol, Leptosol, and Vitric Andosol.

3.1.6. Geology

The geologic profile includes Quaternary sedimentary layers, volcanic products, and Mesozoic-era deep sedimentary North American rocks. Quaternary sediments, which include lake, river,

fan, and talus layers, range in size from clay to gravel and contain some pyroclastic material such as pumice and ash. These deposits, which can be more than 200 meters thick, are the main aquifers here. The Ziway plain, Kuntane-Inseno-Kela plain, and the Crescent of Butajira, a little piece of gravel and sand, are all major aquifer areas (Mitiku, 2011b).

Precambrian metamorphic rocks such as Biotitic gneiss can be found on the north side of the research area, as well as east of the Guraghe Mountains. These rocks are coated in Adigrat sandstone and pegmatite veins, although they are not suitable for groundwater storage (Dipola, 1972; Mitiku, 2011b). Volcanic formations are primarily composed of Quaternary pyroclastic deposits, but also include Tertiary rhyolites and basalts on escarpments and beneath Quaternary layers. As volcanic rocks age, they can serve as excellent water reservoirs in rocky terrain, particularly in fracture zones (Ayenew, 2008b; Mitiku, 2011b).

Limestone and sandstone are Mesozoic sedimentary strata found over 1,000 meters below earth beneath Tertiary igneous rocks. Even though these sediments are prospective aquifers, their depth limits their exploitability, as seen in the Kela Village context; thus, they are not the ideal option for groundwater extraction (Mitiku, 2011b). The geological architecture reveals that Quaternary deposits and volcanic formations are the primary sources of groundwater in the area.

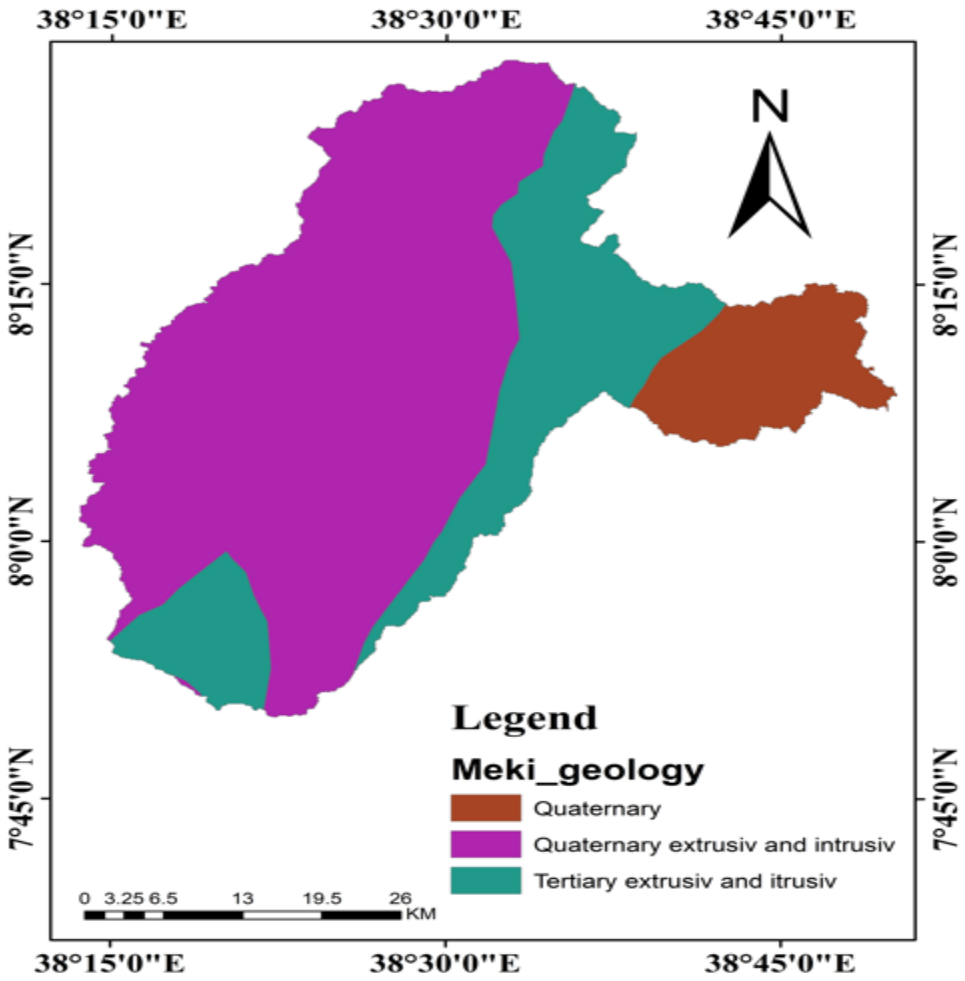

Figure 3.9 Geology of meki river catchment

3.2. Data collection methods

Historical meteorological data from meteorological stations (rainfall, temperature, evaporation, etc.) and historical flow data of rivers in the research area were obtained from the National Meteorological Statistical Agency and the Ministry of Water and Irrigation, respectively. Data on river discharges were also required for model calibration and validation. The Hydrology Department of the Ministry of Water, Irrigation, and Energy (MoWIE) in Ethiopia collected daily data from the Meki River gauging station. MoWIE, the Oromia Water Work Construction Enterprise office, and the Meki town water supply office all provided data on well/pump tests, land use, and soil conditions. Groundwater levels and borehole elevations were measured in the field. Catchments were delineated using a high-resolution Digital Elevation Model (DEM) from

the Shuttle Radar Topography Mission (SRTM-version 4; HTTP://srtm.csi.cgiar.org/). Geological and topographic sheet data were obtained from the Ministry of Water, Irrigation, and Electricity.

3.3 Model inputs

3.3.1 SWAT model inputs

Groundwater levels and borehole heights were measured on the field. Catchments were identified using a high-resolution Digital Elevation Model (DEM) from the Shuttle Radar Topography Mission (SRTM-version 4; http://srtm.csi.cgiar.org/). Geological and topographic sheet data were gathered from the Ministry of Water, Irrigation, and Power.

3.3.2. Digital Elevation Model (DEM)

SWAT model required a spatial data set consisting of digital representations of topographic surfaces. DEM serves as the foundation for delineating watershed boundaries, stream networks, and sub-basins. Digital elevation model defines the elevation of any point in a study region at a given spatial resolution. It is also used to study the drainage patterns of the land surface terrain and calculate subbasin parameters such as slope gradient and slope length, as well as stream network characteristics such as channel slope, length, and width. In this study, a DEM with a resolution of 30 m x 30 m was employed, obtained from the USGS.

3.3.3. Land Use/land covers data

Land use/cover statistics for the study region were received from the Ethiopian Ministry of Water, Irrigation, and Electricity (MoWIE, 1999). SWAT uses predefined land use types denoted by four-letter codes to connect land use maps to its database using GIS interfaces. To ensure conformity with the model's input needs, a lookup table was created that aligned the land use types with SWAT's standards.

3.3.4. Soil data

The Ethiopian Ministry of Water, Irrigation, and Electricity (MoWIE, 1999) provided soil data for the research region. The SWAT model necessitates a variety of soil textural and physicochemical parameters, such as soil texture, accessible water content, hydraulic conductivity, bulk density, and organic carbon content across soil layers. These attributes were gathered from a variety of sources, including the Africa CD-ROM (FAO, 1998), the Harmonized

World Soil Database Viewer V1.2 (HWSD), and Ethiopia's GIS-based hydrological zones and soil geodatabases.

3.3.5. Climate data or meteorological data

In order to calculate the reference evapotranspiration, SWAT model was used monthly maximum and minimum temperature, relative humidity, sunshine hour, and wind speed data that would be collect from Meki station and National meteorological agency.

3.3.6. MODFLOW model inputs

In order to achieve satisfactory outputs from MODFLOW model it is necessary to specify the required parameters or datasets like well data, borehole elevation, ground water level, DEM and base map.

3.3.7. Hydrogeological data

Hydrogeological data from boreholes were gathered from various government, non-governmental, and private drilling contractors, as well as water point inventories. The goal of gathering this borehole data was to determine input parameters for the MODFLOW model, such as hydraulic conductivity (K), aquifer thickness, specific storage, specific yield, hydraulic conductivity of riverbed material, and initial hydraulic head.

3.4. SWAT model development and input data

This study used the SWAT2012 version (Neitsch et al., 2011) running under ArcSWAT2012 in the ArcGIS10.3 interface. The Meki sub-basin was divided into sub-catchments, and a refined or developed stream network layer was created based on a threshold, which represents the minimum drainage area required to start a stream. These sub-watershed and stream network layers were created using a digital elevation model (DEM), with the smallest unit of spatial discretization resulting from a unique combination of land-use, slope, and soil layer overlays.

This spatial unit is expected to behave similarly to hydrological inputs in SWAT. SWAT models the hydrologic cycle by applying the water balance equation 3.1:

$$SW_T = SW_0 + \sum_{I=0}^{t}(R_t - Q_{surf} - E_a - W_{seep} - Q_{gw} - - - -3.1$$

Where SWt is the final water content (mm), SW0 is the initial water content in time i (mm), t is the time (in days, months, or years), Rt is the amount of rainfall in time i (mm), Qsurf is the amount of surface runoff in time i (mm), Ea is the amount of evapotranspiration in time i (mm), Wseep is the amount of water entering the vadose zone from the soil profile in time i (mm), and Qgw is the amount of return or base flow in time i (mm). SWAT can simulate at daily, monthly, and annual scales, therefore the time scales vary depending on the analysis. Each term in the water balance equation contains complex physical processes that are linked in a harmony with the atmosphere-vegetation-soil consortium. The SWAT input/output, theoretical documentations, and literature provide extensive information on these processes and physical occurrences. The key terms in water balance equation 3.1 are discussed below.

Surface runoff, also known as overland flow, is the excess rainfall from infiltration that flows along slopes. SWAT calculates surface runoff using the Soil Conservations Service's curve number (CN) approach. Equation 3.2 (SCS, 1972) expresses surface runoff as.

$$Q_{surf} = \frac{(R_{day} - I_a)^2}{R_{day} - I_a + S} \text{ and } I_a = 0.2 * S \quad \text{---------- 3.2}$$

Where S is soil storage or retention, Rday is daily precipitation, and Ia is the initial surface abstraction, which comprises surface storage, interception, and infiltration to the moist soil surface up to runoff generation, all in millimeters of water. Soil storage or retention volume is denoted by the curve number CN.

$$S = 25.4\left(\frac{1000}{CN} - 10\right) \quad \text{---------- 3.3}$$

By substituting Ia and S in equation 3.4.4, surface runoff is expressed as:

$$Q_{surf} = \frac{(R_{day} - 0.2S)^2}{R_{day} + 0.8S} \quad \text{---------- 3.4}$$

Surface runoff occurs when rainfall surpasses the initial abstraction and infiltration into the soil's root zone. For a reason, CN is determined by land use, soil, and antecedent soil moisture content. The SWAT manual and user guide contain information on functional relationships and

CN values (Neitsch et al., 2011). Evapotranspiration: This phrase refers to the conversion of water in a certain watershed into water vapor. It is the interaction of water from the soil/vegetation surface with the atmosphere. Evapotranspiration exceeds runoff at the continental level (Valiantzas, 2006).

The Penman-Monteith (Monteith, 1965; Allen, 1986; Allen et al., 1989) methods are one of SWAT's three methods for calculating PET in this study. The Penman-Monteith technique calculates PET by taking into account solar radiation, maximum and minimum air temperature, relative humidity, and wind speed. The Penman-Monteith approach combines energy, aerodynamic, and surface resistance components to account for water vapor evacuation to the atmosphere, as indicated by equation 3.5:

$$\lambda \mathrm{PET} = \frac{\Delta * (\mathrm{H_{net}} - \mathrm{G}) + \rho_{\mathrm{air}} * \mathrm{C_p}[{\mathrm{e_z}}^0 - \mathrm{e_z}]/\mathrm{r_a}}{\Delta + \gamma * (1 + \mathrm{r_c}/\mathrm{r_a})} \quad ---------- 3.5$$

The Penman-Monteith equation calculates potential evapotranspiration (PET) using energy balance and aerodynamic concepts. The model takes into consideration several elements, including net radiation (H), soil heat flux (G), air density (ρ), and the difference between saturation and real vapor pressure (${\mathrm{e_z}}^0 - \mathrm{e_z}$), as well as aerodynamic resistance ($\mathrm{r_a}$). The equation uses the slope of the saturation vapor pressure curve (Δ) and the psychrometric constant (γ) to relate temperature and humidity. Canopy resistance ($\mathrm{r_c}$) accounts for vegetation properties and provides a thorough framework for calculating PET in different climatic circumstances.

Lateral flow describes the subsurface water movement in soils with high hydraulic conductivity. The saturated soil zone is generated when water ponds above a local impermeable soil layer (perched water). This water is at atmospheric or lower pressure. SWAT simulates subsurface flow in a two-dimensional portion of a hillslope using Sloan and Moore's (1984) kinematic storage model. As seen in equation 3.6, the saturated hydraulic conductivity of the soil influences lateral flow.

$$\mathrm{Q_{lat}} = 0.024 \left(\frac{2 * \mathrm{SW_{ly,excess}} * \mathrm{K_{sat}} * \mathrm{slp}}{\emptyset_{\mathrm{d}} * \mathrm{L_{hill}}} \right) \quad ---------- 3.6$$

In this equation, Qlat represents the lateral flow discharged at a hillslope outlet on a given day (mm), SWly represents the excess volume of drainable water stored in a saturated soil layer for a

given day (mm), ϕd represents the drainable porosity of the soil layer (mm/mm), slp represents the slope of the soil layer given by tan(αhill), αhill represents the hillslope segment angle to the horizontal, Ksat represents the saturated hydraulic conductivity of the soil layer (mm h-1), and Lhill represents the hillslope length (m). The drainable volume of water stored in a saturated soil layer for a given day is computed as extra soil water from the field capacity, as shown in equation 3.7.

$$SW_{ly,excess} = SW_{ly} - FC_{ly} \quad \text{if } SW_{ly} > FC_{ly};\ SW_{ly,excess} = 0 \quad ---------- 3.7$$

SWly,excess is the stored portion of drainable water in a saturated soil layer (ly) for a given day (mm), SWly is the soil moisture content of a soil layer on a given day (mm), and FCly is the field capacity soil water content of the given soil layer (mm). Groundwater is water in the saturated zone that has a pressure greater than atmospheric pressure (positive pressure). Water can enter the groundwater system through infiltration, percolation, and/or seepage from water bodies. It is mostly discharged into rivers or bodies of water (return flow or base flow). It can also travel upward to the unsaturated zone before evapotranspiration via the capillary fringe.

Groundwater in SWAT is separated into two aquifer systems. The first is a shallow, unconfined aquifer that provides return flow to streams (also known as groundwater flow or baseflow). The second is a deep, restricted aquifer that does not provide return flow to streams within the watershed. Water percolates deep into the constrained aquifer and is thought to be lost from the given watershed. The time required to recharge the shallow aquifer through the vadose zone by bypass flow or percolation is critical for separating water into surface and groundwater flow. The hydraulic parameters of the geological formation determine this number. SWAT employs an exponential decay weighing function (Sangrey et al., 1984) to calculate the aquifer recharge time delay. Water passing the soil layer and refilling the two aquifers is represented by the following equation.

$$W_{rchrg,i} = \left(1 - \exp\left[-\frac{1}{\delta_{gw}}\right]\right) * w_{seep} + \exp\left[-\frac{1}{\delta_{gw}}\right] * W_{rchrg,i-1} \quad --------3.8$$

Where wrchg,i is the recharge amount entering the aquifers on i day (mm), and δgw is the groundwater delay time or drainage time of the underlying geologic formation (days). Wseep is

the amount of water at the bottom of the soil profile on day i (mm), while wrchrd, i-1 is the recharge amount entering the aquifers on day i-1 (mm).

Part of the recharged water is channeled to the deep aquifer, as shown in equation 3.9.

$$w_{deep} = \beta_{deep} * W_{rchrg} \quad ---------- \quad 3.9$$

In this equation, Wdeep represents the quantity of water moving to the deep aquifer on a given day (mm), βdeep is the aquifer percolation constant, and wrchrg is the recharge amount entering the aquifers (mm). The groundwater delay time (δgw) and aquifer percolation constant (βdeep) are crucial parameters for SWAT parameters GW_DELAY and RCHRG_DP, respectively. Groundwater delay time varies depending on the depth of the water table, the hydraulic qualities of the soil, and the geological structure. It is computed indirectly by simulating aquifer recharge in a given watershed or by optimizing groundwater level simulations using measured values. Once calibrated for a given watershed, the GW_DELAY value can be applied to other watersheds in similar geomorphic locations (Sangrey et al., 1984). GW_DELAY can be used to correct lagging curves by shifting the simulation's hydrograph limbs.

Equation 3.10 uses Hooghoudt's (1940) steady-state groundwater response to a given recharge to estimate baseflow to a specific reach.

$$Q_{gw} = \frac{800 * K_{sat}}{Lgw^2} * h_{wtbl} \quad ---------- \quad (3.10)$$

Where Qgw is the baseflow of the reach on a particular day (mm), Ksat is the saturated hydraulic conductivity of the shallow aquifer (mm day-1), Lgw is the distance from the sub-watershed division to the reach (m), and hwtbl is the water table height (m). Equation 3.11 can be used to simplify groundwater discharge when there is no recharging time.

$$Q_{gw} = Q_{gw,0} * \exp[-\alpha_{gw} * t] \ if \ aqsh > aqshthr, q \ otherwise \ Q_{gw}$$
$$= 0 ---- \ (3.11)$$

Where Qgw,o is the baseflow into the given reach at the beginning of the recession curve (mm), αgw is the baseflow recession constant (vary from 0 to 1) in days, aqsh is amount of water stored in the shallow aquifer on a given day (mm), and aqshthr,q is the threshold water level in the shallow aquifer which groundwater starts to contribute baseflow (mm). αgw and aqshthr,q are important parameters in SWAT parameters ALPHA_BF and GWQMN, respectively.

Baseflow alpha factor in days (ALPHA_BF) is the baseflow recession constant of proportionality between groundwater flow and recharge changes to the aquifer (Smedema and Rycroft, 1983).

ALPHA_BF ranges from 0.1 to 0.3 for watersheds that adapt slowly to groundwater change and from 0.9 to 1.0 for fast-responding watersheds (Sisay, 2013). It can be determined by evaluating the recession curve of a watershed's recorded flow hydrograph during the no-recharge period. Baseflow to a reach occurs when the water table in the shallow aquifer exceeds GWQMN; otherwise, there is no baseflow. Changing this value allows you to manage the amount of water that flows directly into baseflow and indirectly into AET as "revap" flow. This indicates that boosting GWQMN can reduce baseflow, and vice versa. When the upper soil surface is dry and the underlying layer is wet, water diffuses up and evaporates.

Deeply rooted plants also drain water from the shallow aquifer. In the SWAT model, this elimination procedure is known as "revap". It occurs only when the water content of the shallow aquifer surpasses a predetermined revap threshold level during a dry season. Equation 3.12 describes the maximum amount of water that can travel via the revap process.

$$w_{revap,mx} = \beta_{rev} * PET \quad ---------- \quad 3.12$$

In this equation, wrevap.mx represents the maximum quantity of water moving into the soil zone (mm), βrev represents the revap coefficient (GW_REVAP in SWAT), and PET is the potential evapotranspiration for the day (mm). The real amount of revap is then estimated using equation 3.13:

$$w_{revap} = w_{revap,mx} - \alpha q_{shthr,rvp} \text{ if } \alpha q_{shthr,rvp} > \alpha q_{sh} < (\alpha q_{shthr,rvp} + w_{revap,mx})$$

$$w_{revap} = w_{revap,mx} \text{ if } \alpha q_{sh} > (\alpha q_{shthr,rvp} + w_{revap,mx})$$

$$\text{otherwise}, \quad w_{revap} = 0 \quad 3.13$$

Where wrevap is the actual amount of water moving into the soil zone (mm), aqsh is the amount of water stored in the shallow aquifer for a particular day (mm), and aqshthr,rvp (REVAPMN in SWAT) is the minimum water level in the shallow aquifer for a revap to occur (mm).

The GW_REVAP coefficient affects the aquifer's revap flow. There is no revap flow if GW_REVAP is zero, and revap equals PET when its value is 1.0*GW_REVAP, which ranges from 0.02 to 0.20.

3.4.1. SWAT Model Parameterization

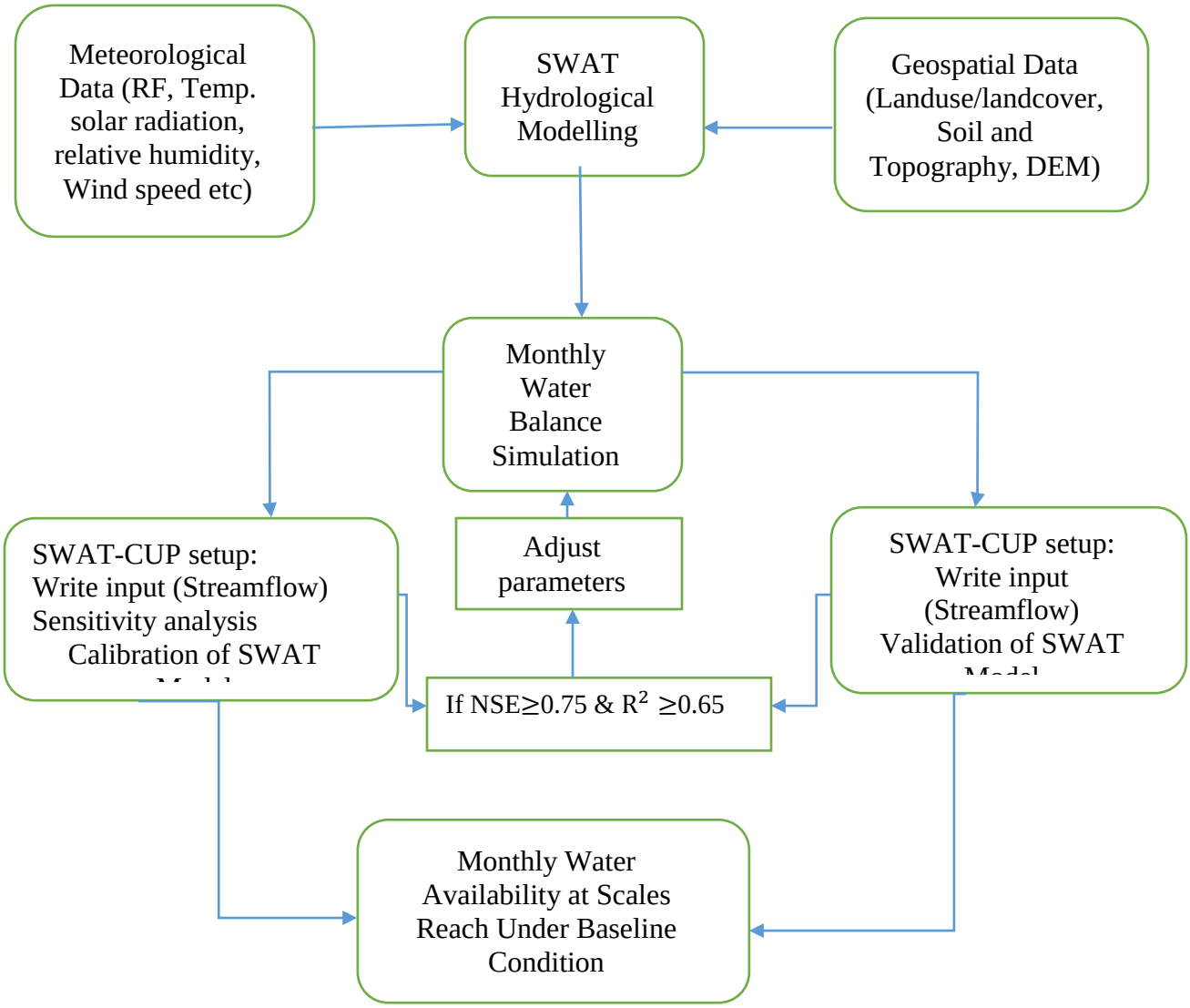

Figure 3.10: Methodology or conceptual frame work of SWAT model

SWAT allows a catchment to represent a number of different physical processes. A catchment was divided into several sub-catchments. Climate, HRUs, groundwater, and the principal channel or reaches draining the subbasin are the categories into which the input data for each sub

catchment or subbasin is classified. HRUs are land regions within a sub-basin or sub-catchment that have specific soil, land cover, and management characteristics (Neitsch et al. 2011).

3.4.2. Watershed and channel delineation

The Meki River catchment served as the aperture for the Digital Elevation Model (DEM) of 30 m x 30 m resolution, which portrayed the sub-basins, channel network, and watershed boundaries. The catchment's outlet point, which also served as the watershed's departure, marked the top of this river basin. The entire area was separated into smaller basins using the Arc-SWAT algorithms, and each of them supplied a specific stream channel. Stream channels were calculated using DEM cells with a surface area of at least 3000 hectares. To specify the sub-basins, 18 outlet sites were manually set, one of which was selected using Arc-SWAT.

The SWAT model initialization procedure begins with the determination of the catchment and subbasin boundaries. The DEM is made up of grid cells with elevation values and was utilized in conjunction with Arc-SWAT's watershed delineation tool, which uses flow direction and accumulation algorithms to build the stream network. A threshold area was developed to define the stream origin, and the catchment's outflow was manually completed to complete the delineation. The catchment area was 2242.042 km² and divided into 18 sub-basins, as illustrated in Figure 3.11.

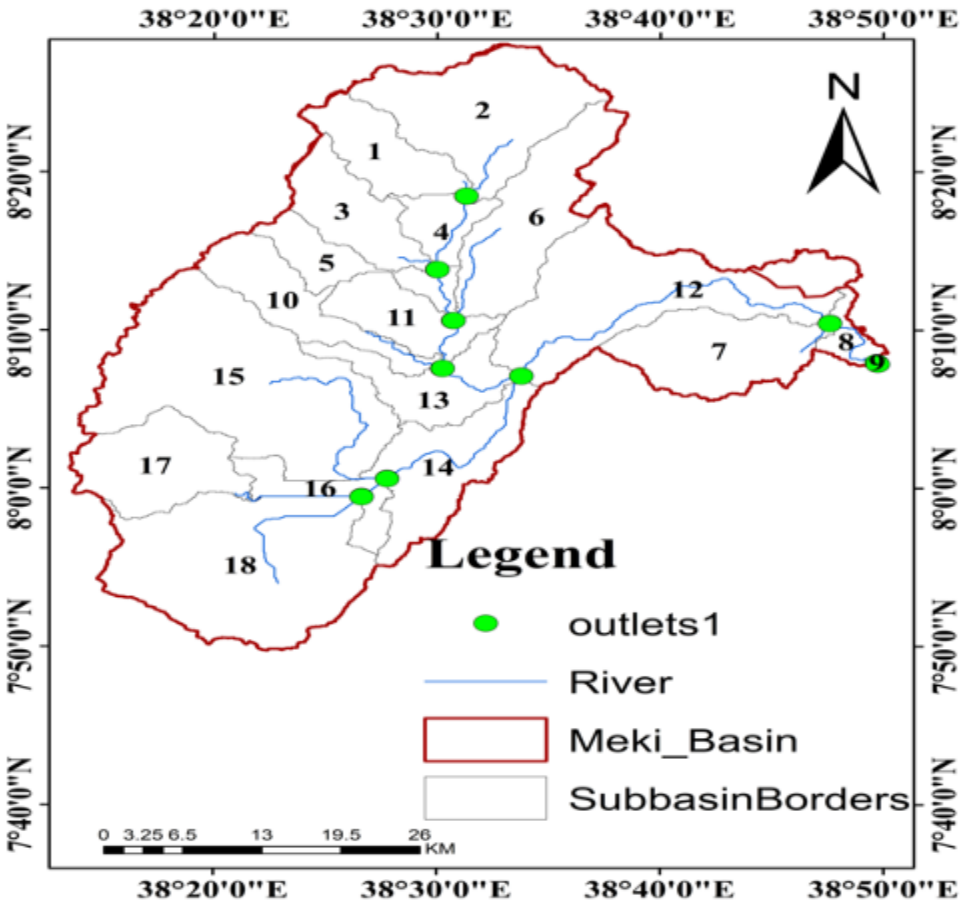

Figure 3.11 Sub-basin of meki river sub basin

3.4.3. Hydrologic Response Unit (HRU) Analysis

Hydrologic Response Units (HRUs) are sub-basin areas that represent unique combinations of soil, land cover, and management, allowing the model to account for differences in hydrological parameters such as evapotranspiration. Runoff is estimated for each HRU and routed, resulting in better flow estimates and a more realistic representation of the water balance.
To define HRUs, land use and soil data in shapefile format were entered into the SWAT interface. A look-up table linked land cover classes to associated SWAT codes. Following reclassification, the soil map was linked to the soil database, and slope classification was determined using DEM data.

The HRUs were then assigned to sub-basins, with a threshold level used to eliminate minor soil types, land uses, and slope classes. In accordance with SWAT user recommendations, a 10%

threshold for land use and 5% for soil were utilized to reduce the amount of HRUs while keeping adequate detail.

The slopes were classified into three categories: level to gently undulating (0-8%), rolling to hilly (8-15%), and sharply dissected to mountainous (over 15%). The HRU approach yielded 86 HRUs over 18 sub-basins, ensuring that only the most important land uses, soils, and slopes were considered for accurate modeling.

3.4.4. SWAT Model Input

SWAT's major channel length and catchment area were computed using the Arc-SWAT GIS interface and the research region's 30m x 30m resolution DEM. Arc-SWAT uses the Digital Elevation Model (DEM) and mapped land use and soil data to create a set of basic model input files.

SWAT requires particular information on the geography, land use/coverage, soil types, weather patterns, and watershed management strategies. To capture varied watershed features, the model adopts a two-level scheme: first, catchment and sub-catchment delineation is performed using topographic information, followed by further breakdown into HRUs based on land use and soil type consideration.

3.4.4.1. Spatial data Digital Elevation Model (DEM)

A DEM defines topography by specifying the elevation of each point in a given area at a certain spatial resolution. The data for the digital elevation model with a resolution of 30m came from the Ministry of Water, Irrigation, and Energy. The DEM was utilized to identify the Catchment and investigate drainage patterns on the terrain's land surface, as well as sub-basin metrics such as slope gradient and length, and stream network elements.

3.4.4.2. Soil data

The SWAT criteria take into account numerous soil textural and physicochemical parameters such as soil texture, accessible water content, soil hydraulic conductivity, bulk density, and organic carbon content, as well as different strata of each soil type. The soil map raster and look-up table for the SWAT database were developed. After being received from MoWIE, these soil data were analyzed in ArcGIS 10.3 along with the soil types (FAO 2005). The predominant soil types in the study catchment were lithic leptosol (Lp), which accounted for 12.84% of the

research area, eutric vertisols (VR), 5.02%, eutric leptosols (Lp), 16.33%, and cambisol (37.93%) (Figure 3.12).

The user soil was also created, and the soil lookup table was converted into a soil database file and loaded into the ArcSWAT database.

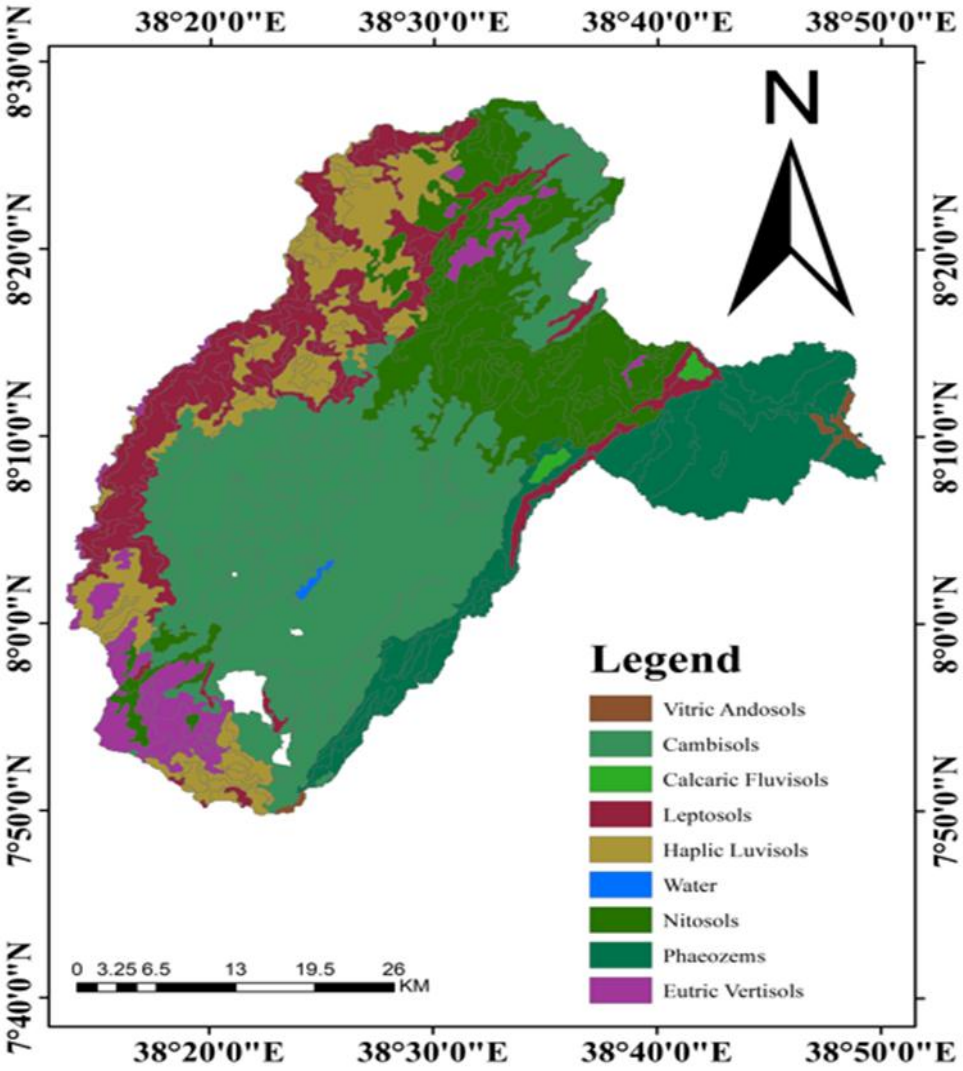

Figure 3.12 Dominant soil types of study area

Table 3.2. Dominant soil types of study area

Dominant Soil Group	Area (KM2)	Percentage (%)
AN	10.68	0.48
PH	320.69	14.3
CM	850.35	37.93
FL	9.93	0.44
LV	241.43	10.77
NT	405.45	18.08
VR	112.64	5.02
V/R	3	0.14
LP	287.87	12.84

3.4.4.3. Land use

Land use is a major element influencing catchment runoff, evapotranspiration, and surface erosion. The land use information for the research area was located using MoWIE. After using the raster map and lookup table as input for ArcSWAT, the study region's land use map was classed. The land use map has been updated to reflect the rendering of specific land cover types, such as cropland (AGRL), grassland or pastureland (RNGE), shrubland or brushland (RNGB), forestland (FRST), barren land (BARR), natural forestland (FRSE), woodland or deciduous forestland (FRSD), and wetland or marshland (WETN) (Figure 3.13). The ArcSWAT database file was imported, with the land use lookup table converted to a land use and land cover database.

Table 3.3 Study area LULC area and percentage

Classes of LULC	Area (KM)	Percentage (%)
Grassland	263.3	11.74

Forest	352.31	15.71
Cropland	1441.99	64.32
Shrub/bush	74.26	3.31
Wetland	0.14	0.03
Barren land	50.02	2.2
Woodland	28.37	1.27
Settlements	15.62	0.7

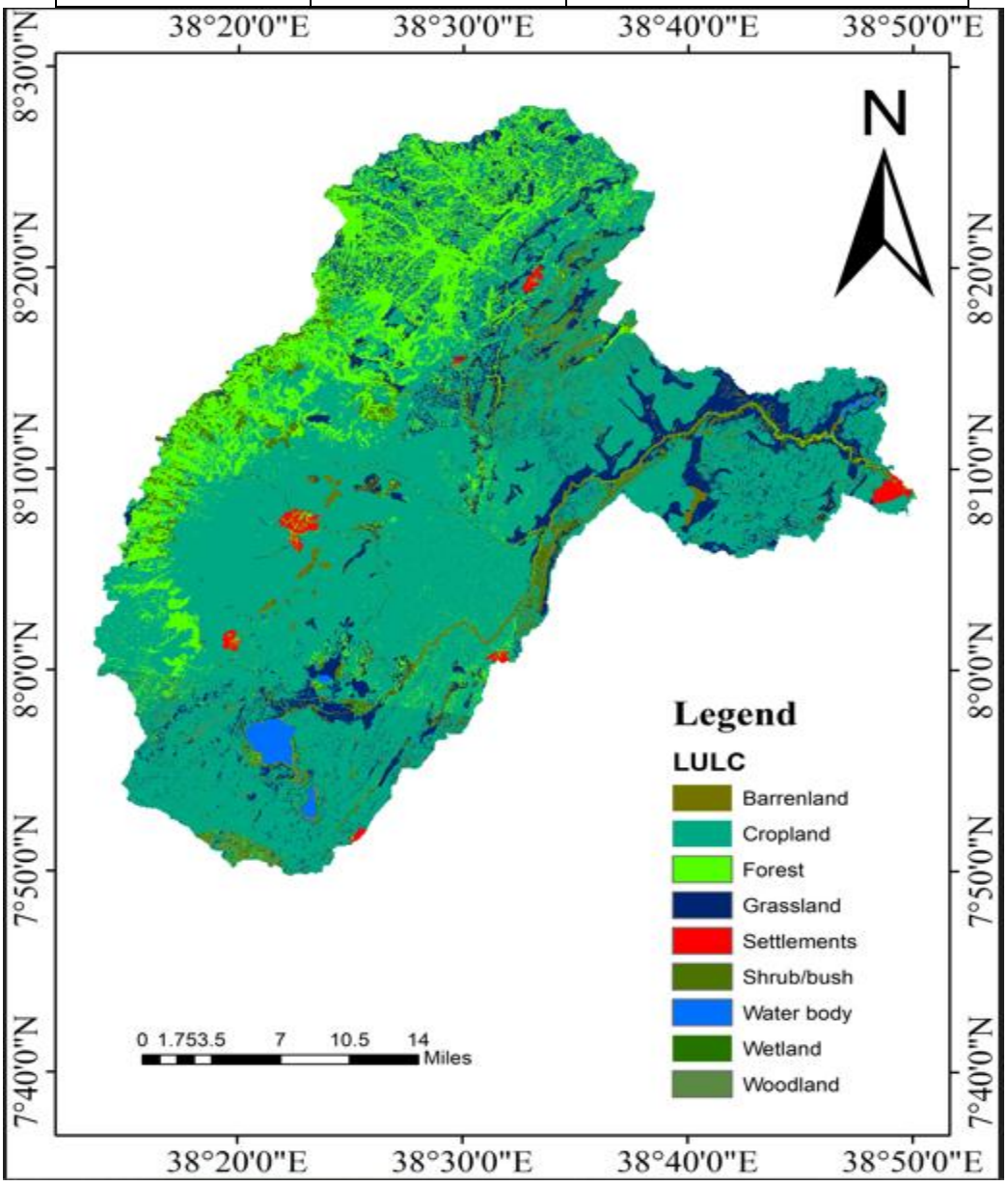

Figure 3.13 Land use and land cover map

3.4.4.4. Slope of the study area

Mountains surround the research area on both the west and east sides of the basin. The slope map of the research region reveals that the majority of the watershed is covered in exceptionally steep slopes. The slope map created from a DEM using ArcGIS software specifies mild slope (0-8%), fairly steep slope (8-15%), moderately steep slope (15-20%), and extremely steep slope (20-35%). However, for the SWAT input, the slope was divided into three categories: class 1 (0-8%), class 2 (8-15%), and class 3 (>15%).

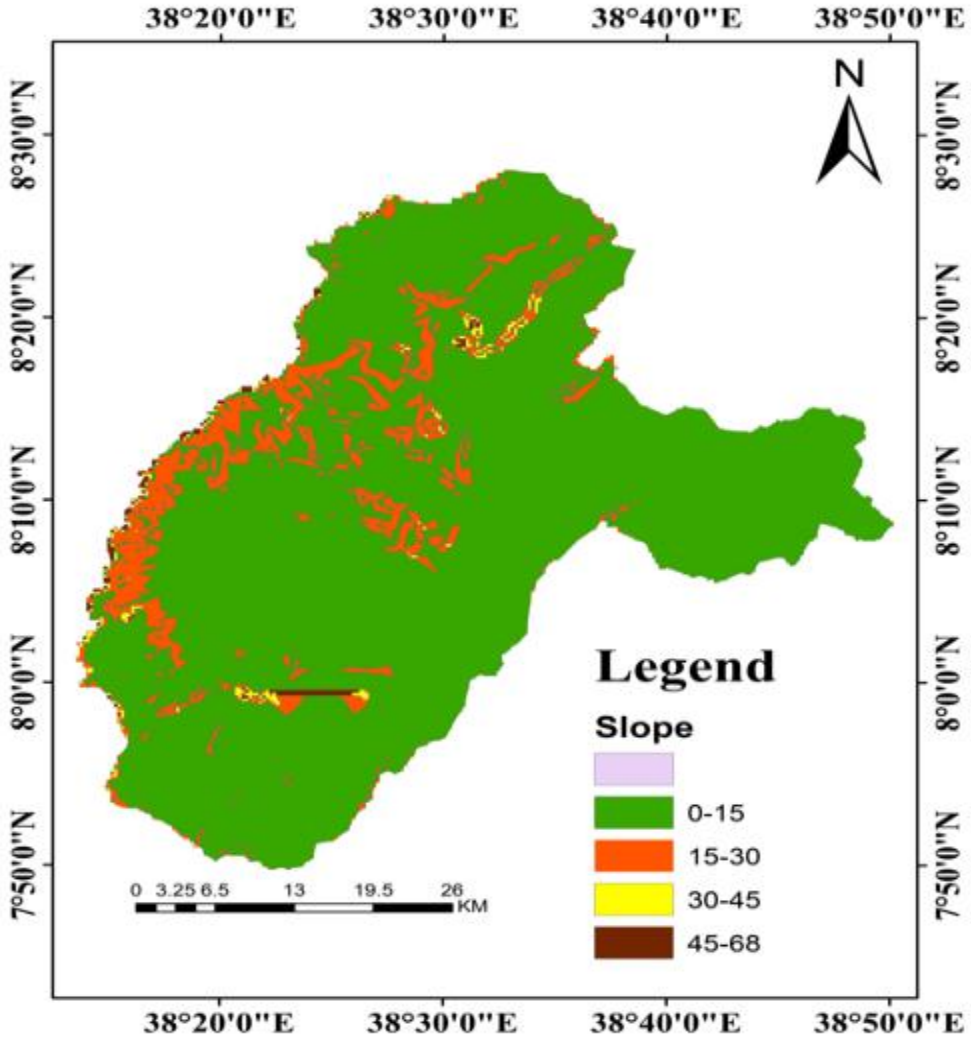

Figure 3.14 Slope of study area

Table. 3.4 Percentage of slope in study area

Slope	Area	Percentage (%)
0 – 15	231.14	10.3
15 – 30	22.1	0.99
30 – 45	1976.53	88.16
45 - 68	12.27	0.55

3.4.4.5. Weather data preparation (Weather Generator)

The WGN Parameter Estimation Tools prepares WGN files for SWAT using daily meteorological data. Before the WGN Parameter Estimation Tools could begin to prepare, the 21 years' worth of meteorological data (including precipitation, temperature, relative humidity, solar radiation, and wind speed) were compiled in a single folder and processed to create a directory for them. Weather data from the single station with full climate data (Bui Stations) as WGN files for Arc-SWAT input via the ArcMap interface. The climate data was constructed using daily data from 2000 to 2020. The WGEN was created, converted to a database file, and then imported into the Arc-SWAT reference database. The WGEN file is useful for simulating weather variables such as wind speed, relative humidity, sun radiation and temperature.

Table 3.5 Station locations added to Arc-SWAT database

STATION NAME	**LAT**	**LONG**	**ELEVATION**
Bui	8.330833	38.55444	2054

3.4.4.6. River discharge

The MoWIE's Hydrology Department offers data on the Meki River's daily discharge. This data was developed to be used as input to the SWAT-CUP model and for model validation. The collected river flow data comprised daily river flows from 2000 G C to 2013 G C. The river discharge station at Meki Outflow gets flow data from the Meki River Outlet.

3.5. SWAT calibration and validation

Calibrating and testing the SWAT model is critical to assuring the accuracy and dependability of its simulations. The SWAT-CUP model, which uses optimization methods to match simulated and observed hydrological responses, is critical to this process (Abbaspour et al., 2007). During calibration, observable data such as streamflow, sediment output, and nutrient concentrations are utilized to fine-tune model parameters, improving the model's capacity to simulate real-world scenarios. The iterative method adjusts settings until an acceptable match is found.

Following calibration, validation tests the model's prediction capabilities with independent datasets that were not utilized during calibration to ensure generalizability (Abbaspour et al., 2007). Parameter sensitivity analysis is essential during calibration to discover key parameters that influence model performance (Abbaspour, 2015). Despite the uncertainties, calibration and validation are required to determine the model's resilience. SWAT-CUP's Sequential Uncertainty Fitting version 2 (SUFI-2) interface is widely used for calibration and uncertainty analysis (Abbaspour et al., 2004). SUFI-2 is more effective than other approaches and requires less runs (Setegn et al., 2008; Yang et al., 2008). Model performance is assessed using statistical methods such as the Nash-Sutcliffe efficiency (NSE) and coefficient of determination (R2) (Moriasi et al., 2007; Nash & Sutcliffe, 1970).

This study employed streamflow data from Meki town (2000-2013) for calibration (2003-2009) and validation (2010-2013), with monthly data aggregated for analysis. SWAT model calibration and validation, which are enabled by SWAT-CUP, are crucial for maintaining the model's reliability in hydrological process simulations and assisting with water resource management decisions.

Table 3.6: Model performance rating for stream flow at the monthly time scale.

	Equations	
Performance rate	$\text{NSE}=1-\frac{\sum_{i=1}^{N}\left(Q_{si-Q_{oi}}\right)^2}{\sum\left(Q_{o-}\overline{Q_o}\right)^2}$	$R^2=\frac{\sum_{i=1}^{n}(Q_{si}-\overline{Q_s})(Q_{oi-}\overline{Q_o})^2}{\sum_{i=1}^{n}(Q_{si}-Q_s)^2\sum_{i=1}^{n}(Q_{oi}-\overline{Q_o})^2}$
V. good	$0.75 < \text{NSE} \leq 1.00$	$0.75 < R^2 \leq 1.00$
Good	$0.65 < \text{NSE} \leq 0.75$	$0.65 < R^2 \leq 0.75$

Satisfactory	$0.50 < \text{NSE} \leq 0.65$	$0.50 < R^2 \leq 0.65$
Unsatisfactory	$\text{NSE} \leq 0.50$	$R^2 \leq 0.50$

Source: (Moriasi et al., 2007) where, NSE is Nash-Sutcliffe efficiency Q_{obs}, and Q_{sim} are measured and simulated flows respectively, R^2 is the coefficient of determination.

3.5.1. Sensitivity Analysis

To guarantee effective calibration, sensitive parameters have to be identified using sensitivity analysis. Sensitivity analysis helps establish which model parameters have the most influence on predictions, allowing for the reduction of parameters that must be estimated and therefore shortening calibration time. This research was validated with the Sequential Uncertainty Fitting (SUFI-2) algorithm, which identifies critical parameters influencing streamflow in the Meki River subbasin.

A global sensitivity analysis approach, which assesses the influence of one parameter in comparison to others, was applied. Fourteen parameters were chosen for this analysis based on previous research and their relevance to the subject. These metrics included CN2 (SCS CN II value), SOL_K (saturated hydraulic conductivity (mm/hr), GWQMN (threshold water depth for flow), and others associated with soil, groundwater, and channel properties. The 14 most sensitive parameters identified were then chosen for model calibration. Section 4 of the results discusses the specific values for these parameters and how they affect the model output.

3.6. Ground water model conceptualization

In groundwater modeling, creating a conceptual model is an important initial step. This model lays the groundwork for the following numerical model by defining hydrostratigraphic units, system boundaries, and the groundwater balance. Kresic and Mikszewski (2013) define the conceptual model as a schematic representation that captures knowledge about the studied area. According to Anderson et al. (2015), the model covers important elements such as boundary conditions, hydrostratigraphy, hydrogeological properties, flow dynamics, sources, sinks, and an initial water balance, allowing for a qualitative understanding of groundwater movement and the processes that regulate it.

A hydrological conceptual site model, as defined by Anderson and Woessner (1992) and Neven and Alex (2011), clarifies the complicated relationships that influence groundwater fluxes by identifying groundwater sources and sinks, as well as the porous media through which it flows. It also provides insights into past groundwater behavior and forecasts future changes caused by numerous activities. Furthermore, boundary conditions, as stated by Anderson and Woessner (1992) and Lekula et al. (2018), play an important role in shaping the mathematical framework of the numerical model. These characteristics, which can be physical (e.g., surface topography, faults, and water bodies) or hydraulic (e.g., flow and head conditions), have a substantial impact on groundwater flow patterns and must be carefully considered when developing the conceptual model.

3.6.1. Hydro-stratigraphic units

Quaternary Sedimentary Deposits: These deposits, identified as the region's principal geological feature (Mesele and Mechal, 2020; MoWS, 2008), comprise the Meki River Basin's key aquifer systems. However, the heterogeneity in thickness and composition across the region results in a very varied aquifer nature (MoWS, 2008). Mesozoic sedimentary formations and Precambrian metamorphic rocks: These geological structures, found primarily along the escarpment, form low groundwater potential aquifers, while little is known about their characteristics (MoWS, 2008). These hydrostratigraphic units define groundwater flow pathways and storage features in the Meki River Basin, impacting the distribution of sources, sinks, and flow directions, which is necessary for building a full conceptual model of the groundwater system.

3.6.2. Sources and sinks

The escarpment area, particularly the Guraghe Mountains, is an important recharge zone for the Meki River Basin (Ayenew, 2008). This region is dominated by volcanic aquifers, which allow groundwater to flow through worn surfaces, cracks, and fractures. The Butajira-Pediment Aquifer, with a complicated combination of alluvial, talus, and debris formations, has moderate productivity and serves as a local relief region. Its shallow groundwater table supports a large number of private and hand-dug wells, as well as springs with low to moderate productivity.

The Butajira-Kibet Aquifer, formed by scoria cones, is famous for its high transmissivity and

hydraulic conductivity, but its deeper groundwater table means fewer springs, necessitating pump-powered water abstraction. The Enseno-Kela Aquifer, which is covered in various lacustrine, pyroclastic, and alluvial deposits, supports a dense network of hand-dug wells and springs used for drinking and small-scale irrigation. The Tora-Koshe-Dugda Ridge Aquifer, which is made up of deep ignimbrite, tuffs, and pyroclastic rocks, has cracks and joints that restrict groundwater flow. Because of their depth, family-owned wells are rare in this area. In contrast, the Meki Area Aquifer is a shallow, unconfined, and extremely productive system made up of poorly sorted gravel, sand, silt, clay, and volcanic deposits that support a variety of water supply strategies. Understanding these various geological and hydrogeological characteristics is critical for effective groundwater management and the sustainable use of resources in the Meki River Basin.

3.6.3. Flow direction

Groundwater flows largely through worn surfaces, fissures, and cracks, with the escarpment area serving as the basin's primary recharge zone (Ayenew, 2008). Specific Aquifer properties: Aquifers vary in composition and properties across the basin, with volcanic formations, alluvial, talus, and debris deposits influencing groundwater flow patterns and storage capacity (Halcrow, 2008; JICA and MoWE, 2012).

Regional groundwater flow comes mostly from the high rainfall plateau that borders the rift to the rift valley aquifers, which is largely determined by the structure of the bounding faults (Ayenew, 2008; Kebede et al., 2008). Escarpment to Rift Valley: As the plateaus give way to lacustrine deposits on the valley floor, particularly near the lake, the depth to the groundwater table decreases. Furthermore, transmissivity increases from the escarpment to the rift bottom (Mesele and Mechal, 2020; MoWS, 2008).

3.6.4. Boundary conditions

Boundary conditions are determined using either physical barriers like vast bodies of water and impermeable rocks, or stable hydraulic features like water splits and streamlines (Anderson et al. 2015). The Escarpment (Guraghe Mountains) was characterized by volcanic aquifers that covered a large region, with groundwater flowing predominantly through worn surfaces, cracks and fractures. This area acts as an important recharging zone for the basin (Ayenew, 2008).

Butajira-Pediment: This aquifer, which consists of a complex mixture of alluvial, talus, and debris deposits underlain by Tertiary Volcanic strata, has modest productivity and functions as a local relief region (Halcrow, 2008).

Butajira-Kibet: This aquifer, formed by scoria cones of basaltic composition, spans along the Butajira-Kibet region, with relatively high transmissivity and hydraulic conductivity but deeper groundwater tables (Halcrow, 2008). Enseno-Kela: This aquifer, which is covered in lacustrine, pyroclastic, and alluvial deposits, has varying thickness and depth to the groundwater table, as well as a high density of hand-dug wells and springs developed for local water supply (Mesele and Mechal, 2020; MoWS, 2008). Tora-Koshe-Dugda Ridge: This aquifer is made up of deep ignimbrite, tuff, and pyroclastic rocks, with cracks and joints controlling groundwater flow (MoWS, 2008). The Meki Area (Lacustrine Deposits) is distinguished by shallow and unconfined highly productive aquifers made primarily of gravel, sand, silt, clay, diatomite, and volcanic deposits with intergranular permeability (JICA and MoWE 2012).

3.6.5. Aquifer properties

Despite recent study efforts, aquifer properties in the Meki River Basin remain challenging due to data scarcity (JICA and MoWE, 2012; Kebede et al., 2008; Mesele and Mechal, 2020; MoWS, 2008). Groundwater data are primarily derived from project-based testing and observations. Over 2000 water abstraction projects were collected, including information on hand-dug and pumping wells, as well as geological and hydrogeological data. Table 3.7 highlights the parameters of important aquifers, which show hydraulic conductivity changes ranging from 0.6 to 20.86 m/day. The escarpments and Tora-Koshe-Dugda Ridge are characterized by fractured aquifers. Lacustrine and alluvial deposits dominate Enseno-Kela, whereas lacustrine sediments predominate in the Meki area.

Butajira-Pediment's aquifer is defined by alluvial and debris flows from the escarpments, whereas Butajira-Kibet and other minor aquifers are largely basaltic. Despite the limitations, understanding aquifer features is critical for effective groundwater management and sustainable resource exploitation in the region. The MoWIE provided geological and hydrogeological data as well. Regardless of these obstacles, understanding aquifer features is critical for effective groundwater management and sustainable use in the region.

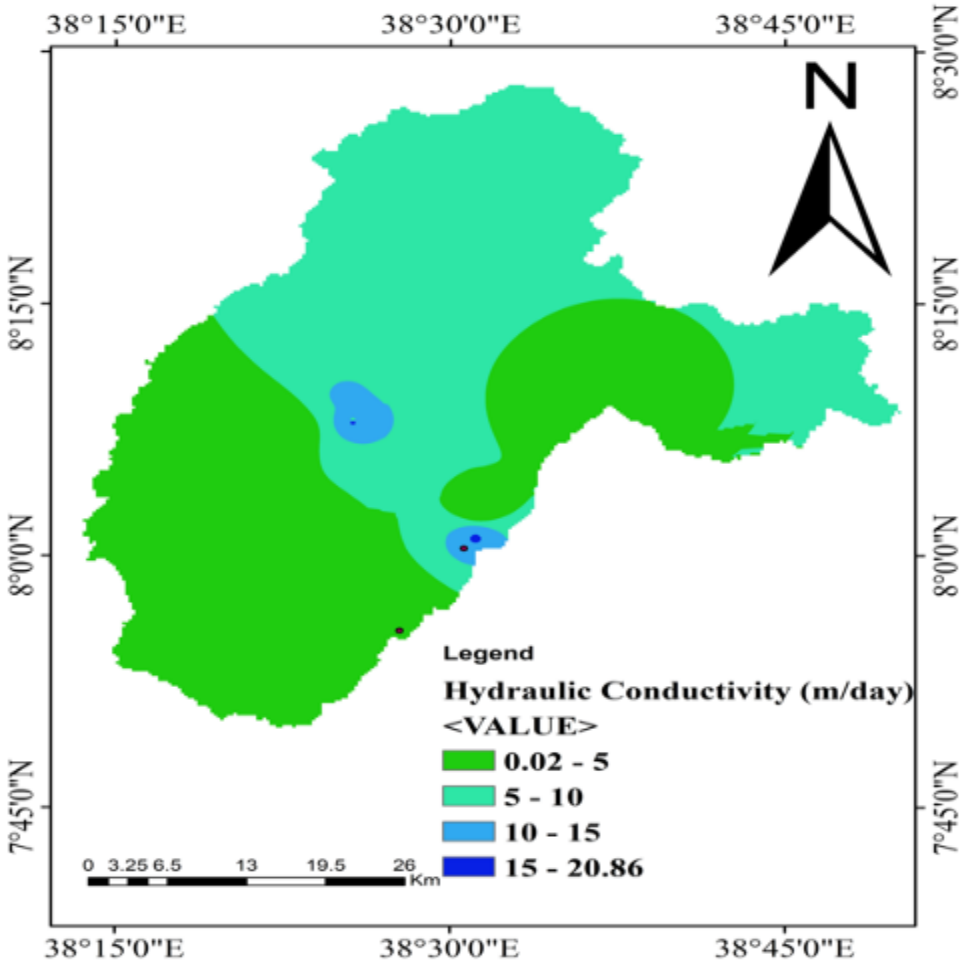

Figure 3.15 Hydraulic conductivity range map, in m/day

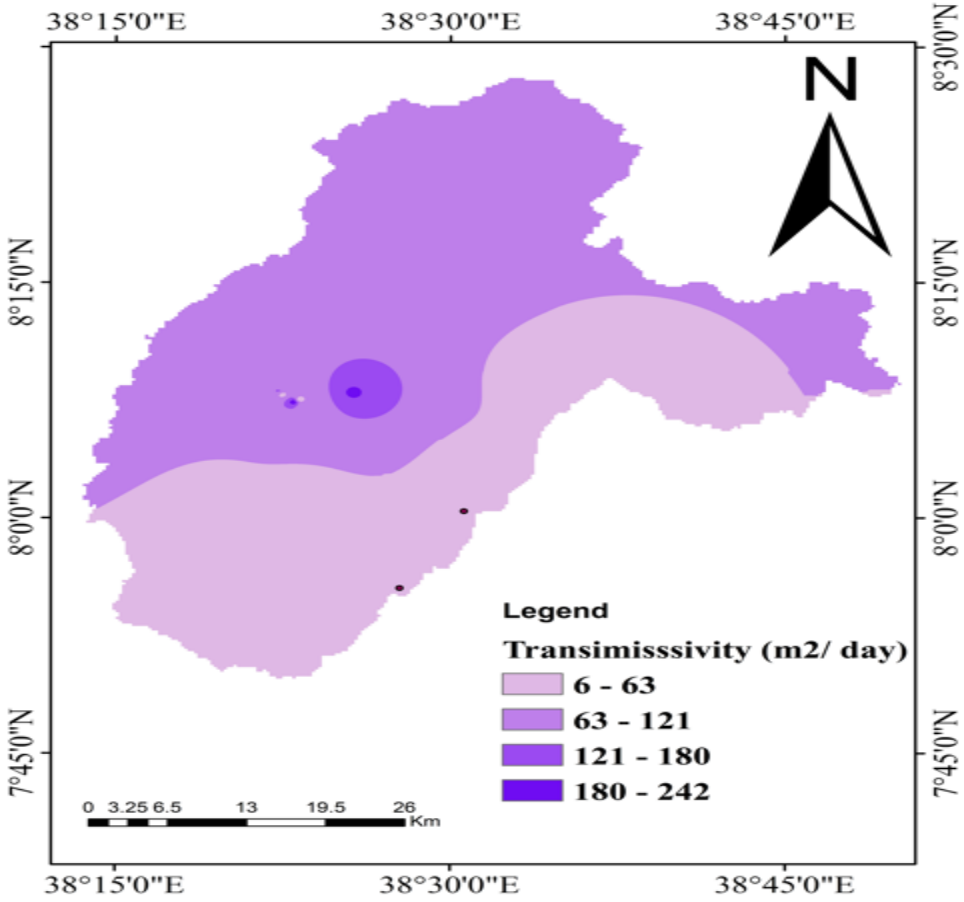

Figure 3.16: Transmissivity range map, in m/day

3.6.6. Groundwater recharge

Groundwater recharge is accomplished through natural processes such as precipitation, rivers, lakes, and human-caused events. Recharge rates are influenced by terrain, geology, climate, soil qualities, land use, vegetation, and drainage patterns. The western rift escarpment of the Meki River watershed receives the most recharge because of its plentiful rainfall, rugged terrain, and steep, dissected slopes. In this work, the recharge was applied to the top active model layer with spatially variable flow generated from the SWAT model. The model takes into account the daily average recharge distribution, emphasizing oscillations caused by land surface permeability, which varies according to soil properties and land usage. The catchment's annual recharge rate is projected to be 124.72 mm/year, or around 0.346 mm/day. These values were calculated using SWAT model simulations that link surface and groundwater dynamics.

3.7. Numerical model

Numerical models are computer simulations that evaluate groundwater systems, providing information on flows and water levels based on groundwater data. There are two basic types of numerical modeling approaches: steady-state and transient (non-steady state). Steady-state modeling implies a constant hydraulic head throughout time, which represents long-term situations. Darcy's law is commonly used to represent both confined and unconfined environments (Anderson et al., 2015). For the Meki River Catchment, a 3D groundwater flow model was created using MODFLOW-NWT, a Newton-based version of MODFLOW-2005.

This model entails defining geographical and temporal discretization, establishing boundary and beginning conditions, and describing aquifer features. Hydraulic parameters were initially based on published estimations and then refined to match observed data. GIS data, such as layer extent and elevation, were maintained in ArcGIS version 10.3, and MODFLOW-NWT input files were created with ModelMuse (Winston, 2009). MODFLOW-NWT mimics groundwater flow by dividing time into stress periods, which are further subdivided into time steps. For the Meki River Basin, a single stress period spanning January 1, 2000 to 2020 was employed, with a monthly time step connecting the model to the SWAT data.

The model activates grid cells where SWAT hydrological units exist and specifies hydrogeological units' hydraulic attributes using the Upstream Weighting (UPW) package. Confined layers have a constant saturated thickness, whereas convertible layers vary depending on head levels. MODFLOW-2005, the foundation for MODFLOW-NWT, is a 3D finite-difference groundwater model created by the USGS. It can mimic both constant and transient flow in aquifer systems, whether confined, unconfined, or mixed. The three-dimensional equation for incompressible groundwater flow through porous media (Equation 3.14) lies at the heart of the model, governing flow in multiple directions (x, y, z) and accounting for water sources and sinks.

$$\frac{\partial}{\partial x}\left(K_{xx}\frac{\partial h}{\partial x}\right)+\frac{\partial}{\partial v}\left(K_{yy}\frac{\partial h}{\partial v}\right)+\frac{\partial}{\partial z}\left(K_{zz}\frac{\partial h}{\partial z}\right)+W=S_s\frac{\partial h}{\partial t}\text{----------(3.14)}$$

In this formula, Kx, Ky, and Kz represent hydraulic conductivity values in the x, y, and z directions, which are assumed to be parallel to the primary axes of hydraulic conductivity (L/T),

and h is the potentiometric head (L). Furthermore, W is defined as volumetric flux per unit volume, indicating sink and/or source of water. When W < 0.0, water exits the system; when W > 0.0, water enters (T-1). Ss represents the specific storage of porous materials (L-1), and t stands for time.

3.7.1. Model selection and description

The model was chosen for its ability to mimic surface-groundwater interactions in unconfined aquifers, including drying and rewetting effects (Niswonger et al. 2011). It is open-source, publicly available, and operates on the ModelMuse graphical user interface (GUI), which allows for both 3D visualization and model manipulation. Calibration is done manually through trial and error, which provides a better grasp of parameter correlations than automated approaches. MODFLOW-NWT distinguishes itself by being able to calculate groundwater heads for dry cells, something conventional MODFLOW-2005 cannot do. ModelMuse supports variable model configuration by allowing users to describe spatial inputs using 3D objects and formulas, making it easy to change grid sizes and simulation periods without affecting spatial data or boundary conditions.

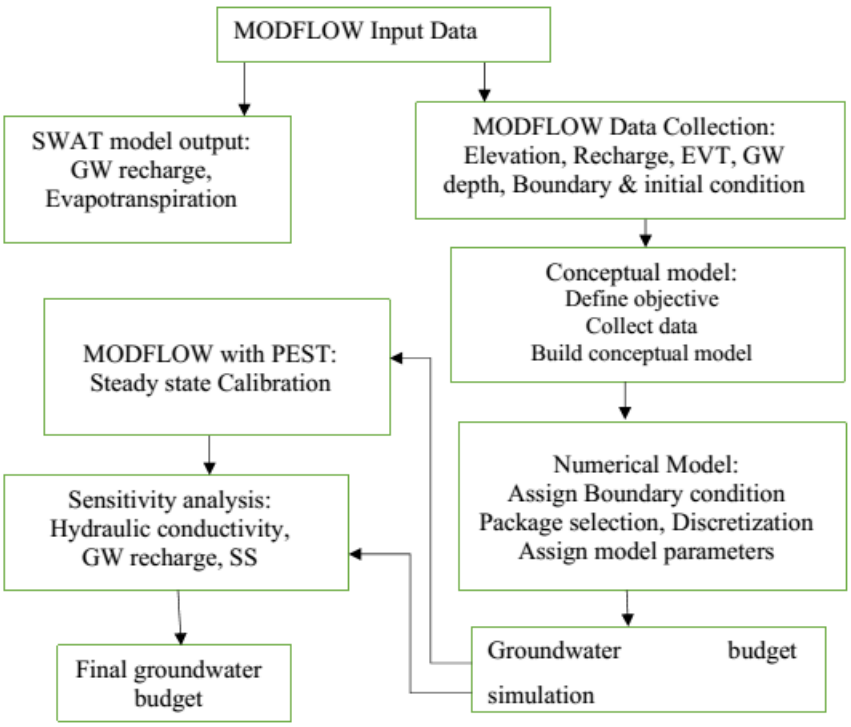

Figure 3-17 MODFLOW-NWT methodology under Modelmuse environment

3.7.2. Layer definition

This study comprises single layers that are unconfined. The reason for assuming convertible circumstances in these layers is to employ. DEM defined the model top elevation, which was then combined with the starting heads for the Meki River subbasin. The variance in well depth describes the bottom of the catchment.

3.7.3. Grid design

The study region was divided into 300-meter square grids, yielding 235 rows and 224 columns with a model domain area of approximately 2242.04 km2. Because raising cell size increases uncertainty and reducing cell size makes the model slower and more time-consuming, this resolution was thought to be sufficient. The grid smoothing criterion value is set to 1.2, which is the default value in the ModelMuse GUI. In total, there are 52,640 cells in the model domains, with 25,526 active and 27,114 inactive on both levels.

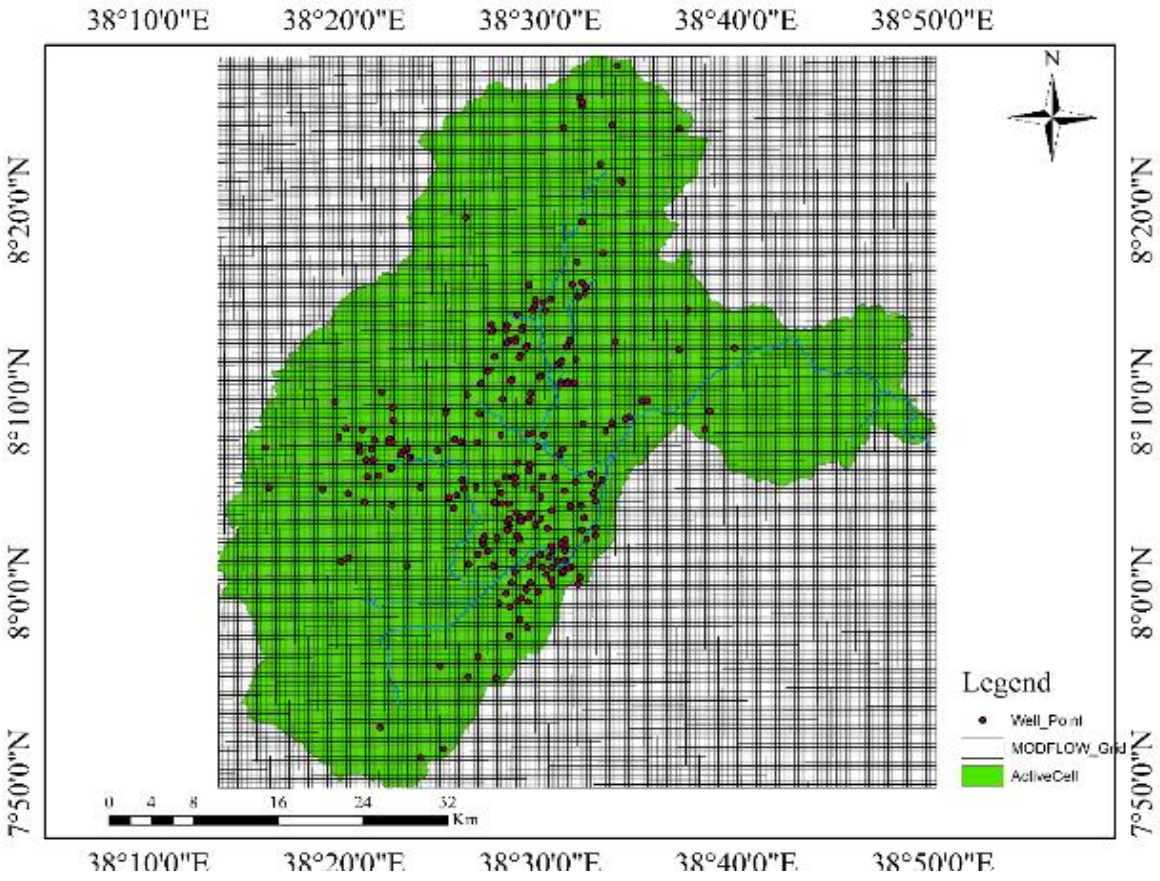

Figure 3. 18 Model grid and boundary condition

3.7.4. Model top of layer

Layer thicknesses are extensively defined to allow for the depiction of important geologic units. The aquifer layer's top elevation is taken into account. This study assessed the aquifer as unconfined and single-layered. The top layer is interpolated from the USGS's 30-meter resolution digital elevation model and placed at the land's surface (DEM) since, in general, the top layer height was assumed to be equal to the elevation of the ground surface, which was then supplied into the MODFLOW top elevation array.

3.7.5. Upper aquifer bottom of layer

Layer thicknesses are well specified, allowing for the representation of major geologic units. The aquifer layer's top elevation is taken into account. This study classified the aquifer as unconfined and single-layered. The top layer is interpolated from the USGS's 30-meter resolution digital elevation model and placed at the land's surface (DEM), as the top layer height is often regarded to be equal to the elevation of the ground surface, which is then fed into the MODFLOW top elevation array.

3.7.6. Initial hydraulic head

The model's initial circumstances are the distribution of water levels at each active cell within its layers. The structural model used input from model layers to simulate the physical stratigraphy of the aquifer system. Because the model consists of only one layer, the surfaces of the aquifers' top and bottom were precisely characterized and imported into Modflow (ModelMuse5.0). The top model of the research region is a digital elevation model (DEM) created by the USGS. It was then calculated by subtracting water level from top elevation across a large area using aquifer topography and a conceptual hydrogeological map. Following that, the actual value of water level elevation was assigned as initial heads in active cells.

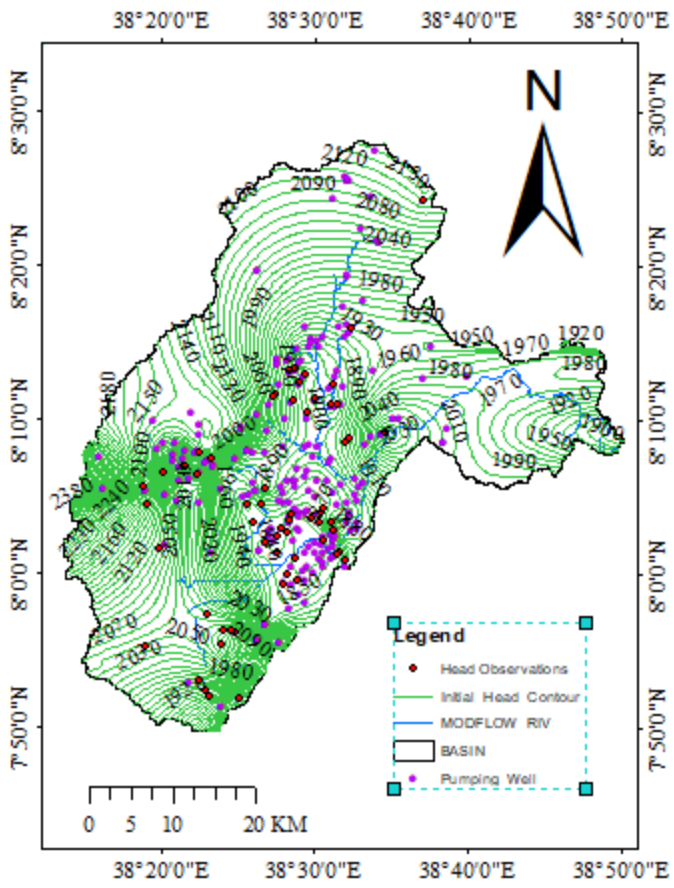

Figure 3.19 Initial hydraulic head

3.7.7. Model boundary conditions

Boundary conditions in groundwater modeling are critical for accurately reflecting the flow of water into and out of a system. They are distinguished by physical features such as vast quantities of water and impermeable rocks, as well as stable hydraulic structures such water splits and streamlines (Anderson et al., 2015). MODFLOW distinguishes three types of boundary conditions: specified heads, specified fluxes, and head-dependent fluxes. Specified heads fix the hydraulic head in specific model cells, whereas specified fluxes govern the flow of fluid entering or exiting the groundwater system, as seen in the Recharge package. Head-dependent fluxes, on the other hand, are based on a given conductance and a far-field hydraulic head value; examples include evapotranspiration, general head boundary, river, and well packages (Harbaugh 2005).

The function of boundary conditions extends to determining how water flows through the groundwater system. Water migration from groundwater to streams is an example of a boundary condition. Properly identifying these boundaries is an important step in any groundwater modeling study since it allows us to understand the hydrological system in the study area. Anderson and Woessner (1992) define boundary conditions as mathematical expressions that specify either the hydraulic head (dependent variable) or the flow (dependent variable derivative) at the system's limits.

In steady-state simulations, barriers have a substantial impact on the flow pattern in the system. They manage water entry and departure locations, making precise characterization an essential part of the modeling process. Because boundary conditions can change across time and place, it is critical to ensure that they accurately reflect the system's dynamics.

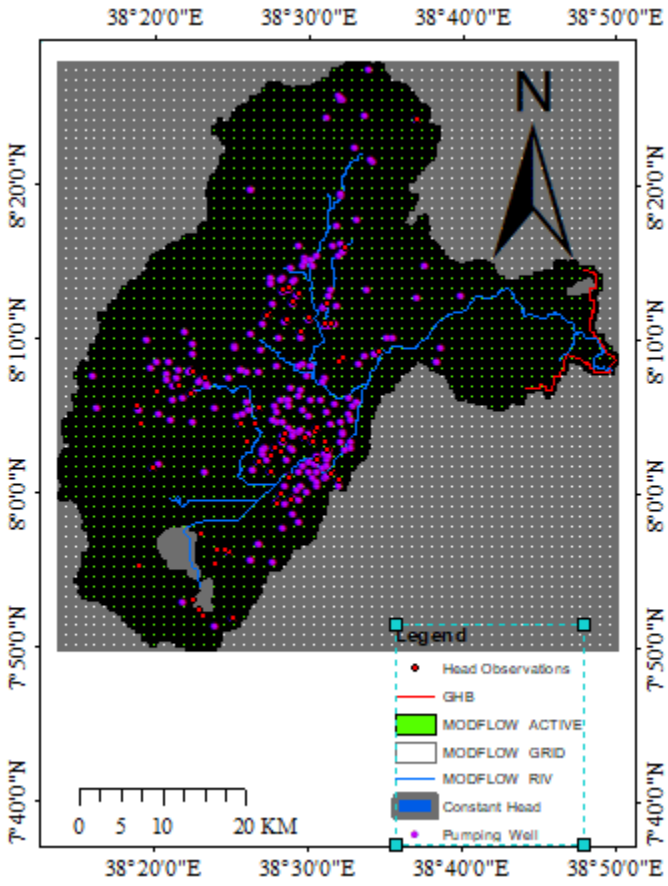

Figure. 3.20 Model boundary conditions

3.7.7.1. Time-Variant Specified-Head (CHD)

The Time-Variant Specified-Head Package (CHD) allows constant head cells to have different values at each time step, also known as constant head boundaries. These limits are especially well-suited for modeling huge bodies of water such as major rivers, lakes, reservoirs, and seas that are untouched by system stresses (Anderson and Woessner, 1992). In this study, the constant head boundary is represented by a polyline object located along the northwestern boundary. The CHD package enables the model to accurately replicate the dynamic behavior of these key water features, improving the overall depiction of the hydrological system. This package enables the user to specify the head in model cells.

3.7.7.3. Groundwater evapotranspiration

The amount of groundwater extracted via evapotranspiration (ET) is evaluated using MODFLOW's EVT package, which assumes that in semi-arid irrigated areas with shallow water tables, the ET rate varies linearly with depth below the water table. The EVT software takes into account the effects of direct evaporation and plant transpiration in depleting water from the saturated groundwater regime, subject to the following conditions: (1) when the groundwater elevation is at or above the root zone (bottom layer of SWAT soil profile), ET from the water table occurs at a maximum user-specified rate; (2) when the groundwater elevation is below a specified extinction depth, ET from the saturated zone ceases; and (3) between these two circumstances, ET from the water table varies linearly (Harbaugh et al. 2000). The EVT package's maximum evapotranspiration rate (EVTR) is calculated as the difference between the potential evapotranspiration rate (PET rate) calculated by SWAT and the actual evapotranspiration rate (AET rate) simulated by SWAT, assuming that the shallow water table can satisfy some of the PET rate.

$EVTR = PET - AET$ ---------- (3.15)

For this coupling technique to be successful under the new coupling code, the groundwater table must be located within the root zone.

3.7.7.4. River package

The MODFLOW River Package simulates water exchange between an aquifer and a river using a head-dependent flux technique, which is determined by the hydraulic head in the groundwater system and the river stage. Perennial rivers provide crucial boundary conditions for simulating surface-groundwater interactions (Kinzelbach, 2014). The flux (Q_riv) is estimated using the relationship between aquifer head (h) and river stage (h_riv), as well as characteristics such as streambed conductance (Criv), river width (Wriv), riverbed thickness (M_riv), and vertical hydraulic conductivity (K_riv). The key equations are:

$$Q_{riv} = C_{riv}(h_{riv} - h) \quad , \quad h > B_{riv} \quad \text{.......} (3.16)$$

$$Q_{riv} = C_{riv}(h_{riv} - B_{riv}) \quad , \quad h < B_{riv} \quad \text{.......} (3.17)$$

$$C_{riv} = \frac{K_{riv} L_{riv} W_{riv}}{M_{riv}} \text{.......} (3.18)$$

Where: Q_riv is the leakage rate [L3 T−1], h_riv is the river head [L], h is the aquifer head below the river [L], B_riv is the streambed bottom [L], and C_riv is the streambed conductance [L2T−1]. W_riv = river width [L]; Mriv = riverbed thickness [L]; Kriv = vertical hydraulic conductivity [LT−1].

The Meki River model's stream stages were calculated using field data and DEM, with a river stage of 0.5 m assumed (JICA, 2012). During calibration, parameters like streambed conductance and hydraulic conductivity were changed, and a river package file (modflow_MRW.riv) was generated to accurately describe groundwater-surface water interactions.

Table 3.7 Major stream model input summary (modified from Makin et al., 1976)

No	**Major Stream**	**Conductivity(m/day)**	**Thickness Bed (m)**	**Head of the River (m)**	**Width (m)**
1	Meki river	0.09-0.12	0.75-0.9	1637.3-2001	7.25-15
2	Lebu river	0.12	1	1879.66-2164.54	7
3	Akamuja river	0.12-0.27	1	1834.43-2371.59	8.5
4	Irinzaf river	0.076-0.27	1	1815.54-2296.69	7-8.5
5	Weja River	0.13	1	1808.68-1938	6 -10

3.7.7.5. General-head boundaries (GHB)

In groundwater modeling, General-Head Boundaries (GHB) are a third-type boundary condition that follows head-dependent flow principles. They are especially useful when the model boundaries cannot be specified as no-flow or constant head, allowing for the simulation of groundwater interactions with adjacent aquifers. GHBs require two critical parameters: conductance and a remote constant-head border. GHBs were used in the Meki River boundary model to simulate lateral groundwater inflow and outflow, and their calibration was based on steady-state groundwater levels obtained at neighboring monitoring wells. The initial conductance was determined using the following formula:

$$C = \frac{(L*W)*K}{D} \quad (3.19)$$

The surface area of the grid cell faces that exchanges flow with the external source or sink is denoted by (LxW), K is the average hydraulic conductivity of the aquifer material separating the source or sink from the model grid, and D is the distance between the source or sink and the model grid. This arrangement allows for precise depiction of lateral head gradients, which is critical for understanding groundwater dynamics in the research area.

3.7.7.6. Head observations (HOB)

The MODFLOW Head Observation module streamlines the process of collecting groundwater head data at specific sites. By adding observation points to the model and attaching them to the package, MODFLOW generates a file including simulated head values, observed heads, and residuals. Table 3.9 (in the Appendix) summarizes these data. A point object is used to assign a unique ID to each piezometer, as well as the time step and observed head. The observation site locations were loaded into ModelMuse as a shapefile. During steady-state simulations, the observed heads were utilized to calibrate the model and compare them to the simulated ones. Since groundwater head is vertically uniform over the aquifer, this simplification does not introduce inaccuracy.

3.7.7.7. Recharge Package (RCH)

The Recharge Package is required for simulating specific fluxes across the model's surface in groundwater modeling. To compute the volumetric recharge flux, multiply the user-defined recharge rates by the horizontal areas of the respective cells. Consistency in recharge data is critical for the proper integration of hydrological models such as SWAT and groundwater models. The groundwater model uses recharge data directly from the SWAT model, guaranteeing that recharge values remain consistent after the models are coupled, resulting in realistic hydrological predictions.

To import recharge data into ModelMuse, values are taken from the SWAT model's "output.hru" file, which contains the model's whole output. These recharge zones and values are then loaded into ModelMuse to ensure proper representation in the groundwater model. The addition of SWAT recharge data (124.72 mm/year) to ModelMuse improves the model's ability to properly reproduce real-world hydrologic processes.

3.7.7.8. WELL package

The WELL package in MODFLOW simulates groundwater extraction from aquifers for agricultural, municipal, industrial, and domestic applications. It permits water to be collected from cells (individually or collectively) inside a certain model layer, as long as the cells are saturated. Required zone polygons were imported from ArcGIS into ModelMuse, and each zone was allocated an average abstraction rate. ModelMuse then applied the flow to the cells covered by the polygon. Wells were installed in the upper aquifer layer to keep the afflicted cells saturated and supply the required flux.

The model defined the pumping wells using the Cell-by-Cell input approach. A well's pumping rate is independent of its cell area and hydraulic head. MODFLOW assumes that a well has completely penetrated the cell. To imitate water withdrawal, the well's recharge entry was set to a negative daily abstraction rate (m^3/d). The well data for this simulation, which entailed collecting and preparing about 257 wells, is included in an appendix. This simulation also included the creation of MODFLOW input file packages.

3.7.7.9. Zone budget

Groundwater budgets for the research region are computed using Modelmuse, a groundwater flow modeling software. Finding a groundwater budget for a specific portion of the research area can sometimes be more advantageous. The USGS's open-source ModelMuse application incorporates the ZONEBUDGET package. USGS developed the ZONEBUDGET software suite. It uses MODFLOW data to calculate sub-regional water budgets. It also computes water budgets using tabular budget data produced by USGS MODFLOW's cell-by-cell flow option. The ModelMuse software divides the entire model area into nearly uniform subregions, allowing water budgets to be calculated for each.

3.8. Steady state model calibration and performance evaluation

In this study, a steady-state MODFLOW model was calibrated using both a manual and the Parameter Estimation (PEST) module, with parameter values optimized through numerous iterations to match observed and measured head values and create realistic fluxes. The calibration procedure was first performed manually, then automated. Forward calibration entails modifying characteristics like hydraulic conductivity and recharging to imitate heads. Calibration continued until the difference between the simulated and observed heads was within an acceptable error range (Anderson et al., 2015).

The study used several error measures, such as mean error, mean absolute error, and root mean square error for groundwater levels, as well as discrepancy values for water balance (with an acceptable value of ≤ 0.02). The calibration centered on hydraulic conductivity and recharge, with primary K values established from earlier work and adjusted throughout calibration. Using realistic parameter values within a recognized range is critical for successful calibration, as unrealistic values can cause severe model errors (Anderson et al., 2015).

3.9. Error assessment and sensitivity analysis

To establish the model's uncertainties, sensitivity analysis is required. Uncertain parameters and boundary conditions are the sources of some of the model's uncertainties.

$$ME = \frac{1}{n}\sum_{i=1}^{n}(Head_{obs} - Head_{sim})_i \quad \ldots\ldots\ldots\ldots \quad (12)$$

Equation 13 calculates the mean absolute value by averaging the absolute differences between the observed head (Headobs) [m] and the model-calculated head (Headsim) [m].

$$MAE = \frac{1}{n}\sum_{i=1}^{n}|(Head_{obs} - Head_{sim})_i| \quad \ldots\ldots\ldots\ldots\ldots\ldots\ldots\ldots\ldots\ldots\ldots\ldots\ldots\ldots\ldots \quad (13)$$

The root means square error (RMSE) is determined using Equation 14:

$$RMSE = \sqrt{(\frac{1}{n}\sum_{i=1}^{n}(Head_{obs} - Head_{sim})_i{}^2)} \quad \ldots\ldots\ldots\ldots\ldots\ldots\ldots\ldots\ldots\ldots\ldots\ldots\ldots \quad (14)$$

3.10. Sensitivity analysis

In this study, sensitivity analysis was performed utilizing the automated calibration method PEST (Parameter Estimation), with a focus on three essential model parameters: hydraulic conductivity (HK), specific storage (Ss), and recharge. These parameters were iteratively adjusted to determine their impact on model performance, while the remaining parameters remained constant. PEST changed these parameters in repeated iterations to reduce the disparity between simulated and observed heads, offering a statistical evaluation of the model's sensitivity to changes in each parameter (Anderson et al., 2015).

PEST identified the most relevant parameters by methodically modifying HK, Ss, and recharge, hence enhancing the calibration process and ensuring the model accurately mirrored real-world conditions (Hassan et al., 2014). In conclusion, employing PEST for sensitivity analysis with HK, Ss, and recharge allowed for a complete examination of the model's performance, resulting in a more accurate calibration and improved knowledge of the important elements impacting groundwater behavior in the study area.

3.11. Structure of integrated SWAT and MODFLOW model

Figure 22a depicts the integrated SWAT and MODFLOW model structure, which combines the surface water model (SWAT) with the groundwater model (MODFLOW). Within this structure, the higher layers, which include the root zone, vadose zone, and shallow aquifer, are assigned to the SWAT model, while the lower layer, which represents the deep aquifer, is assigned to the MODFLOW model (Dowlatabadi et al., 2015). In this study, SWAT and MODFLOW were set up to function separately before being connected via recharge rate exchange. These recharge

rates were initially predicted by the SWAT model and are shown as groundwater recharge values at the Hydrological Response Unit (HRU) level.

Subsequently, during the integration phase, each HRU's recharge rate is exchanged with cells and used as input data for MODFLOW, as shown in Fig. 3.22. However, the semi-distributed structure of SWAT makes it difficult to determine the spatial location of each HRU inside subbasins. To solve this issue, a pragmatic approach is taken, with one HRU developed for each subbasin based on dominant land use, soil type, and slope choice (Dowlatabadi et al., 2015). This approach also helps to understand the catchment's surface and groundwater hydrology, as well as identify the river-aquifer interaction using a surface-groundwater modeling strategy, as explained by Molla et al. (2023).

The schematic diagram provided by Kim et al. (2008) (Fig. 3.22) further emphasizes the exchange of recharge rates from SWAT to MODFLOW, corroborating the integration approach adopted in our study. Through this integration, our model effectively captures the complex interactions between surface water and groundwater systems, providing valuable insights for sustainable water resource management and decision-making.

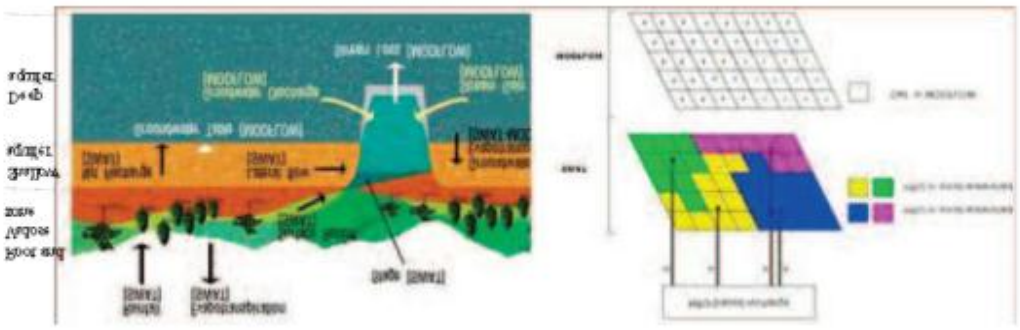

Fig. 22. Schematic diagram of a) combining SWAT and MODFLOW b) exchange recharge rate from SWAT to MODFLOW (Kim et al., 2008)

4. RESULT AND DISCUSSION

4.1. SWAT model run

The SWAT model was executed for the Meki River sub-basin by initially splitting the watershed into 18 sub-basins, which were further divided into 86 Hydro-Logical Response Units. The boundary and HRU analysis were conducted following which the model uses the data from five meteorological stations to simulate the streamflow from 2000 to 2020. The first three years (2000-2002) were used as a warm-up period to stabilize the model before the entire 21 years were simulated. For ensuring that the model was right, calibration and validation procedures were carried out, and the model was run 1000 times over both periods for tuning and testing its predictions.

4.1.1 Sensitivity analysis

Before calibrating the model, a sensitivity analysis was conducted to identify the most influential parameters on streamflow. This step is critical for optimizing model calibration and improving its predictive accuracy. In this study, global sensitivity analysis was performed using the SUFI-2 algorithm, which ranks parameters based on their statistical significance, using p-values and t-statistics. Parameters with smaller p-values and higher absolute t-statistics are considered more sensitive and play a greater role in model outcomes.

A total of fourteen parameters were assessed for sensitivity. The most sensitive parameters identified were R__CN2.mgt, R__SOL_K(..).sol, and V__GWQMN.gw, which had the lowest p-values, indicating their critical importance for calibration. Moderately sensitive parameters like R__ESCO.hru and R__REVAPMN.gw also significantly influenced streamflow predictions. Though less sensitive parameters, such as V__ALPHA_BF.gw and R__SOL_AWC(..).sol, had higher p-values, they still required careful attention to ensure accurate model calibration.

By focusing calibration efforts on the most sensitive parameters, the model's predictive performance was significantly improved, leading to more reliable simulations of watershed hydrology. This is essential for effective water resource management and decision-making.

Table 4.1: The most sensitive parameters in SWAT-CUP for streamflow calibration.

Rank	Parameter Name	Fitted Value	Min Value	Max Value	t-Stat	P-Value
1	R__CN2.mgt	-0.0103	-0.02	0.11	0.9855	0.0191
2	R__SOL_K(..).sol	92.5	0	100	0.982	0.0237
3	V__GWQMN.gw	0.1885	0	0.26	0.9788	0.028
4	R__ESCO.hru	0.0385	0	0.22	-0.9758	0.0319
5	R__REVAPMN.gw	4.199	0	8.84	0.9591	0.0539
6	V__ALPHA_BF.gw	0.05625	0	0.45	-0.9534	0.0614
7	R__SOL_AWC(..).sol	0.00275	0	0.01	-0.938	0.0818
8	R__CANMX.hru	30.595	0	42.2	0.9023	0.1291
9	R__SOL_Z(..).sol	146.25	0	150	-0.8863	0.1504
10	R__CH_K2.rte	1.5255	0.01	8.67	0.8704	0.1717
11	R__HRU_SLP.hru	0.22275	0	0.33	0.8695	0.1729
12	R__GW_REVAP.gw	0.03775	0.02	0.162	0.8443	0.2068
13	R__CH_N2.rte	0.1315	0.01	0.19	0.8044	0.2611
14	V__GW_DELAY.gw	120.675	30	147	0.7533	0.3321

4.1.2. Calibration of model

Calibration is the process of modifying model parameters to match observed data, ensuring the accuracy of the model's predictions. In this study, calibration was carried out on a monthly basis using observed streamflow data from the Meki River subbasin covering the years 2000 to 2009. The SUFI-2 algorithm was employed for calibration, with two key performance metrics the Nash-Sutcliffe Efficiency (NSE) and coefficient of determination (R^2) used to compare observed and simulated streamflow data and assess the model's accuracy. The calibration results showed a strong correlation between observed and simulated streamflow. The model obtained a R^2 value of 0.76, explaining 76% of the variabilities. The NSE value was 0.61, indicating good performance based on Moriasi et al. (2007)'s criteria. The model modestly underestimated streamflow during the calibration period, with an observed mean annual

streamflow of 12.05 m³/s and a simulated value of 7.9 m³/s, resulting in a disparity of roughly 4.15 m³/s. Regardless, the model's performance was deemed satisfactory for calibrating purposes.

Table 4.2. Model performance statistics for calibration period.

Monthly Time Step	Mean monthly stream flow (m3/s)		R2	NSE	P-factor	r-factor
	Observed	Simulated				
2003-2009	12.05	7.9	0.76	0.61	0.61	0.34

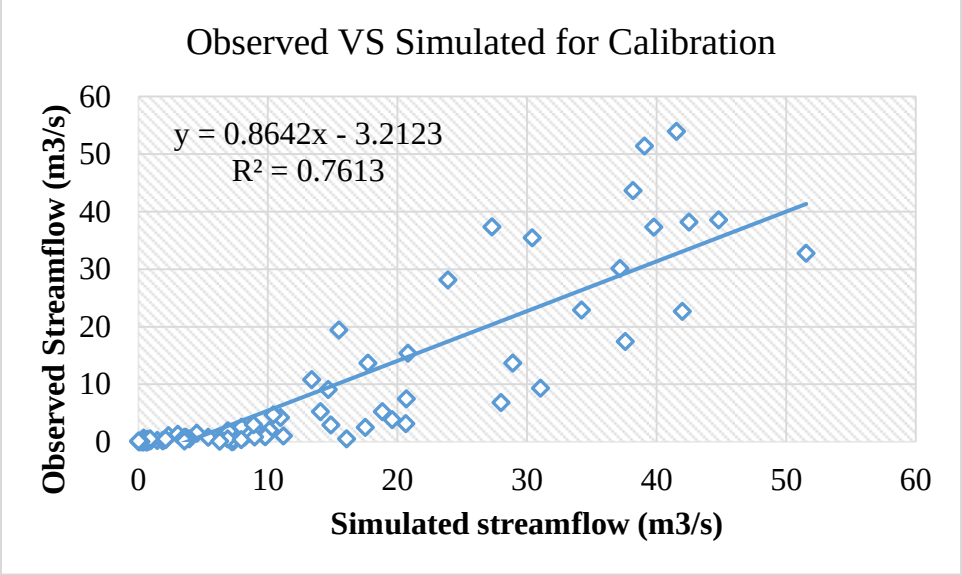

Figure 4.1 Correlation performance of calibration

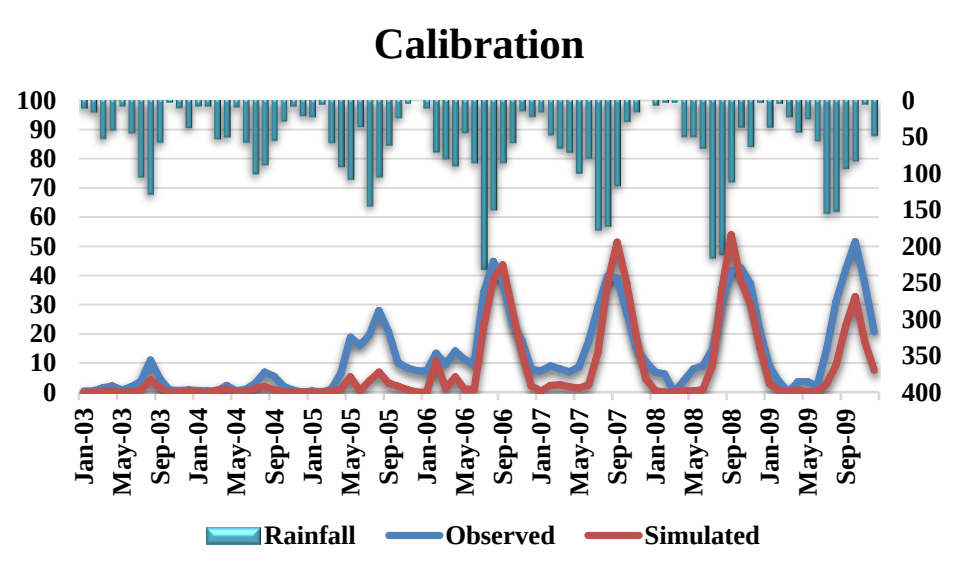

Figure 4. 2 Performance of the model during the 2003–2009 calibration period

4.1.3. Validation of model

Once the model was calibrated, it was tested using data from 2010 to 2013, with no further changes to the parameters. The validation phase evaluated the model's ability to predict streamflow under conditions different from those used during calibration. The results showed that the model successfully predicted streamflow, demonstrating a strong correlation between observed and simulated values. In the validation phase, the R^2 value of 0.85 indicated a strong correlation, while the NSE value of 0.74 reflected solid model performance. The validation results showed better alignment between observed and simulated flow values compared to the calibration period. This suggests that the model's predictive ability improved during calibration and remained stable during validation, underscoring its potential for future water resource management.

Table 4.3: Model performance statistics for validation period

Monthly Time Step	Mean monthly stream flow (m3/s)		R^2	NSE	P-factor	r-factor
	Observed	Simulated				
2010-2013	7.84	4.29	0.85	0.74	0.67	0.29

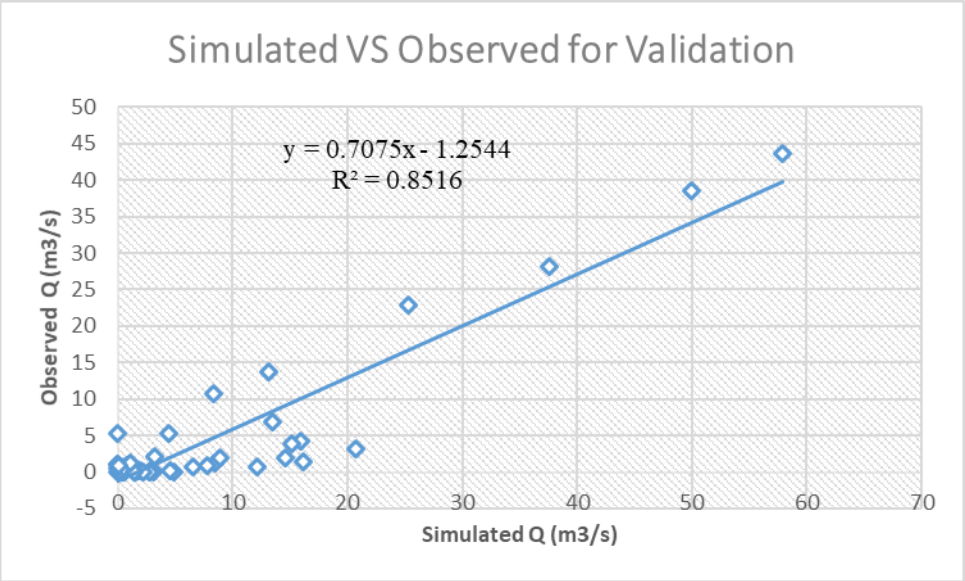

Figure 4.3 Correlation performance of validation

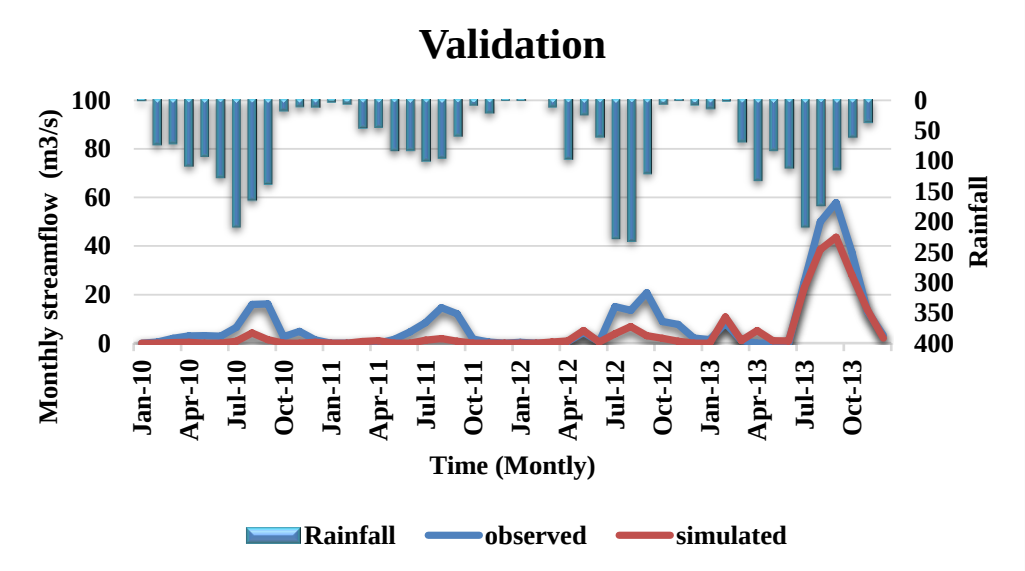

Figure 4.4 Performance of the model during the 2010–2013 validation period

4.1.4. Model performance

The model's overall performance was evaluated based on the graphical comparison of observed and simulated streamflow for both the calibration and validation periods. Figures 4.2 and 4.4 show the strong match between observed and simulated flows, with high R^2 and NSE values

during both periods. The results indicate that the SWAT model is capable of reliably and consistently simulating streamflow, making it a valuable tool for future hydrological research and water resource management in the Meki River sub-basin.

In conclusion, the sensitivity analysis helped identify key calibration parameters, while the calibration and validation outcomes affirmed the model's ability to accurately replicate streamflow. The model's strong performance in both phases supports its application in watershed management decision-making, ensuring that future water resource planning is grounded in reliable and precise hydrological simulations.

4.4. Surface water availability

4.4.1 Mean annual water budget of Meki River sub basin

The calibrated SWAT model parameters have been edited in the SWAT model, and water balance components have been computed for the years 2003 to 2020. Table 4.4 shows the water balance components.

The temporal variation of water balance components in the Meki River watershed demonstrates significant annual variability, mostly influenced by precipitation patterns. Annual precipitation averages 932.8 mm, fluctuating notably from a low of 587.44 mm in 2006 to a peak of 1275.63 mm in 2017. Higher precipitation years, such as 2017, correlate strongly with increased surface runoff, highlighting a direct relationship between rainfall intensity and runoff volumes. Despite a moderate average, the watershed experiences pronounced year-to-year fluctuations, underscoring its sensitivity to climatic changes and the consequential impact on water availability and distribution.

Surface runoff, averaging 337.82 mm annually, demonstrates similar variability, with peaks observed in high precipitation years like 2017 (519.08 mm) and lows in drier periods such as 2007 (139.42 mm). This variability suggests rapid responses to rainfall events, influenced by infiltration capacities and land cover conditions. Lateral flow, averaging 21.25 mm per year, remains relatively stable across different years, indicating consistent subsurface flow paths unaffected by annual precipitation variations.

Groundwater flow averages 101.7 mm annually, ranging widely from 0.53 mm in 2006 to 263.63 mm in 2018, aligning closely with periods of increased percolation and precipitation. Percolation rates, which reflect infiltration into groundwater, vary significantly, with a low of 1.59 mm in 2006 and a high of 287.82 mm in 2018. Higher percolation years coincide with increased groundwater flow and precipitation, suggesting substantial groundwater recharge events.

The components of evapotranspiration (ET) and potential evapotranspiration (PET) further clarify the watershed's hydrological dynamics. Evapotranspiration (ET) averages 448.69 mm annually, reflecting a stable pattern influenced by vegetation and soil conditions. In contrast, potential evapotranspiration (PET) averages 817.07 mm annually, consistently exceeding actual ET due to water availability constraints rather than atmospheric demand. Water yield, which averages 466.95 mm annually, exhibits wide fluctuations from 153.61 mm in drier years like 2007 to 706.51 mm in wetter years such as 2018. These variations underscore the watershed's sensitivity to climatic shifts, impacting water availability and distribution dynamics.

In summary, the Meki River watershed exhibits significant variability in water balance components, particularly influenced by annual precipitation variations. These dynamics impact surface runoff, groundwater flow, and percolation rates, crucial for understanding water availability and sustainability. Effective water resource management strategies must consider these fluctuations to mitigate risks associated with climatic variability and ensure sustainable use of water resources across the watershed.

Table 4.4 Water balance components of Meki river watershed.

TIME	PREC	SURQ	LATQ	GWQ	PERC	ET	PET	WATER YIELD
Year	(mm/yr)	(mm/yr)	(mm/yr)	(mm/yr)	(mm/yr)	(mm/yr)	(mm/yr)	(mm/yr)
2003	910.9	303.44	17.38	56.34	81.9	424.5	833.6	382.4
2004	963.13	329.64	25.51	126.05	152.41	499.81	849.79	483.44
2005	1024.28	482.16	20.55	120.23	126.88	438	834.78	635.24
2006	587.44	188.41	9.22	0.53	1.59	420.18	921.77	199.86
2007	691.81	139.42	12.97	0.69	22.24	457.65	858.54	153.61

2008	914.36	320.56	20.85	81.81	121.27	451.48	804.59	428.37
2009	1014.63	408.78	17.83	58.2	75.54	444.84	816.62	489.01
2010	823.51	298.92	15.48	44.59	72.37	444.75	816.67	362.33
2011	836.63	362.03	14.8	28.4	46.82	488.3	918.3	408.07
2012	1044.43	289.52	28.81	173.26	196.63	477.43	788.41	498.98
2013	869.99	370.66	22.52	109.5	141.94	403.69	815.97	509.49
2014	917.71	264.41	23.22	133.9	158.01	431.59	758.67	430.43
2015	897.83	427.02	17.14	94.44	113.26	392.42	752.05	544.77
2016	941.75	245.26	23.91	121.44	146.07	480.32	792.85	397.05
2017	1275.63	519.08	25.63	136.71	157.45	479.97	799.84	687.79
2018	1099.94	392.87	35.53	263.63	287.82	454.67	759.2	706.51
2019	1043.63	400.76	29.88	179.14	223.61	438.09	768.54	620.83
Average	932.8	337.82	21.24882	101.6976	125.0476	448.6876	817.07	466.9518

The time series graph depicting several simulated components shows the behavior of parameters over time (Fig. 4.5). All components vary temporally in response to rainfall patterns, with larger concentrations found in wetter years such as 2018. Conversely, the lowest values were observed in 2006, the driest year. This graph depicts the dynamic variations in the behavior of various components in response to rainfall and time.

Fig. 4.5 illustrates the temporal dynamics of these components, showing heightened concentrations during high rainfall years like 2018 and diminished concentrations in low rainfall years such as 2006. This temporal variability underscores the sensitivity of water balance components to annual rainfall fluctuations, crucial for understanding watershed hydrology and guiding effective water management strategies.

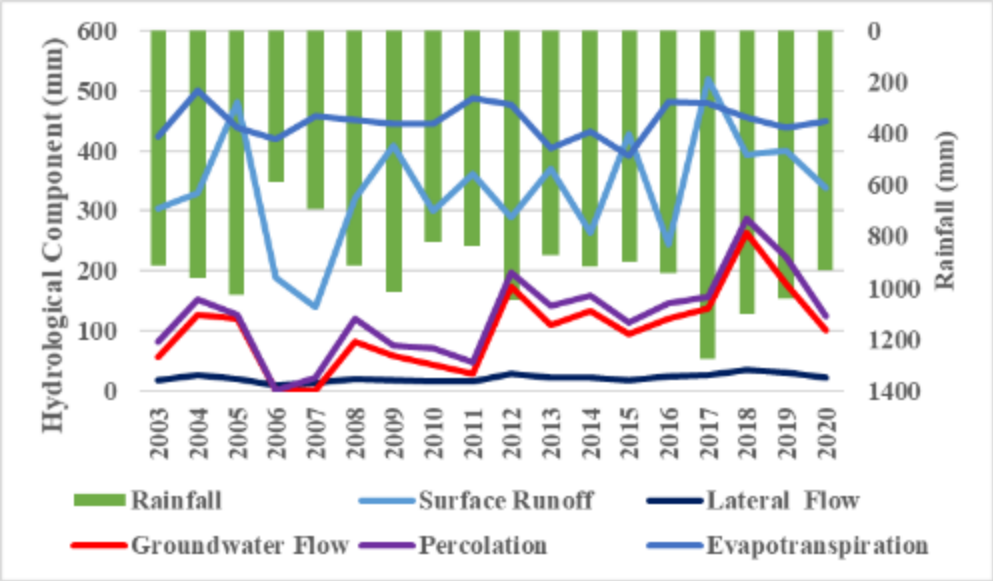

Fig.4.5. Yearly water balance components.

4.4.2. Average monthly water balance components

Table 4.6 displays the average monthly surface water balance components calculated by the SWAT (Soil and Water Assessment Tool) model for a specified location. Precipitation (PRECIP) averages 932.8 mm per year, with seasonal fluctuations including peaks in June (94.5 mm) and lows in March (56.03 mm). Surface runoff (SURQ) peaks in March (84.73 mm) and April (77.97 mm), most likely due to heavy rainfall or limited soil infiltration capacity, then falls to a low in May (11.17 mm) and June (10.98 mm).

Lateral flow (LATQ) remains relatively low throughout the year, increasing slightly in April (1.55 mm), May (2.64 mm), June (3.03 mm), and July (3.06 mm). Groundwater flow (GWQ) or baseflow reaches its highest in July (15.31 mm) and is lowest in February (1.71 mm) and March (0.41 mm), indicating significant recharge during the rainy season and reduced flow in drier months.

Percolation (PERC), reflecting water moving from soil to groundwater, peaks in April (20.21 mm) and May (20.15 mm), suggesting high infiltration rates during these months. Soil water content (SW) peaks in January (488.08 mm) and decreases steadily to its lowest in August (119.9 mm). Evapotranspiration (ET), including evaporation and plant transpiration, peaks in July (77.49 mm) and is lowest in January (3.7 mm). Potential evapotranspiration (PET) peaks in

July (145.79 mm) and is lowest in January (8.01 mm), indicating higher atmospheric water demand during warmer months.

The data reveals distinct seasonal patterns with peak precipitation, surface runoff, and water yield during the rainy season (March to September). Conversely, the dry season (October to February) shows significantly reduced surface runoff and water yield, along with lower soil water content and evapotranspiration. Groundwater dynamics exhibit seasonal fluctuations, with peak groundwater flow coinciding with mid-rainy season (July) and minimal flow towards the end of the dry season (March), reflecting recharge and depletion cycles.

The contrast between actual ET and PET throughout the year indicates that the region experiences water limitations affecting evaporation and transpiration rates. This suggests potential water stress periods when actual evapotranspiration falls short of potential under optimal conditions. Understanding these seasonal dynamics is essential for effective water resource management, informing strategies to enhance water use efficiency, mitigate drought risks, and sustain ecosystem health in the studied area. Overall, this table provides a complete overview of the hydrological behavior of the watershed, showing how different components of the water balance vary seasonally.

Table. 4.5. Mean monthly surface water balance component by SWAT model.

Month	PREC (mm)	SURQ (mm)	LATQ (mm)	GWQ (mm)	PERC (mm)	ET (mm)	PET (mm)	YIELD(mm)
Jan	62	21.43	0.12	5.22	0	3.7	8.01	27.63
Feb	62.32	23.14	0.04	1.71	0	7.52	17.63	24.93
Mar	56.03	84.73	0.14	0.41	2.03	19.9	36.08	85.37
Apr	60.64	77.97	1.55	3.6	20.21	35.76	60.02	83.87
May	86.42	11.17	2.64	10.33	20.15	57.28	123.66	24.68
Jun	94.5	10.98	3.03	13.86	17.73	61.15	121.45	28.35
Jul	94.24	13.69	3.06	15.31	14.54	77.49	145.79	32.81
Aug	88.69	10.81	2.58	11.98	8.07	71.49	130.21	25.93
Sep	83.53	12.96	2.51	7.79	11.5	49.82	84.55	23.79
Oct	81.86	13.2	2.77	9.09	15.82	38.72	55.51	25.37
Nov	90.93	32.95	2.11	11.75	13.87	17.46	21.63	47.18
Dec	71.64	24.8	0.69	10.65	1.12	8.4	12.54	37.04
Mean	932.8	337.82	21.25	101.7	125.04	448.69	817.07	466.96

4.4.3. Sub basin spatial variation of water balance

The table presents averaged hydrological data across various sub-basins, revealing insights into the dynamics of water balance components. Water yield (WYLDmm) remains relatively stable, ranging from 36.33 to 39.06 mm, closely tied to precipitation, evapotranspiration (ETmm), and surface runoff (SURQmm) dynamics. Groundwater discharge (GW_Qmm) exhibits variability from 5.84 to 9.46 mm, indicating fluctuations in groundwater recharge and baseflow contributions. Evapotranspiration levels vary notably, with values ranging from 11.30 to 38.10 mm, including an outlier scenario at 11.30 mm, likely influenced by unique environmental conditions affecting water loss through evaporation and plant transpiration.

Surface runoff shows moderate variability, ranging from 25.70 to 30.08 mm, reflecting differences in precipitation intensity and soil characteristics impacting water movement over the land surface. Percolation (PERCmm) ranges from 7.63 to 11.45 mm, highlighting variations in soil properties and processes governing water infiltration into the groundwater system. Soil water content (SWmm) varies significantly from 138.90 to 164.36 mm, indicating diverse soil moisture regimes across the sub-basins. Precipitation (PRECIPmm) ranges from 22.22 to 77.77 mm, with lower values potentially indicating periods of reduced rainfall affecting overall water availability. Potential evapotranspiration (PETmm) ranges widely from 19.47 to 68.13 mm, with an outlier at 19.47 mm suggesting distinct conditions impacting water loss potential due to factors such as climate variability or land use changes.

In scenarios with high water yield and groundwater discharge (WYLD = 39.06 mm, GW_Q = 9.34 mm), abundant water resources and significant groundwater contributions are evident, accompanied by high surface runoff and effective percolation processes. Conversely, scenarios with low evapotranspiration (ET = 11.30 mm) indicate exceptionally low water loss through evaporation and plant transpiration, paired with high soil water content (SW = 164.36 mm) and minimal precipitation (PRECIP = 22.22 mm), possibly indicating drought conditions or limited vegetative cover.

A scenario with high percolation (PERC = 11.45 mm) suggests effective water infiltration into the groundwater system, supported by high groundwater discharge (GW_Q = 9.46 mm) and

moderate surface runoff (SURQ = 27.93 mm), indicating favorable conditions for groundwater recharge and sustainable water availability.

Estimating the spatial distribution of runoff source areas has significant consequences for watershed operations. The spatial distribution of surface runoff, groundwater flow, and percolation has been calculated. Figure 4.8 shows that the watershed's surface runoff was lower in the northern part and higher in the eastern region. The southern region produced a higher concentration of runoff due to agricultural landuse and hilly slope. The northern portion has areas with depths ranging from 292 to 303 mm. Surface runoff in the River watershed ranged from 332 to 343 mm in the eastern section of the study area (the highest surface runoff area), with 323 and 332 mm primarily observed in the southern region.

Increased runoff might be caused by a loss in canopy interception, percolation, and evapotranspiration, while a decrease in runoff indicated a reduction in soil water storage. Groundwater flow in the watershed was very high in the southern part and low in the eastern region (Fig.4.8). Groundwater flow increased on higher slopes and decreased on lower slopes. The northern region has a larger concentration of groundwater flow to the stream due to significant infiltration, while agricultural areas have lower concentrations due to tile drainage domination. Compared to surface runoff, lateral flow was higher in high-infiltration regions and lower in flat terrain. Fig.4.6 shows that the northern region contributes significantly to streamflow through lateral flow.

The groundwater contribution to streamflow (GW_Q) exhibits notable variability, with maximum and minimum values observed in 2018 (263.63 mm) and 2006 (0.53 mm), respectively. Interestingly, 2018 marked the second-highest rainfall year, indicating a strong correlation between rainfall intensity and groundwater flow dynamics. During the calibration period, the highest annual groundwater flow was recorded, underscoring the influence of precipitation on groundwater recharge. This trend is further supported by Table 4.5, which shows an increasing trend in GW_Q with rising rainfall amounts.

Lateral flow (Lat-Q) similarly shows significant variability, peaking in 2018 (35.53 mm) and hitting its lowest in 2006 (9.22 mm). This pattern aligns with rainfall data, where 2018 stands as the second-highest rainfall year and 2006 as the lowest. Percolation (PERCO) follows a

comparable trend, reaching its highest in 2018 (287.83 mm) and its lowest in 2006 (1.59 mm), highlighting its sensitivity to rainfall variations.

Evapotranspiration (ET) exhibits maximum and minimum values in 2004 (499.81 mm) and 2013 (403.69 mm), respectively. These variations are influenced by factors such as vegetation canopy development and solar radiation fluxes, crucial for water loss from the watershed. Water yield (WYLD) peaks in 2018 (706.51 mm), contrasting sharply with its minimum in 2007 (153.61 mm), aligning with the highest rainfall year observation. The dependence of water yield on runoff, groundwater flow, and lateral flow underscores its direct relationship with precipitation patterns.

The simulation model indicates that approximately 39-50% of rainfall is lost through evapotranspiration, while lateral flow contributes minimally to overall water loss. Groundwater flow and percolation contribute 0.1–4% and 0.3–26% of total rainfall, respectively, with variations linked closely to rainfall variability. High rainfall years see significant proportions of rainfall converted into surface runoff (around 40%), groundwater flow (24%), and lateral flow (3%), highlighting their responsiveness to precipitation dynamics. Conversely, low rainfall years result in reduced surface runoff (32%) and minor contributions from groundwater flow (0.1%) and lateral flow (1.6%).

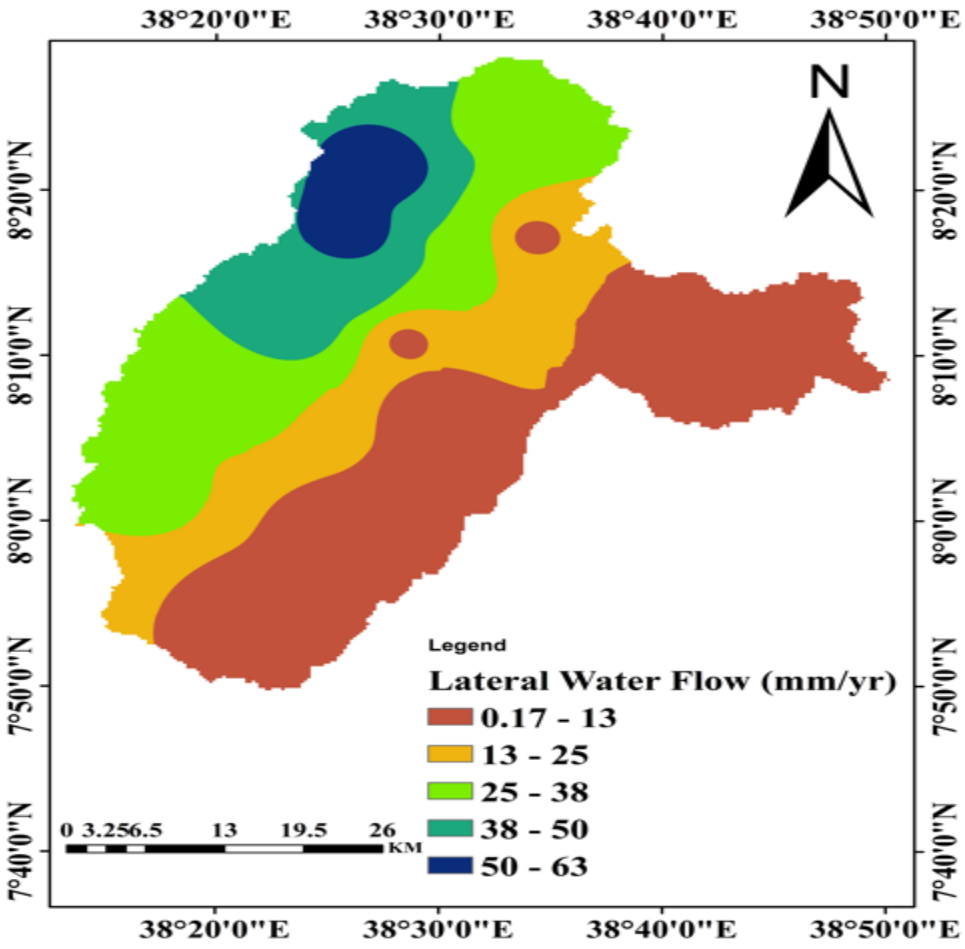

Fig. 4.6. Spatial distribution of lateral flow contribution to streamflow in subbasin.

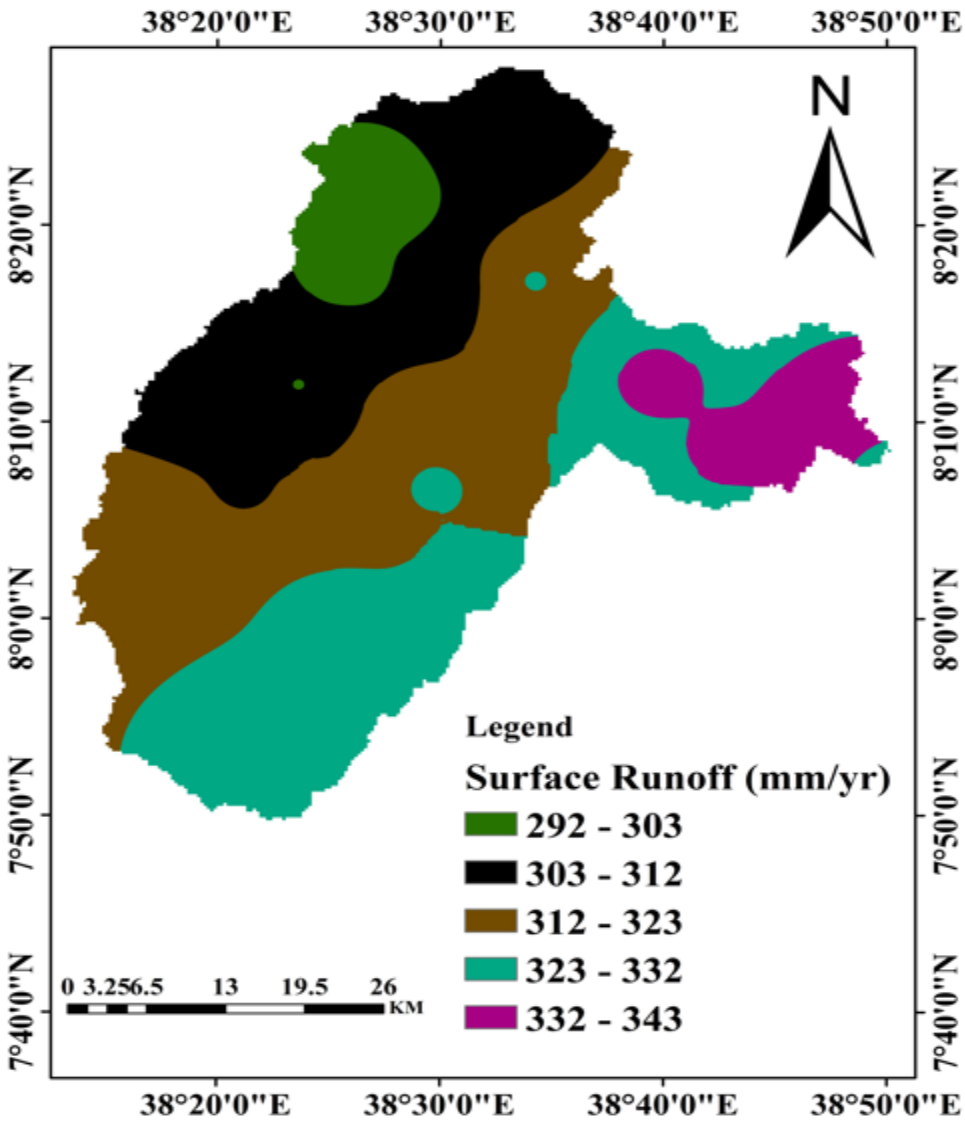

Fig.4.7. Spatial distribution of surface runoff contribution from streamflow.

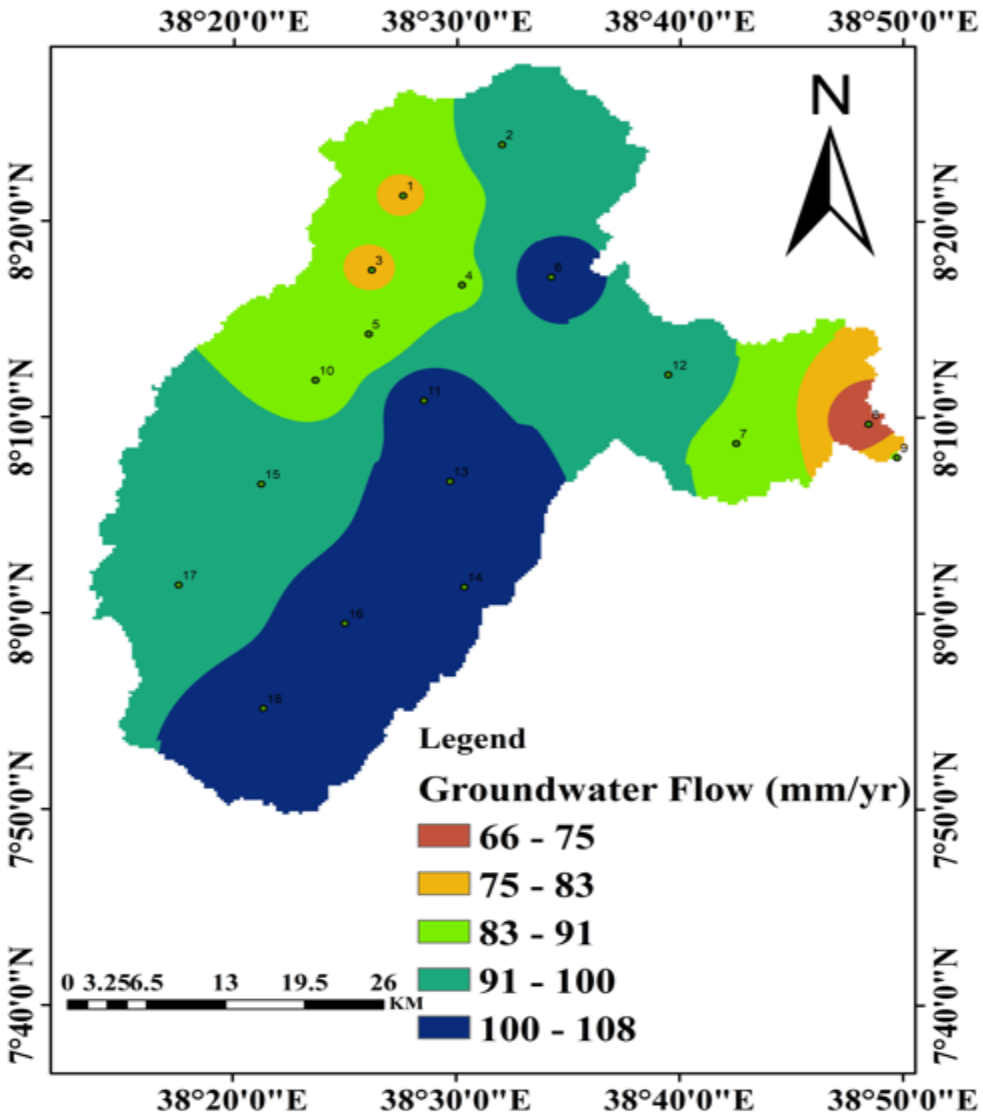

Fig.4.8. Spatial distribution of groundwater contribution to stream in subbasin.

4.5. Groundwater modelling

After the aquifer's recharge and evapotranspiration were estimated using the calibrated model in the SWAT software, the aquifer was modeled for steady state circumstances using Modelmuse software. The measured water levels in the Meki river catchment aquifer were utilized for calibration. The steady state period was chosen from January 1st, 2000 to December 31st, 2020, based on the availability of observed groundwater data.

4.6. Head calibration

4.6.1. Calibrated heads and error assessment

Calibrated heads and error assessment reveals several key findings about the groundwater model's accuracy and reliability. Figure 4.9 depicts a scatter plot of residuals that shows the relationship between observed and computed heads across 62 piezometers. It shows a substantial relationship between observed and computed values. This is supported by the coefficient of determination (R2) of 0.9922, which indicates that the model accurately represents the variability in groundwater levels across the research area. The observed head values ranged from 1682m to 2171m, with a total change of 489m, which helps to comprehend the dataset's variability. Notably, the largest absolute values for model residual, RMSE, and MAE are 35.699m, 9.46m, and 7.22m, respectively (see Appendix IX).

When these metrics are compared to Anderson et al. (2015)'s suggested thresholds, the results are good, with estimated RMSE, MAE, and maximum absolute residuals falling well within acceptable ranges of 1.9%, 1.5%, and 0.7%, respectively. These results are compatible with the criteria established by Anderson et al. (2015), which state that RMSE, MAE, and MA should be less than 2%, 2%, and 10%, respectively. Further analysis shows a mean absolute inaccuracy of -3.369 m, demonstrating an overall tendency to overestimate heads. This observation is supported by the presence of negative residuals in the scatter plot, which confirms the model's performance features. The model effectively meets the evaluation requirements, indicating its viability for future applications.

The strong correlation coefficient of 0.99967 between observed and estimated values supports the model's correctness and fit to the observed data. This suggests that the optimized parameters employed in the model accurately reflect the behavior of the groundwater system.

To summarize, groundwater calibration utilizing the PEST methodology resulted in a well-fitted model with optimal parameter values, allowing for credible simulations and predictions of groundwater behavior. The extensive study of residuals and correlation coefficients provides vital insights in the model's performance.

Table 4.6 Shows the calculated error assessment and comparison to the indicated values by Anderson et al. (2015). The units are in meters.

	ME	MAE	RMSE
The steady state model calibration results	-3.31	7.22	9.46
Suggested value of MAE, RMSE and MA (2%, 2%, 10% of total head changes) respectively	0.7	1.5	1.9

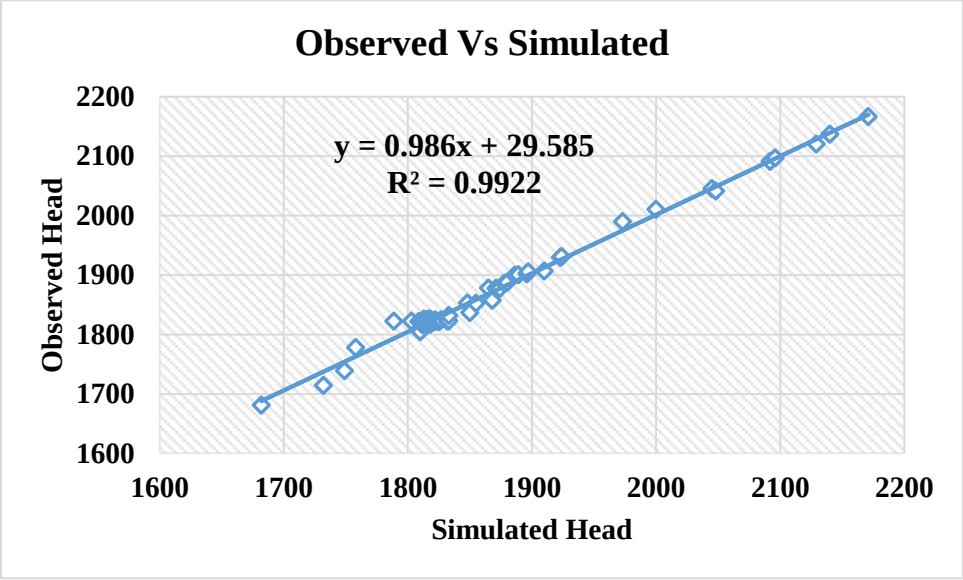

Figure 4.9. Scatter plot of observed and simulated hydraulic head

4.6.2. Residual analysis

The graph depicted in Figure 4.6 displayed residual plot after model calibration. Residuals signify the disparity between measured and simulated values. Examination of these residuals offers valuable information about the model's performance and the accuracy of its simulation. As depicted in Figure 4.6, the residuals exhibited fluctuations around zero, indicating that, on average, the model neither consistently overestimated nor underestimated the measured values. The magnitude of residuals varied across observations, spanning from -35.6993 to 13.6238. Positive residuals denoted instances where the simulated value exceeded the measured value, whereas negative residuals indicated the opposite. The trend of residuals showcased a mixture of positive and negative values across observations, illustrating spatial variability in the model's

performance. Outlying residuals, such as -35.6993 and 13.6238, potentially highlighted areas warranting attention, where the model significantly diverged from observed values.

Further analysis of residuals revealed that the majority clustered around zero, suggesting satisfactory model performance. The mean value of non-zero weighted residuals approximated -3.210, implying a slight overall underestimation. The standard variance of weighted residuals stood at 89.53, signifying variability in model performance across observations.

Additionally, in Figure 4.10, the distribution of observed head and residual distribution were compared. Among the 62 piezometers, 22 were found to be underestimated while the remaining 40 were over-simulated, indicating a balanced model with no predominant systematic errors in either direction.

Overall, the significant correlation coefficient and residual distribution showed that the calibrated model accurately represented the hydrogeological processes that influence groundwater flow and recharge.

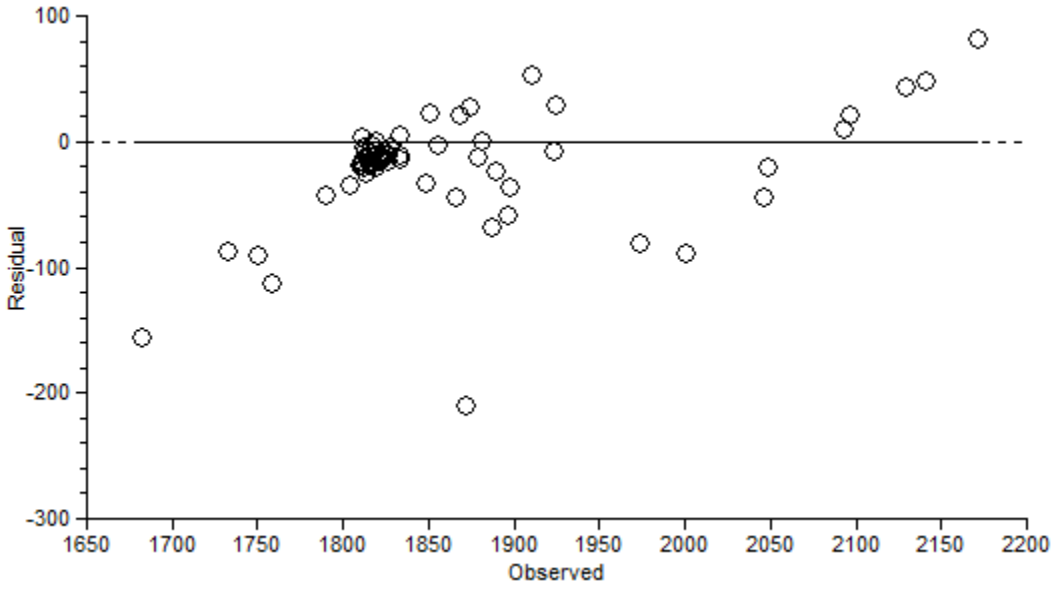

Figure.4.10. Residual and observed head distribution

4.7. Groundwater head simulated distribution spatial

After calibrating the groundwater model, a groundwater contour map was created using MODFLOW simulated heads (Modelmuse 5.1). Figure 4.11 depicts the distribution of heads throughout each active cell in the groundwater flow model, which is an important conclusion.

This distribution reveals that groundwater primarily flows from the western escarpment and Butajira pediment (northeast) sectors of the catchment towards the Tora-koshe-dugda ridge boundaries. Notably, closely spaced contours in the upper catchment or western escarpment to denote areas with low aquifer hydraulic conductivity, while the central and southeastern regions exhibit more widely spaced contours, indicating relatively higher hydraulic conductivity (Molla et al., 2023; Cohen and Cherry, 2020).

Furthermore, the image shows that at the upper portions of the catchment, the groundwater head contours are tightly spaced, indicating low hydraulic conductivity of the aquifers and significant groundwater recharge. Conversely, the Butajira pediment and koshe-dugda ridge boundaries predominantly feature more widely spaced contours, indicative of relatively higher hydraulic conductivity of aquifers (Molla et al., 2023; Cohen and Cherry, 2020).

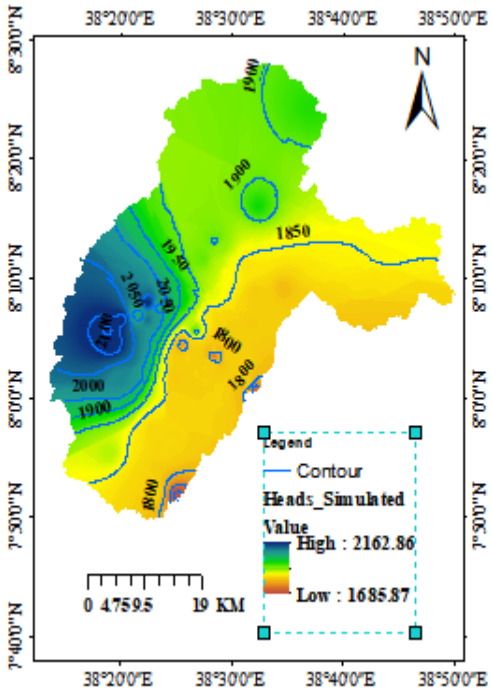

Fig. 4.11 Groundwater head distribution

4.8. Spatial variability of river-groundwater interactions

The interactions between rivers and groundwater were investigated using MODFLOW-NWT's river package to model water leaks into and out of the groundwater system. The research shows that water exchange happens in practically every cell along the river, with significant spatial variation and connectivity between rivers and the aquifer. Figure 4.12 shows the MODFLOW-

simulated river-groundwater interactions, which highlight the gaining (groundwater discharge/baseflow) and losing (groundwater recharge) river stretches. Integrated modeling results show that around 9.1 Mm^3 of water leaks into the groundwater system each year, while the flux from groundwater to rivers is around 35.1 Mm^3.

The Tora-Koshe-Dugda area has the highest gaining reaches of the Meki River, with fluxes of up to 96,198.128 m^3/day. The center catchment areas have the lowest gaining reaches. The western escarpment has the largest losing reaches, with medium loss at the catchment outflow and the lowest loss in the center of the Meki River subbasin. Gaining stretches occur mostly in the Tora-Koshe-Dugda river network, particularly near the basin's major exit, where the topography is practically flat and groundwater heads are high and close to the land surface. Most portions of the Meki River are integrated with the groundwater system, and groundwater inflow to streams is greater.

The river network has an average groundwater discharge of 96,118.128 m^3/day and a recharge rate of 24,866.406 m^3/day. This balance suggests a near-equilibrium state in surface-groundwater exchange, albeit the spatial distribution of these interactions varies greatly across the basin. The type of interaction is impacted by the region's topography. In high-elevation places, river cells mostly receive groundwater, but in flatter regions, the river discharges water into the aquifers. The majority of tributaries in the modeled aquifer area are losing (influent) rivers, which recharge groundwater by seepage via riverbeds and banks. However, the overall groundwater recharge in these parts is minor when compared to the groundwater outflow from the gaining reaches.

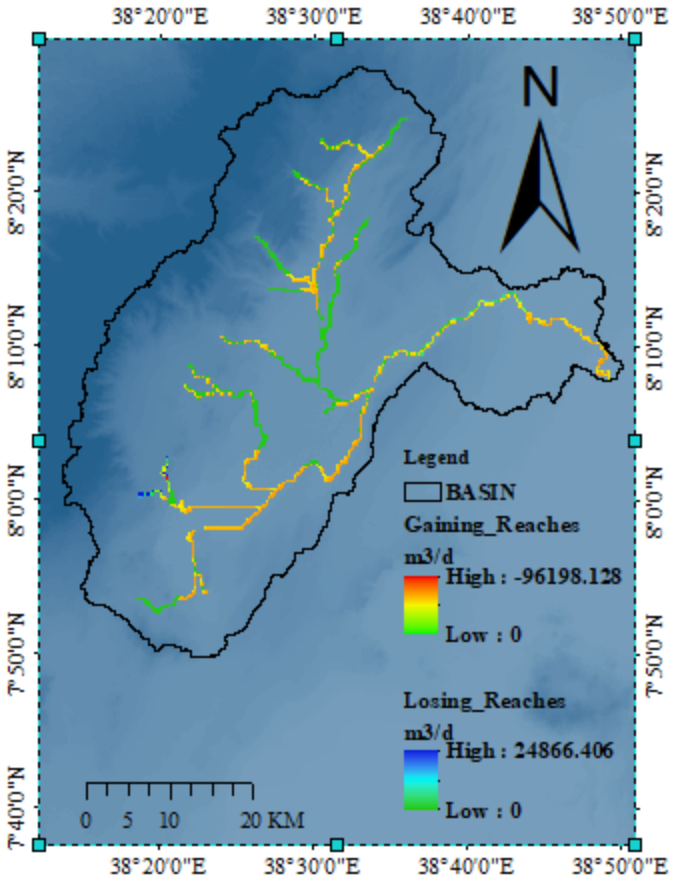

Fig. 4.12; Spatial variation of Surface Water-Groundwater interaction.

4.9. Groundwater budgets

The volumetric budget for the full steady state model at the conclusion of time step 1, stress period 1, provides vital information about the flow dynamics in the system. This budget includes both inflows and outflows, providing insight into the model's water sources and sinks. Table 4.7 provides details on the water balance results obtained from the ModelMuse model listing files. Groundwater balance data show that the research region has a total input and outflow of 40.947189 million cubic meters per year (Mm^3/year). The research area's recharge rate is predicted to be 23.5 Mm^3/year, accounting for 57.4% of total inflow. This substantial recharge emphasizes the importance of natural replenishment in sustaining the aquifer.

The STORAGE component indicates no changes in storage, meaning there is no net addition or removal of water from the groundwater storage. This suggests that the aquifer is in a steady state with respect to storage changes over the simulation period. The CONSTANT HEAD

package simulates boundaries where the head (water level) is kept constant. A significant inflow (23,002.698 M^3/day) compared to the outflow (888.8766875 M^3/day) suggests that water is predominantly entering the system from these boundaries. This could indicate recharge from constant head boundaries like lakes or reservoirs. Wells are extracting groundwater (outflow only). The total extraction rate is 243.4445469 M^3/day, which over a year sums up to 88,857.25962 M^3/year. This is the volume of water being pumped out of the groundwater system by wells.

This package demonstrates a substantial relationship between the river and the groundwater system. A significant amount of water is seeping from the river into the groundwater (24,866.406 M3/day), while an even greater volume (96,198.128 M3/day) is leaving the groundwater for the river, indicating that the river is a key discharge location for the groundwater system. ET reflects the loss of groundwater caused by evaporation and plant transpiration. The findings show a daily loss of 9,178.56 M3/day, totaling 3,350,174.4 M3/year, indicating considerable groundwater release via ET. River and stream leakage are important aspects of groundwater dynamics. River leakage adds 24,866.41 m^3/day to the inflow and 96,198.13 m^3/day to the outflow, showing significant groundwater discharge onto surface water bodies. This interaction plays an important role in the subbasin's entire hydrological cycle.

HDB often indicates boundaries where flow is determined by the hydraulic head difference. The outflow (5,675.0715 M3/day) indicates that water is leaving the system via these boundaries. Recharge is the addition of water to the groundwater system, usually via precipitation. The findings show a strong influx (64,314.976 M3/day), indicating a high recharge rate into the groundwater system. In general, total input equals total outflow, showing a balanced model with no disparities in the water budget. This balance is critical for determining the model's correctness. A percent disparity of 0 means that the model's water budget is entirely balanced, with no errors or losses in the calculations.

This groundwater model demonstrates a well-balanced water budget with considerable interactions among several components such as constant head boundaries, river leakage, and recharge.

Model accuracy: The difference between inflows and outflows is 0.000%, which is well within the allowed range of ≤1%. This high level of accuracy in the model's water balance contributes

to the simulation findings' trustworthiness. Large inflows from stable head borders and recharging. Significant outflows into rivers and by evapotranspiration. Groundwater extraction using wells and head-dependent barriers. Understanding these components aids in the successful management of groundwater resources, forecasting the effects of diverse activities, and assuring the long-term usage of the aquifer system.

Understanding the various components of inflow and outflow, as well as their consequences for water resource management and sustainability, is required to interpret and analyze the groundwater budget results provided for the Meki River sub-basin. The groundwater budget analysis shows that the groundwater system in the Meki River sub-basin remained largely stable during the chosen time step and stress period. The balance of inflows and outflows indicates that the model accurately reflects the water balance in the research area. The equal total inflows and outflows indicate a balanced groundwater system, implying that the aquifer is not being drained or overly refilled. This stability is critical to long-term water resource management.

Table 4.7. Steady state Groundwater budget

Package	IN (M^3/day)	OUT (M^3/day)	IN (M^3/year)	OUT (M^3/year)
STORAGE	0	0	0	0
CONSTANT HEAD	23002.7	888.8767	8395985	324440
WELLS	0	243.4445	0	88857.26
RIVER LEAKAGE	24866.41	96198.13	9076238	35112317
ET	0	9178.56	0	3350174
HEAD DEP BOUND	0	5675.072	0	2071401
RECHARGE	64314.98	0	23474966	0
TOTAL	112184.1	112184.1	40947189	40947189
PERCENT DISCREPA			0	0
IN	-	OUT	=	0

4.10. MODFLOW sensitivity analysis

Model calibration and sensitivity analysis were carried out using a parameter estimation software (PEST). The sensitivity analysis offered in the output sheds light on how changes in model parameters affect model outputs, as well as the relative importance of each parameter in

explaining the observed data. Sensitivity measures the effect of a parameter change on the objective function (often the model output) and is critical for determining which parameters are most significant in driving model behavior.

As shown in fig. 4.13, the sensitivity analysis provided shows the impact of parameter variations on the model's output, with a particular focus on three parameters: specific storage, horizontal hydraulic conductivities, and recharge, to determine their influence on groundwater level. Figure 4.13 demonstrates that the groundwater model was most responsive to horizontal hydraulic conductivity, followed by recharge and specific storage.

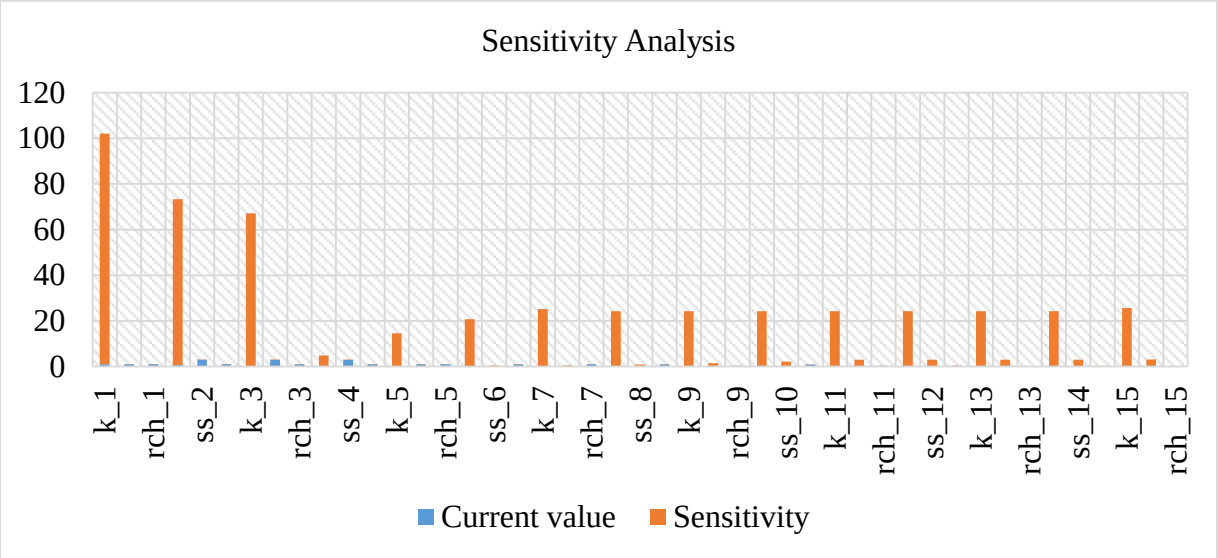

Fig. 4.13. MODFLOW Sensitivity Analysis

5.CONCLUSION AND RECOMMENDATION

5.1. Conclusion

In this work, the SWAT and MODFLOW models were utilized to simulate surface and groundwater in the Meki River subbasin. The SWAT and MODFLOW were conducted separately and then joined together using recharge rates. The hydrological input for the MODFLOW cells was the recharge values taken from the SWAT model's HRUs. The simulation results for two corresponding models, including stream flow and groundwater level, were then compared, and they agreed well with the observed data. According to statistical criteria (NSE= 0.61, R2= 0.76) for calibration and (NSE= 0.74, R2= 0.85) for validation, the river discharge at the watershed's outlet was accurately simulated. Furthermore, the RMSE and R2 for 62 observation wells throughout the calibration period were 9.46 m and 0.9922, respectively, indicating a strong agreement between observed and simulated groundwater level trends.

The MODFLOW groundwater model enhances SWAT by incorporating HRU-based recharge rates into aquifer simulations. The model achieves a strong correlation (R^2 = 0.9922) between observed and simulated groundwater levels across 62 piezometers, indicating excellent agreement. Error metrics such as RMSE (9.46 m) and MAE (7.22 m) validate model accuracy within acceptable limits. Spatial analyses reveal heterogeneous groundwater flow influenced by local hydrogeological conditions and surface-water interactions, supporting reliable hydrogeological assessments.The groundwater head distribution analysis shows flow primarily from the western escarpment towards the Tora-Koshe-Dugda ridge boundaries, with varying hydraulic conductivity influencing head distributions across different sectors of the catchment. Areas with low hydraulic conductivity, such as the western escarpment and Butajira pediment, exhibit closely spaced contours, indicating slower groundwater movement and higher recharge rates. In contrast, regions with higher hydraulic conductivity, particularly in the central and southeastern parts, display widely spaced contours, reflecting faster groundwater flow and lower recharge rates.

The study of river-aquifer interactions reveals large transfers between rivers and the aquifer. The model forecasts an average groundwater discharge into the river of 91,198.128 m^3/day,

exceeding recharge from the river to the aquifer by 24,866.406 m^3/day. This highlights the importance of these interactions in the sub-basin's hydrological balance. The MODFLOW model's calibration provides a solid foundation for studying the hydrogeological processes of the Meki River subbasin. Despite considerable overestimation, the model's performance indicators, such as RMSE and MAE, are within acceptable limits, indicating its trustworthiness for future applications. However, the model's trustworthiness is limited by the lack of precise hydrostratigraphic data, the presence of uncertainties and assumptions for model simplification, and the removal of geothermal impacts, abstractions, and groundwater evapotranspiration.

5.2. Recommendations

Based on the study's findings, various comprehensive recommendations can be made to improve water resource management and secure long-term water use in the Meki River Basin. These proposals address the geographical and temporal variability in streamflow, groundwater, and surface water-groundwater interactions throughout the basin. Managing the observed geographical and temporal fluctuations in streamflow needs a multifaceted strategy. Seasonal water allocation strategies should be designed and implemented to meet water shortages during dry years while also managing excess water during wet seasons. These strategies should prioritize water availability for vital purposes such as home supply, agriculture, and environmental protection.

It is critical to strengthen the basin-wide data gathering and monitoring networks. Continuous monitoring of streamflow, precipitation, and evaporation rates will give the accurate and timely data required for model calibration and decision making. To fill data gaps in underserved areas, sophisticated hydrometeorological stations and community-based reporting systems may be deployed. To prevent high runoff and soil erosion, land-use methods should be maximized. Reforestation, terracing, and the use of no-till farming techniques can improve soil water retention and infiltration, which is essential for maintaining base flows during dry periods. Long-term research on the effects of land-use changes and climate variability on streamflow should also be considered in planning efforts

Decision-makers should employ streamflow estimates under various climate and land-use scenarios to prepare for and mitigate future difficulties. Groundwater management is crucial for sustaining the basin's water supplies, especially in locations where groundwater is the principal water source. Groundwater recharge zones in the highlands of the western escarpment must be protected and restored. This can be accomplished through afforestation and soil conservation methods that increase water percolation into aquifers.

Groundwater abstraction should be closely monitored and restricted, particularly in locations with low aquifer conductivity and limited recharge potential. Creating community-managed water user associations can help ensure that extraction is done fairly and sustainably. Over-extraction and contamination hazards can be further reduced by encouraging the use of contemporary irrigation techniques like drip or sprinkler systems, which reduce water waste and make better use of existing resources. It is advised that extensive aquifer characterization studies be conducted to better understand the spatial variability of groundwater flow throughout the basin. These studies should include assessments of hydraulic conductivity, storage capacity, and recharge potential in order to improve groundwater resource planning.

The interactions between surface water and groundwater in the basin are critical and must be controlled to ensure the sustainability of both resources. Interventions such as the installation of artificial recharge structures or check dams in areas with declining river reaches can aid in water retention and aquifer recharge. An integrated water resource management (IWRM) framework should be implemented to ensure that surface and groundwater resources are planned and managed in a coordinated way. This method would involve stakeholders from several sectors, including as agriculture, urban growth, and environmental conservation, in order to balance competing water demands.

To avoid over-reliance on either resource, efficient irrigation practices that take into account both surface and groundwater availability should be encouraged. Techniques like conjunctive water usage, which uses surface water and groundwater in tandem, can help improve resource utilization and assure sustainability. Finally, promoting collaboration among all basin stakeholders, including government agencies, local communities, and non-governmental groups, is vital. This collaboration will ensure a comprehensive strategy to managing the

interconnectedness between surface and groundwater systems, improving resilience to climatic unpredictability, and encouraging sustainable behaviors.

Overall, by applying these detailed recommendations, water resource management in the Meki River basin can be greatly improved. These steps will improve the basin's water systems' sustainability and resilience while also ensuring equal access for all water users. Policymakers, researchers, and communities must collaborate to implement these measures, drawing on scientific insights and local knowledge to establish a more sustainable and flexible water resource management framework for the future.

6. REFERENCES

Abate, H. (2007). Impact of land use change and climate variability on catchment runoff: A modeling study of the Meki River Basin (Master's thesis).

Abbott, M. B., Bathurst, J. C., Cunge, J. A., O'Connell, P. E., & Rasmussen, J. (1986). An introduction to the European Hydrologie System—Systeme Hydrologique Europeen "SHE" 2: Structure of a physically based, distributed modelling system. *Journal of Hydrology, 87*(1-2), 61-77.

Abebe, A., Yohannes, H., & Dereje, A. (2014). Impact of disappearance of Lake Haramaya on the livelihood of the surrounding community: The case of Haramaya District in Oromia National Regional State, Ethiopia. *Journal of Economics and Sustainable Development, 5*(18), 141-148.

Aliyari, F., Bailey, R. T., Tasdighi, A., Dozier, A., Arabi, M., & Zeiler, K. (2019). Coupled SWAT-MODFLOW model for large-scale mixed agro-urban river basins. *Environmental Modelling & Software, 115*, 200-210.

Anderson, M. P., & Woessner, W. W. (1992). Applied groundwater modeling: Simulation of flow and advective transport. *Academic Press*.

Aquanty Inc. (2018). HydroGeoSphere (HGS) version 2332: User manual documents.

Arnold, J. G., Srinivasan, R., Muttiah, R. S., & Williams, J. R. (1998). Large area hydrologic modeling and assessment part I: Model development. *Journal of the American Water Resources Association, 34*(1), 73-89.

Arnold, J. G., Kiniry, J. R., Srinivasan, R., Williams, J. R., Haney, E. B., & Neitsch, S. L. (2012). SWAT 2012 Input/Output Documentation. *Texas Water Resources Institute Technical Report, 439*.

Ayenew, T. (1998). The hydrogeological system of the Lake District Basin, Central Main Ethiopian Rift (Doctoral dissertation). Free University of Amsterdam, The Netherlands.

Ayenew, T. (2001). Numerical groundwater flow modelling of the Central Main Ethiopian Rift lakes basin. *SINET: Ethiopian Journal of Science, 24*(2), 167-184.

Ayenew, T. (2003). Evapotranspiration using thematic mapper spectral satellite data in the Ethiopian rift and adjacent highlands. *Journal of Hydrology, 279*(1-4), 83-93.

Ayenew, T. (2004). Environmental implications of changes in the levels of lakes in the Ethiopian Rift since 1970. *Regional Environmental Change, 4*(4), 192-204.

Ayenew, T. (2008). Hydrological system analysis and groundwater recharge estimation using semi-distributed models and river discharge in the Meki River watershed. *SINET: Ethiopian Journal of Science, 31*(1), 29-42.

Ayenew, T., & Legesse, D. (2007). The changing face of the Ethiopian rift lakes and their environs: Call of the time. *Lakes & Reservoirs: Research & Management, 12*(3), 149-165.

Bailey, R. T., Wible, T. C., Arabi, M., Records, R. M., & Ditty, J. (2016). Assessing regional-scale spatio-temporal patterns of groundwater-surface water interactions using a coupled SWAT-MODFLOW model. *Hydrological Processes, 30*(24), 4420-4433.

Bailey, R., Rathjens, H., Bieger, K., Chaubey, I., & Arnold, J. (2017). SWATMOD-Prep: Graphical user interface for preparing coupled SWAT-MODFLOW simulations. *Journal of the American Water Resources Association, 53*(2), 400-410.

Birhanu, M. (2012). Numerical groundwater flow modeling of the Meki River Catchment, Central Ethiopia (Master's thesis).

Brunner, P., & Simmons, C. T. (2012). HydroGeoSphere: A fully integrated, physically based hydrological model. *Groundwater, 50*(2), 170-176.

Chernet, T. (1982). Hydrogeology of the lakes region. *Ethiopian Institute of Geological Surveys*.

Chung, I. M., Kim, N. W., Na, H., Lee, J., Yoo, S., Kim, J., & Yang, S. (2011). Integrated surface-groundwater analysis for the Pyoseon Region, Jeju Island in Korea. *Applied Engineering in Agriculture, 27*(6), 875-886.

Chung, I. M., Lee, J., Kim, N. W., Na, H., Chang, S. W., Kim, Y., & Kim, G. B. (2015). Estimating exploitable amount of groundwater abstraction using an integrated surface water-groundwater model: Mihocheon watershed, South Korea. *Hydrological Sciences Journal, 60*(5), 863-872.

Chunn, D., Faramarzi, M., Smerdon, B., & Alessi, D. S. (2019). Application of an integrated SWAT–MODFLOW model to evaluate potential impacts of climate change and water withdrawals on groundwater–surface water interactions in West-Central Alberta. *Water, 11*(1), 1-28.

Conan, C., Bouraoui, F., Turpin, N., de Marsily, G., & Bidoglio, G. (2003). Modeling flow and nitrate fate at catchment scale in Brittany (France). *Journal of Environmental Quality, 32*(6), 2026-2032.

Consult, I. (1970). Meki River Diversion Scheme I. Volume 2: Hydrology.

Deb, P., Kiem, A. S., & Willgoose, G. (2019). A linked surface water-groundwater modelling approach to more realistically simulate rainfall-runoff non-stationarity in semi-arid regions. *Journal of Hydrology, 575*, 273-291.

DiPaola, G. M. (1972). The Ethiopian Rift Valley (7000' and 8040' lat North). Reprinted from Bulletin Volcanologique, Tome XXXVI-4, 517-560. Francesco Giannini and Figli, Napoli, Italy.

Dogrul, E. C., Brush, C. F., Chung, F. I., & Goyal, A. (2016). Groundwater modeling in support of water resources management and planning under complex climate, regulatory, and economic stresses. *Water, 8*(12), 592.

Doherty, J. (2018). Model-independent parameter estimation and uncertainty analysis: User manual. Watermark Numerical Computing.

Dowlatabadi, H., & Zomorodian, M. (2016). Conjunctive simulation of surface water and groundwater using SWAT and MODFLOW in Firoozabad watershed. *KSCE Journal of Civil Engineering, 20*(1), 485-496.

Eshtawi, T., Evers, M., & Tischbein, B. (2015). Potential impacts of urban area expansion on groundwater level in the Gaza Strip: A spatial-temporal assessment. *Arabian Journal of Geosciences, 8*(12), 10565-10584.

Fleckenstein, J. H., Krause, S., Hannah, D. M., & Boano, F. (2010). Groundwater-surface water interactions: New methods and models to improve understanding of processes and dynamics. *Advances in Water Resources, 33*(11), 1291-1295.

Galbiati, L., Bouraoui, F., Elorza, F. J., & Bidoglio, G. (2006). Modeling diffuse pollution loading into a Mediterranean lagoon: Development and application of an integrated surface-subsurface model tool. *Ecological Modelling, 193*(1-2), 4-18.

Gao, F., Feng, G., Han, M., Dash, P., Jenkins, J., & Liu, C. (2019). Assessment of surface water resources in the Big Sunflower River watershed using coupled SWAT-MODFLOW model. *Water, 11*(3), 1-21.

Gashew, H. (1998). Hydrogeology and hydrochemistry of Lake Ziway area and the surrounding. *Addis Ababa University*, 117 pp.

Guevara-Ochoa, C., Medina-Sierra, A., Vives, L., Zimmermann, E., & Bailey, R. T. (2020). Spatio-temporal patterns of the interaction between groundwater and surface water in plains. *Hydrological Processes, 34*(6), 1371-1392.

Guzman, J. A., Moriasi, D. N., Gowda, P. H., Steiner, J. L., Starks, P. J., Arnold, J. G., & Srinivasan, R. (2015). A tool for mapping and spatio-temporal analysis of hydrological data. *Environmental Modelling & Software, 68*, 109-116.

Guzman, J. A., Moriasi, D. N., Gowda, P. H., Steiner, J. L., Starks, P. J., Arnold, J. G., & Srinivasan, R. (2015). A tool for mapping and spatio-temporal analysis of hydrological data. *Environmental Modelling & Software, 68*, 109-116.

Haitjema, H. M. (1995). Analytic element modeling of groundwater flow. *Academic Press*.

Harbaugh, A. W. (2005). MODFLOW-2005, The US Geological Survey modular ground-water model—the ground-water flow process. *US Geological Survey Techniques and Methods 6-A16*.

Hulluka, M., Ahmed, K., & Mesele, B. (2023). Groundwater management and development in Ethiopia: Current trends and future perspectives. *Water*, 15(2), 310.

Hunt, R. J., Strand, M., & Walker, J. F. (2006). Measuring groundwater-surface water interaction and its effect on wetland stream benthic productivity, Trout Lake Watershed, Wisconsin, USA. *Journal of Hydrology*, *320*(3-4), 370-384.

Kalbus, E., Reinstorf, F., & Schirmer, M. (2006). Measuring methods for groundwater-surface water interactions: A review. *Hydrology and Earth System Sciences Discussions, 10*(6), 873-887.

Kashyap, P. S., & Singh, R. P. (2020). Quantitative comparison of SWAT-MODFLOW and GSFLOW for watershed-scale hydrologic modeling. *Water, 12*(7), 1-20.

Kim, J., Shin, Y., Chung, I., Lee, J., Yoo, S., Park, D., & Kim, G. (2008). Assessment of groundwater availability in Jeju Island using SWAT-MODFLOW simulation. *Journal of Hydrology*, *356*(1-2), 247-259.

Legesse, D., & Ayenew, T. (2006). Effect of improper water and land resource utilization on the central Main Ethiopian Rift lakes. *Quaternary International, 148*(1), 8-18.

Legesse, D., Vallet-Coulomb, C., & Gasse, F. (2004). Analysis of the hydrological response of a tropical terminal lake, Lake Abiyata (Main Ethiopian Rift Valley) to changes in climate and human activities. *Hydrological Processes, 18*(3), 487-504.

Lerner, D. N., Issar, A. S., & Simmers, I. (1990). Groundwater recharge: A guide to understanding and estimating natural recharge. *International Contributions to Hydrogeology, Vol. 8*, Verlag Heinz Heise.

Li, X. (2018). Integration of hydrological modeling and data assimilation in the characterization and prediction of streamflow and groundwater dynamics (Doctoral dissertation). *The University of Arizona*.

Lindzen, R. S., & Farrell, B. (1980). Some realistic modifications of simple climate models. *Journal of the Atmospheric Sciences, 37*(5), 894-907.

Liu, Y. (2009). Groundwater recharge in the arid and semi-arid regions: Climate variability and anthropogenic activities (Doctoral dissertation). *University of Florida*.

López, D. (2005). Impact of Climate and Land Use Change on the Hydrology of the Peruvian Andes (Doctoral dissertation). *Swiss Federal Institute of Technology Zurich*.

López, D., & Graham, D. W. (2005). Peruvian highlands hydrology: Impact of precipitation variability on streamflow generation processes and water availability. *Advances in Water Resources, 28*(6), 611-625.

Massoud, M. A., El-Fadel, M., Scrimshaw, M. D., & Lester, J. N. (2003). Land use impact on the distribution and environmental implications of petroleum hydrocarbons in sediments. *Environmental Pollution, 124*(1), 25-34.

McDonald, M. G., & Harbaugh, A. W. (1988). A modular three-dimensional finite-difference groundwater flow model. *US Geological Survey Techniques of Water-Resources Investigations, Book 6, Chapter A1*.

McGregor, J. L., & Dix, M. R. (2008). An updated description of the conformal-cubic atmospheric model. In K. Hamilton & W. Ohfuchi (Eds.), *High Resolution Numerical Modelling of the Atmosphere and Ocean* (pp. 51-76). Springer.

Melese, A., Wagesho, N., & Sime, G. (2019). Assessing the impact of climate change on hydrological components and groundwater recharge in Ethiopia. *Climate, 7*(8), 1-22.

Melese, A., Abegaz, A., Legesse, D., & Ayenew, T. (2018). Hydrogeological study of the northern and central part of the Ethiopian Rift: Implications for groundwater management. *Environmental Earth Sciences, 77*(19), 1-17.

Mengistu, G., & Hurni, H. (2019). Groundwater management in Ethiopia: Current status and future challenges. *Water International*, 44(3), 276-291.

Merkel, B. J., & Planer-Friedrich, B. (2008). Groundwater geochemistry: A practical guide to modeling of natural and contaminated aquatic systems. *Springer*.

Mohammed, Y. A., & Ayalew, L. (2016). Hydrogeological investigation of groundwater potential in the Central Rift Valley Lakes basin, Ethiopia. *Journal of African Earth Sciences*, 114, 35-46.

Moriasi, D. N., Gitau, M. W., Pai, N., & Daggupati, P. (2015). Hydrologic and water quality models: Performance measures and evaluation criteria. *Transactions of the ASABE, 58*(6), 1763-1785.

Neitsch, S. L., Arnold, J. G., Kiniry, J. R., & Williams, J. R. (2011). Soil and Water Assessment Tool Theoretical Documentation. Version 2009. *Texas Water Resources Institute Technical Report, 406*.

Nguyen, H., Le, T. V. H., Macalister, C., & Tran, T. A. (2020). Evaluating the impacts of sea-level rise and climate change on surface water-groundwater interaction and salinity intrusion in the Vietnamese Mekong Delta. *Science of The Total Environment, 727*, 1-14.

Nicholls, R. J., Hoozemans, F. M. J., & Marchand, M. (1999). Increasing flood risk and wetland losses due to global sea-level rise: Regional and global analyses. *Global Environmental Change, 9*(1), S69-S87.

Niyogi, D. (2012). Indian summer monsoon variability and extremes. *Climate Dynamics, 39*(5), 1183-1208.

Owuor, S. O., Butterbach-Bahl, K., Guzha, A. C., Jacobs, S. R., Rufino, M. C., Pelster, D. E., ... & Breuer, L. (2016). Groundwater recharge rates and surface runoff response to land use and land cover changes in semi-arid environments. *Ecological Processes, 5*(1), 1-18.

Pavelic, P., Stutter, M. I., & Muirhead, R. W. (2012). Groundwater and food security in Africa: Opportunities for improving management. *International Journal of Water Resources Development*, 28(4), 617-631.

Rusli, R., Ilham, R., & Farhan, M. (2023). Groundwater resource management: Challenges and opportunities in the context of sustainable development. *Water Resources Management*, 37(5), 1757-1773.

Smerdon, B. D., & Redding, T. E. (2013). Hydrology of wetlands and groundwater dependent ecosystems: Concepts, methods, and recent developments. *Forest Ecology and Management, 302*, 202-211.

Solomon, D. K., & Cook, P. G. (2000). 3. Environmental tracers in subsurface hydrology. In P. G. Cook & A. L. Herczeg (Eds.), *Environmental tracers in subsurface hydrology* (pp. 1-20). Springer.

Szilagyi, J., Jozsa, J., Kovacs, A., & Mika, J. (2009). Estimation of catchment-scale evapotranspiration by a reduced-order, analytical model. *Journal of Hydrology, 371*(1-4), 240-247.

Taye, M. T., Ebrahim, G. Y., Nigussie, L., Hagos, F., Uhlenbrook, S., & Schmitter, P. (2022). Integrated water availability modelling to assess sustainable agricultural intensification options in the Meki catchment, Central Rift Valley, Ethiopia. *Journal Name, Volume*(Issue), pages.

Tessari, G., & Lorenzi, M. (2007). Climate change and surface water-groundwater interactions: Numerical simulation of the Piave River Basin (Italy). *Physics and Chemistry of the Earth, 32*(15-18), 994-1001.

Tigabu, T., Wagner, P. D., Hörmann, G., & Fohrer, N. (2020). Modeling spatio-temporal flow dynamics of groundwater-surface water interactions of the Lake Tana Basin, Upper Blue Nile, Ethiopia. *Hydrology Research, 51*(5), 724–740. https://doi.org/10.2166/nh.2020.046

Voudouris, K. S. (2006). Groundwater balance and safe yield of the coastal aquifer system in NEastern Korinthia, Greece. *Applied Geography*, *26*(4), 291-311.

Wagener, T., Wheater, H. S., & Gupta, H. V. (2004). Rainfall-runoff modelling in gauged and ungauged catchments. *Imperial College Press*.

Wang, Z., Eckhardt, K., & Schumann, A. (2018). An integrated surface-subsurface hydrological model for shallow water table areas. *Journal of Hydrology*, *556*, 180-193.

Wheater, H. S., & Evans, E. (2009). Land use, water management and future flood risk. *Land Use Policy*, *26*(S1), S251-S264.

Zektser, I. S., & Everett, L. G. (2004). Groundwater resources of the world and their use. *UNESCO*.

Zhang, Y., & Schilling, K. E. (2006). Temporal changes in baseflow and baseflow nitrate flux in the Raccoon River, Iowa. *Journal of Hydrology*, *327*(3-4), 612-622.

Zhou, Y., Li, W., & Wang, S. (2011). Integrated hydrological modelling of a karst catchment using SWAT-MODFLOW. *Hydrological Processes, 25*(18), 2873-2884.

7. Appendix

Appendix I: Mean Annual precipitation

Year	Bui	Buta Jira	Ejersa	Koshe	Meki	Sutan	Tora
2000	1464.5	1385.6	1267.4	1244.5	1306.2	580.7	477.6
2001	1501.3	2041.3	1516.9	1371.1	1211.6	620.7	1306.7
2002	1396.8	1724.9	851.1	863.7	926.6	475.7	1131.1
2003	1341.3	1777.8	1270.9	1080.6	1036.5	534.4	819
2004	1328.7	1498.4	1309.8	924.2	855.7	505.8	885.7
2005	1837.5	2508.6	1363.6	1476.5	1232.2	693.8	639.5
2006	1786.2	2272.3	1365.3	1393.6	1372.9	994.3	1351.6
2007	1430.7	1570.3	1116.5	1382.5	1147	940.2	1261.1
2008	1426	2200.4	1407.3	1353.5	1187.2	862.3	992.7
2009	1179.9	1125.3	1277.8	811.6	889.8	761.7	1178.7
2010	2045	2068.3	1433.1	1579.4	906.6	1091	1622.6
2011	1226.5	1985.6	1162.9	885.3	586.7	585.1	1785.9
2012	1222.8	1253.7	1314.7	773.4	1277.5	837.8	898.1
2013	1392.2	1524.9	1522.3	1125.5	1007.3	1068.7	1119.4
2014	1512.4	2261.2	1278.8	1049.5	1317.9	908	1357.8
2015	921.3	883	1127.9	369.9	800.8	657.8	1050.5
2016	1288.1	1260.1	1596.2	1306.2	1183.8	993.1	983.7
2017	1556.9	1222.8	1430.6	644.5	1430	930.3	973.2
2018	1374.9	1498.5	1112.2	939.1	782.9	793.1	1534.2
2019	1693.2	1509.1	492.7	1586.2	576.1	1019.9	1432.3
2020	1994	2084.5	1636.4	1659.5	752.7	1253.5	5515.7

Appendix II: Mean maximum temperature

Gauging Station	Jan	Feb	Mar	Apr	May	Jun	Jul	Aug	Sep	Oct	Nov	Dec
Bui	26.4	27.9	28.5	27.9	28.08	27	24.62	24.44	25.8	26.1	26.1	25.5
Buta	27.3	28.2	29.3	28.1	28.03	27.4	24.82	24.99	26.2	28	28	26.8

Appendix III: Mean minimum temperature

Gauging Station	Jan	Feb	Mar	Apr	May	Jun	Jul	Aug	Sep	Oct	Nov	Dec
Bui	8.1	9.37	10.6	11.3	11.19	10.4	10.43	10.53	10.29	8.97	8.16	7.17
Buta	9.55	10.4	11.6	12.5	11.78	12.29	11.21	11.68	11.5	10.74	9.89	8.95

Appendix IV: Mean wind speed (in m/s) at 2 m

Year	Jan	Feb	Mar	Apr	May	Jun	Jul	Aug	Sep	Oct	Nov	Dec
2000	2.25	2.47	2.53	2.27	1.82	1.73	1.49	1.45	1.2	1.55	1.69	1.79
2001	1.77	2.01	1.69	2.09	1.54	1.42	1.38	1.55	1.47	1.87	2.11	1.96
2002	2.09	2.07	1.82	2.2	1.5	1.5	1.46	1.25	1.33	2.01	2.22	2.05
2003	2.02	2.4	2.24	1.86	1.99	1.54	1.4	1.17	1.09	1.81	1.83	1.91
2004	1.72	2.06	1.87	1.64	1.78	1.43	1.31	1.18	1.18	1.63	1.88	1.86
2005	1.63	1.91	1.74	1.77	1.36	1.22	1.21	1.18	1.1	1.63	1.8	1.83
2006	1.82	1.75	1.65	1.52	1.55	1.23	1.23	1.1	1.15	1.63	1.79	1.92
2007	1.73	1.6	1.86	1.78	1.6	1.18	1.09	1.04	1.07	1.7	1.96	1.85
2008	1.84	1.99	1.98	2.05	1.47	1.18	1.16	0.97	1.07	1.33	1.4	1.38
2009	1.4	1.57	1.48	1.42	1.38	1.35	1.12	0.96	1.07	1.3	1.4	1.25
2010	1.36	1.08	1.33	1.1	0.85	0.89	0.98	0.73	0.9	1.31	1.3	1.22
2011	1.5	1.66	1.57	1.17	1.23	0.94	1.01	0.87	0.8	1.35	1.25	1.35
2012	1.49	1.65	1.57	1.16	1.44	1.12	0.88	0.89	0.92	1.41	1.31	1.33
2013	1.35	1.51	1.24	1.19	0.88	0.97	0.88	0.81	0.9	0.9	1.34	1.26
2014	1.25	1.19	1.28	1.32	1.05	1.41	1.04	1.4	1.06	1.48	1.18	1.17
2015	1.36	1.35	1.38	1.45	0.98	1.57	1.25	0.76	1.45	1.22	1.29	1.23
2016	1.04	1.25	1.28	0.92	0.75	0.82	0.7	0.64	1.11	1.34	1.4	1.22
2017	1.39	1.47	1.16	1.46	1.32	1.36	1.09	0.82	1.68	1.73	1.88	1.77
2018	1.1	1.29	1.24	0.8	0.95	0.64	0.77	0.78	0.8	1.28	1.43	1.36
2019	1.43	1.47	1.3	1.11	1.21	0.7	0.72	0.7	0.59	1.28	1.35	1.21
2020	1.22	1.47	1.2	1.11	0.85	0.63	0.92	0.72	0.57	1.08	1.27	1.25

Appendix V: Mean monthly relative humidity (%)

Year	Jan	Feb	Mar	Apr	May	Jun	Jul	Aug	Sep	Oct	Nov	Dec
2000	38.18	39.57	42.41	49.39	47.67	46.54	51.05	55.95	51.74	50.35	45.9	44.12
2001	44.52	44.57	51.52	45.99	47.98	50.09	56.05	55.31	48.82	47.19	40.31	41.57
2002	45.11	39.83	45.82	44.82	44.05	45.79	46.47	49.29	45.71	40.04	37.09	46.98
2003	43.87	41.71	45.67	49.88	45.07	48.26	55.4	56.23	53.28	43.99	42.47	42.38
2004	48.29	43.27	56.25	61.97	57.64	57.98	62.65	64	60.91	56.2	52.17	52.27
2005	50.02	46.87	56.99	55.31	60.71	57.97	60.51	59.82	58.27	49.02	50.1	44.95
2006	52.56	54.71	55.6	59.71	40.28	43.89	60.89	63.72	36.39	32.74	32.55	30.57
2007	31.47	29.8	29.82	42.87	47.76	58.58	60.29	58.32	56.14	48.76	47.97	43.13
2008	45.49	45.07	41.08	51.01	51.37	53.48	55.88	57.19	52.77	34.88	33.78	33.81
2009	32.85	48.78	51.13	55.56	53.46	49.89	61.43	62.73	57.61	57.05	49.34	55.74
2010	51.11	55.61	57.29	57.83	57.46	54.94	62.75	61.56	57.7	51.72	45.43	46.59
2011	47.92	44.97	49.94	49.6	54.73	51.45	56.69	59.81	55.62	45.67	49.36	50.52
2012	48.45	46.32	48.4	57.78	52.31	52.25	62.7	62.4	57.78	50.78	48.5	48.76
2013	48.69	47.4	49.24	52.56	53.83	53.69	61.71	60.32	53.05	52.06	52.46	45.88
2014	49.78	54.58	53.16	53.45	53.65	50.35	57.91	57.48	49.4	38.33	36.53	37.57
2015	35.84	41.2	49.51	56.66	58.41	63.34	61.89	64.97	61.58	58.43	60.4	56.2
2016	59.51	39.29	57.16	67.04	64.09	61.93	69.22	67.53	62.59	57.08	54.23	50.78
2017	40.94	43.12	39.75	42.73	46.25	40.44	48.89	48.28	47.29	42.34	38.45	36.99
2018	36.44	32.77	43.16	52.84	53.57	54.2	54.1	54.14	50.03	46.23	49.75	43.9
2019	40.32	45.51	45.37	49.23	47.93	52.18	55.6	59.31	54.83	51.59	48.52	48
2020	48.53	45.93	48.52	52.12	27.91	28.68	59.05	57.41	29.12	46.92	43.62	53.83

Appendix VI: Mean monthly sunshine hours (hours/day)

Year	Jan	Feb	Mar	Apr	May	Jun	Jul	Aug	Sep	Oct	Nov	Dec
2000	21.26	22.38	22.86	21.22	21.03	20.73	19.71	19.01	20.24	19.86	19.72	19.45
2001	19.86	21.16	20.43	21.99	20.91	19.87	18.51	19.19	21	20.72	21.09	20.04
2002	19.8	22.33	21.97	22.37	22	20.95	20.94	20.73	21.77	22.46	21.83	18.95
2003	20.11	21.73	22.06	21.08	21.76	20.41	18.72	18.99	19.89	21.49	20.45	19.79
2004	19.16	21.53	19.45	18.05	18.74	18.2	17.05	17.21	18.16	18.58	18.47	17.87
2005	18.72	20.87	19.35	19.96	17.95	18.17	17.63	18.29	18.51	20.13	19	19.25
2006	18.29	18.96	19.66	18.69	19.94	19.84	17.5	17.23	20.27	20.26	20.2	22.55
2007	20.2	20.2	20.43	22.94	21.31	18.01	17.66	18.67	19.36	20.45	19.48	19.81
2008	19.93	21.29	23.45	20.99	20.31	19.22	18.73	18.86	20.2	20.43	20.2	20.2
2009	20.12	20.4	20.99	19.92	19.88	20.35	17.43	17.56	19.06	18.4	19.17	17.18
2010	18.72	18.84	19.23	19.25	18.83	18.83	17.09	17.85	18.93	19.77	20.04	19.12
2011	19.42	21.46	21.15	21.5	19.5	19.79	18.62	18.25	19.44	21.17	19.14	18.09

2012	19.15	20.94	21.48	19.06	19.95	19.47	16.93	17.46	18.76	19.73	19.17	18.51
2013	19.08	20.68	21.28	20.48	19.5	19.09	17.13	17.98	19.96	19.45	18.28	19.06
2014	18.85	18.91	20.16	20.22	19.61	19.92	18.18	18.71	19.31	20.2	20.2	20.2
2015	20.2	19.94	21.16	19.55	18.51	16.72	17.32	16.97	17.95	18.14	16.6	16.99
2016	16.68	20.01	19.45	16.74	16.97	17.13	15.33	16.18	17.68	18.36	17.91	18.09
2017	20.82	21.61	23.55	22.87	21.33	22.25	20.04	20.62	21.28	21.74	20.89	20.2
2018	20.2	20.2	20.65	20.29	19.54	18.9	19.04	19.53	20.72	20.91	18.93	19.57
2019	20.95	21.2	22.3	21.39	21.07	19.43	18.68	18.28	19.5	19.56	19.16	18.61
2020	19.08	20.66	21.44	20.55	20.2	20.2	17.81	18.7	20.2	20.64	20.26	17.35

Appendix VII: Mean monthly river discharge (m3/s) at Meki town (2000 - 2013)

Year	Jan	Feb	Mar	Apr	May	Jun	Jul	Aug	Sep	Oct	Nov	Dec
2000	0.02	0	0	0.04	0.82	0.66	6.24	13.95	10.86	8.09	3.38	0.95
2001	0.03	0.18	3.06	1.53	4.92	10.87	22.1	37.26	23.36	2.46	1.08	0.52
2002	4.15	2.94	1.74	1.61	0.89	3.368	16.37	17.47	9.51	3.36	2.67	2.16
2003	1.43	0.88	4.16	4.81	2.51	4.65	14.74	20.08	13.56	4.18	0.91	1.02
2004	1.11	0.39	0.89	11.25	0.95	2.39	10.61	23.04	14.76	7.42	0.91	0.13
2005	0.55	0.04	1.46	3.65	14.28	9.89	14.66	26.67	21.68	8.73	2.9	1.96
2006	2.52	2.04	9.13	22.39	16.93	11.24	30.59	37.68	21.96	7.31	1.78	1.23
2007	0.7	2.39	1.37	0.39	2.08	15.92	34.01	37.27	24.05	7.58	1.01	0.33
2008	0.2	0.05	0	0.13	1.35	3.98	10.94	21.07	15.86	2	11.65	0.23
2009	0.8	0.01	0.18	0.52	0.67	0.09	4.02	7.71	6.84	5.87	0.56	0.12
2010	0	1.12	3.12	11.56	9.29	2.13	23.36	30.04	19.79	2.61	0.29	0
2011	0	0	0.28	0	2.41	4.79	11.28	23.99	26.07	3.65	0.5	0.09
2012	0.4	0.15	0.01	1.11	3.96	0.56	23.45	24.2	24.67	6.62	0.05	0
2013	0	0	2.82	0.02	0.03	0	0	2.61	3.63	13.32	0.55	0.16

Appendix VIII: Head data (Static water level) and locations

BOREHOLE	Coordinate	Measured

Observation	UTM-X	UTM-Y	Observation
head1	435852	869258	1682
head2	448646	885794	1732
head3	441974	890758	1749
head4	436818	892494	1758
head5	435517	877276	1788.81
head6	431044	871595	1803
head7	442590	886150	1809
head8	453276	901204	1810
head9	447247	889418	1810
head10	446061	888355	1810
head11	445587	890527	1812
head12	448953	900604	1812
head13	442910	883379	1813
head14	431708	870363	1813
head15	447780	886782	1813
head16	441700	884120	1814
head17	445831	891566	1815
head18	447700	886562	1816
head19	431974	879460	1816
head20	441090	883120	1816
head21	433720	875735	1817
head22	446858	890325	1817
head23	432214	869559	1818
head24	448674	899951	1818
head25	445997	892208	1819
head26	444425	890845	1821
head27	440854	889603	1821
head28	434916	877533	1822

head29	441620	889345	1822
head30	439032	888026	1822
head31	440559	886885	1823
head32	440456	888867	1825
head33	442017	891450	1825
head34	434096	877393	1827
head35	438525	892515	1832
head36	437645	890366	1833
head37	447562	904659	1833
head38	444039	903498	1848
head39	446896	904607	1850
head40	447042	906854	1855
head41	442310	904952	1865
head42	444979	905272	1868
head43	429307	897130	1871
head44	424695	875670	1874
head45	443068	907198	1878
head46	443712	908129	1880
head47	440195	905819	1886
head48	442690	908775	1889
head49	440014	905638	1896
head50	441925	908580	1897
head51	438896	894475	1910
head52	449214	913780	1923
head53	432501	898201	1973
head54	426254	887320	2000
head55	426285	887327	2045
head56	430941	896250	2048
head57	429313	897129	2092

head58	431086	898842	2096
head59	426692	896415	2129
head60	424926	892693	2140
head61	424292	894735	2171
head62	458031	929019	1924

Appendix IX: The coordinates, observed and simulated heads of the observation points with calculated error assessment. Observed head and is simulated head.

BOREHOLE	Coordinate		Measured	Modelled	Residual	Abs. of Residual	Sqrt. Residual
Observation	UTM-X	UTM-Y	Observation	Observation	Observation		
head1	435852	869258	1682	1685.488	-3.488	3.488	12.16614
head2	448646	885794	1732	1718.606	13.394	13.394	179.3992
head3	441974	890758	1749	1743.309	5.691	5.691	32.38748
head4	436818	892494	1758	1780.807	-22.807	22.807	520.1592
head5	435517	877276	1788.81	1824.509	-35.699	35.699	1274.419
head6	431044	871595	1803	1824.247	-21.247	21.247	451.435
head7	442590	886150	1809	1821.936	-12.936	12.936	167.3401
head8	453276	901204	1810	1804.159	5.841	5.841	34.11728
head9	447247	889418	1810	1820.504	-10.504	10.504	110.334
head10	446061	888355	1810	1820.859	-10.859	10.859	117.9179
head11	445587	890527	1812	1820.81	-8.81	8.81	77.6161
head12	448953	900604	1812	1815.82	-3.82	3.82	14.5924
head13	442910	883379	1813	1822.115	-9.115	9.115	83.08323
head14	431708	870363	1813	1825.763	-12.763	12.763	162.8942
head15	447780	886782	1813	1820.563	-7.563	7.563	57.19897

head16	441700	884120	1814	1822.261	-8.261	8.261	68.24412
head17	445831	891566	1815	1820.665	-5.665	5.665	32.09222
head18	447700	886562	1816	1820.617	-4.617	4.617	21.31669
head19	431974	879460	1816	1825.296	-9.296	9.296	86.41562
head20	441090	883120	1816	1822.442	-6.442	6.442	41.49936
head21	433720	875735	1817	1825	-8	8	64
head22	446858	890325	1817	1820.548	-3.548	3.548	12.5883
head23	432214	869559	1818	1825.773	-7.773	7.773	60.41953
head24	448674	899951	1818	1816.922	1.078	1.078	1.162084
head25	445997	892208	1819	1820.569	-1.569	1.569	2.461761
head26	444425	890845	1821	1821.039	-0.039	0.039	0.001521
head27	440854	889603	1821	1821.982	-0.982	0.982	0.964324
head28	434916	877533	1822	1824.515	-2.515	2.515	6.325225
head29	441620	889345	1822	1821.833	0.167	0.167	0.027889
head30	439032	888026	1822	1822.57	-0.57	0.57	0.3249
head31	440559	886885	1823	1822.309	0.691	0.691	0.477481
head32	440456	888867	1825	1822.151	2.849	2.849	8.116801
head33	442017	891450	1825	1821.511	3.489	3.489	12.17312
head34	434096	877393	1827	1824.747	2.253	2.253	5.076009
head35	438525	892515	1832	1822.169	9.831	9.831	96.64856
head36	437645	890366	1833	1822.645	10.355	10.355	107.226
head37	447562	904659	1833	1831.376	1.624	1.624	2.637376
head38	444039	903498	1848	1852.359	-4.359	4.359	19.00088
head39	446896	904607	1850	1836.376	13.624	13.624	185.6134
head40	447042	906854	1855	1851.635	3.365	3.365	11.32323
head41	442310	904952	1865	1877.255	-12.255	12.255	150.185
head42	444979	905272	1868	1856.787	11.213	11.213	125.7314
head43	429307	897130	1871	1876.643	-5.643	5.643	31.84345
head44	424695	875670	1874	1876.398	-2.398	2.398	5.750404

head45	443068	907198	1878	1885.359	-7.359	7.359	54.15488
head46	443712	908129	1880	1886.373	-6.373	6.373	40.61513
head47	440195	905819	1886	1898.594	-12.594	12.594	158.6088
head48	442690	908775	1889	1899.476	-10.476	10.476	109.7466
head49	440014	905638	1896	1900.659	-4.659	4.659	21.70628
head50	441925	908580	1897	1904.243	-7.243	7.243	52.46105
head51	438896	894475	1910	1906.666	3.334	3.334	11.11556
head52	449214	913780	1923	1929.285	-6.285	6.285	39.50123
head53	432501	898201	1973	1989.604	-16.604	16.604	275.6928
head54	426254	887320	2000	2010.231	-10.231	10.231	104.6734
head55	426285	887327	2045	2045.401	-0.401	0.401	0.160801
head56	430941	896250	2048	2041.428	6.572	6.572	43.19118
head57	429313	897129	2092	2091.152	0.848	0.848	0.719104
head58	431086	898842	2096	2096.75	-0.75	0.75	0.5625
head59	426692	896415	2129	2119.751	9.249	9.249	85.544
head60	424926	892693	2140	2134.712	5.288	5.288	27.96294
head61	424292	894735	2171	2162.991	8.009	8.009	64.14408
head62	458031	929019	1924	1921.673	2.327	2.327	5.414929
				Min	-35.699	0.039	0.001521
				Max	13.624	35.699	1274.419
				Median	-3.518	6.329	40.05818